EARLY-STAGE ML-BASED NON-INVASIVE BREAST CANCER SCREENING

By

FARRDIN NOWSHAD
21321007
MOHAMMAD FASIUL ABEDIN KHAN
22121092
ABRAR MAKSUD NAHEAN
22121076
MD. ABU ANAS MRIDUL
22121024

A Final Year Design Project (FYDP) submitted to the Department of Electrical and Electronic Engineering partial fulfillment of the requirements for the degree of Bachelor of Science in Electrical and Electronic Engineering.

Department of Electrical and Electronic Engineering
BRAC University
January, 2026

Declaration

It is hereby declared that

1. The Final Year Design Project (FYDP) submitted is my own original work, completed while pursuing my degree at Brac University.
2. The Final Year Design Project (FYDP) does not contain material previously published or written by a third party, except where this is appropriately cited through full and accurate referencing.
3. The Final Year Design Project (FYDP) does not contain material that has been accepted or submitted for any other degree or diploma at a university or other institution.
4. I/We have acknowledged all main sources of help.

Student's Full Name & Signature:

[Farrdin Nowshad] [21321007]	**[Mohammad Fasiul Abedin Khan]** [22121092]
[Abrar Maksud Nahean] [22121076]	**[MD. Abu Anas Mridul]** [22121024]

Approval

1. Project Title

Early-Stage ML-Based Non-Invasive Breast Cancer Screening.

1. FARRDIN NOWSHAD (21321007)
2. MOHAMMAD FASIUL ABEDIN KHAN (22121092)
3. ABRAR MAKSUD NAHEAN (22121076)
4. MD. ABU ANAS MRIDUL (22121024)

Of Fall 2025 has been accepted as satisfactory in partial fulfillment of the requirement for the degree of BSc in EEE (Bachelor of Science in Electrical and Electronic Engineering on 5th January of 2026.

Examining Committee:

Academic Technical Committee (ATC):

(Chair)

_____

NAHID AKHTER JAHAN, PhD
Associate Professor
Department of Electrical and Electronic Engineering
BRAC University

Final Year Design Project Coordination Committee:

(Chair)

_____

Mirza Rasheduzzaman, PhD
Associate Professor
Department of Electrical and Electronic Engineering
BRAC University

Department Chair:

_____

Md. Mosaddequr Rahman, PhD
Professor
Department of Electrical and Electronic Engineering

BRAC University

Ethics Statement

We, the signatory students, Farrdin Nowshad (21321007), Mohammad Fasiul Abedin Khan (22121092), Abrar Maksud Nahean (22121076), Md. Abu Anas Mridul (22121024) - hereby confirm that our submission has been thoroughly analyzed for plagiarism using reliable detection tools, resulting in a similarity index below 35%. Our content's originality is assured, as it is authored by team members and properly cites external resources following academic guidelines. Our work followed the ethical framework provided in the IRB proposal, also including the informed consents from the volunteers, data privacy measures through encryption and anonymization, AI model transparency, participant welfare, and responsible deployment of ML. We pledge to reduce the risks, ensure participant autonomy, and abide by relevant standards, including ISO 13485 for quality management of medical devices and the Digital Security Act for data protection.

Abstract/Executive Summary

Early breast cancer detection in low- and middle-income countries is limited by high screening costs, lack of infrastructure, and dependence on specialized facilities. This project presents a portable, low-cost, non-invasive AI-assisted breast cancer screening system using infrared thermography and machine learning, designed for deployment in resource-constrained settings. The system captures multi-view thermal images and analyzes temperature asymmetry and abnormal heat patterns using a convolutional neural network deployed on an embedded edge-computing platform. A structured engineering approach was followed, including evaluation of multiple design alternatives, optimization, sustainability, economic analysis, ethical compliance, and project management. The system provides an output, Benign or Malignant, to support clinical decision-making without replacing diagnostic procedures. The results demonstrate technical feasibility, affordability, and sustainability, establishing a strong foundation for IRB-guided clinical validation and scalable community-level screening.

Keywords: MobileNet, BSTI, Thermalytx, CNN, SVM, Benign, Malignant.

Acknowledgement

We would like to express our sincere gratitude to the Chair of our ATC Committee, Nahid Akhter Jahan, PhD, for her invaluable guidance and thorough evaluation of our project. We also extend our appreciation to Farjana Akter Jhuma, PhD, Mr. Subhan Zawad Bihan, and Tasfin Mahmud, in the Department of Electrical and Electronic Engineering at BRAC University, for their constructive feedback and valuable recommendations that significantly contributed to improving the quality of this work. Additionally, we gratefully acknowledge Dr. Rahian Bin Sharif for his efforts and for providing essential insights from a clinical perspective, which greatly enriched the project.

Table Content

Chapter 1: Introduction- [CO1, CO2, CO10]

1.1 Introduction

Breast cancer represents the most prevalent malignancy among women globally and remains a major public health concern across both developed and developing regions. Recent epidemiological estimates indicate that breast cancer accounts for more than 2.3 million newly diagnosed cases annually, constituting approximately 23% of all newly identified cancer cases worldwide [1], [2]. The disease is the second leading cause of cancer-related mortality among women, with substantial regional variation in survival outcomes. In the United States alone, breast cancer is responsible for over 40,000 deaths per year, while mortality rates in low- and middle-income countries (LMICs) are often higher due to delayed diagnosis and limited access to timely care [2].

Early detection plays a decisive role in reducing breast cancer–related mortality and improving long-term patient outcomes. Clinical evidence demonstrates that nearly 95% of breast cancer cases diagnosed at early stages exhibit significantly improved survival probabilities and treatment success compared to late-stage diagnoses [1]. Despite this well-established relationship between early detection and prognosis, large segments of the global population remain excluded from routine screening programs. This disparity is particularly pronounced in LMICs, where healthcare systems face persistent challenges related to infrastructure limitations, high diagnostic costs, and shortages of trained medical personnel.

In countries such as Bangladesh, breast cancer is frequently diagnosed at advanced stages, often after the disease has progressed beyond optimal treatment windows. Factors contributing to delayed diagnosis include limited availability of screening facilities outside major urban centers, financial barriers associated with conventional imaging modalities, sociocultural constraints, and insufficient awareness of early symptoms. As a result, breast cancer outcomes in these settings remain suboptimal despite advances in oncological care.

Conventional breast cancer screening techniques, including mammography, ultrasonography, and computed tomography (CT), are clinically effective but impose substantial logistical and economic burdens. Mammography, the gold standard for population-level screening in many high-income countries, requires expensive equipment, radiation exposure management, trained radiologists, and controlled clinical environments. Ultrasonography, while radiation-free, is highly operator-dependent and necessitates specialized probes and skilled sonographers. These requirements limit scalability and accessibility in low-resource settings, particularly for community-based or mobile screening initiatives. Consequently, reliance on conventional imaging modalities alone is insufficient to address the screening needs of underserved populations.

The rapid expansion of healthcare data and advancements in computational capabilities have catalyzed growing interest in artificial intelligence (AI) and machine learning (ML) techniques as powerful tools for addressing complex challenges in cancer detection and

diagnosis [1]. ML algorithms are particularly well suited for analyzing high-dimensional medical data, identifying subtle patterns, and supporting clinical decision-making processes. In oncology, ML has demonstrated strong potential in image-based diagnostics, risk stratification, and early disease detection, complementing traditional medical workflows.

Among non-invasive screening modalities, infrared thermography has gained renewed attention as a potential tool for preliminary breast cancer risk assessment. Thermography measures surface temperature distributions that reflect underlying physiological processes, including metabolic activity and vascular perfusion. Tumor development is commonly associated with angiogenesis and increased blood flow, leading to localized thermal asymmetries that can be captured using infrared sensors. Unlike conventional imaging techniques, thermography is radiation-free, painless, and contactless, making it suitable for repeated screening and for use in asymptomatic populations.

Historically, the adoption of breast thermography has been constrained by technological and methodological limitations. Earlier generations of thermal imaging systems suffered from low spatial resolution and inadequate thermal sensitivity, while diagnostic interpretation relied heavily on subjective visual assessment. These factors contributed to inconsistent diagnostic performance and limited clinical acceptance. However, recent advances in thermal sensor technology, combined with AI-driven image analysis, have significantly enhanced the reliability and reproducibility of thermographic screening.

Convolutional neural networks (CNNs) and other deep learning architectures have demonstrated strong capability in extracting discriminative features from medical images, including thermograms. By learning complex spatial and textural patterns associated with pathological conditions, ML-based systems can detect subtle thermal anomalies that may not be apparent through manual interpretation. Automated analysis also improves consistency and reduces inter-observer variability, which is critical for large-scale screening applications. Furthermore, the integration of ML models with embedded edge-computing platforms enables real-time inference without dependence on cloud connectivity, enhancing privacy, latency, and operational robustness.

Despite these technological advancements, the effective translation of AI-assisted thermography into real-world healthcare settings requires careful system-level consideration. Screening tools must balance diagnostic performance with affordability, computational efficiency with reliability, and innovation with ethical responsibility. Importantly, AI-based screening systems must be clearly distinguished from diagnostic tools to prevent misinterpretation and inappropriate clinical use. Ethical considerations, including informed consent, data security, algorithmic transparency, and compliance with medical device regulations, are central to the responsible deployment of such technologies.

Within the context of Bangladesh and similar LMICs, the development of accessible early-stage breast cancer screening solutions is of particular relevance. Healthcare delivery in these regions is often decentralized, with primary care clinics and mobile health initiatives serving as the first point of contact for large portions of the population. However, these

settings typically lack advanced diagnostic infrastructure. A portable, low-cost, AI-assisted screening system capable of operating in resource-constrained environments could support early risk identification and facilitate timely referral to specialized care, thereby improving overall disease outcomes.

This Final Year Design Project (FYDP) addresses these challenges through the development of a non-invasive, AI-based breast cancer screening system utilizing infrared thermography. The proposed system integrates thermal imaging hardware, machine learning algorithms, and embedded edge computing within a structured engineering framework. Rather than replacing established diagnostic procedures, the system is intended to function as a screening and triage support tool, assisting healthcare workers in identifying individuals who may benefit from further clinical evaluation.

By emphasizing affordability, portability, and ethical deployment, the project aligns with global trends toward decentralized and equitable healthcare technologies. The system-level approach encompasses hardware design, power management, AI model optimization, and user-oriented workflow integration, ensuring practical deployability alongside analytical rigor. Through this work, the project contributes to the growing body of research on AI-assisted non-invasive screening technologies and demonstrates a feasible pathway for community-level breast cancer risk assessment in low-resource settings.

1.1.1 Problem Statement

Despite the well-established importance of early detection in improving cancer survival outcomes, timely access to effective screening remains a major challenge in Bangladesh. According to a population-based cancer registry study conducted in 2025 by Bangladesh Medical University (BMU), formerly known as Bangabandhu Sheikh Mujib Medical University (BSMMU), the national cancer incidence is estimated at approximately 53 new cases per 100,000 people annually, with cancer accounting for nearly 12% of all recorded deaths [3]. These figures reflect not only the growing burden of cancer but also the systemic limitations in early detection and screening accessibility.

The delayed diagnosis of breast cancer in Bangladesh is primarily driven by a combination of structural and socioeconomic factors. These include limited public awareness regarding early symptoms, the high cost and inaccessibility of screening facilities, a shortage of modern diagnostic infrastructure, and fear or lack of understanding surrounding preventive screening practices. Patients residing in rural and peri-urban regions are disproportionately affected, as they are often required to travel long distances to reach tertiary healthcare facilities. Such logistical and financial barriers frequently result in delayed clinical presentation, reducing the likelihood of early-stage detection and effective intervention.

From a healthcare delivery perspective, existing breast cancer screening pathways rely heavily on hospital-based imaging modalities that are poorly aligned with the constraints of low-resource and decentralized settings. Conventional screening techniques such as mammography and ultrasonography, while clinically validated, require expensive equipment,

trained specialists, and controlled clinical environments. Mammography, in particular, involves ionizing radiation and significant operational costs, making it inaccessible to large segments of the population in low- and middle-income countries like Bangladesh. These limitations restrict routine and repeated screening, especially among asymptomatic individuals, and contribute to late-stage diagnosis patterns.

As a result, breast cancer screening in Bangladesh remains largely opportunistic rather than preventive, with detection often occurring only after symptoms become clinically apparent. This reactive screening model undermines the potential benefits of early risk identification and places additional strain on already constrained healthcare resources. The absence of an affordable, scalable, and community-deployable screening solution represents a critical gap in the current healthcare system.

In response to these challenges, non-invasive screening modalities have gained increasing research interest, particularly those enhanced by artificial intelligence (AI). Infrared thermography has emerged as a promising alternative due to its radiation-free, painless, and contactless nature. The technique utilizes infrared sensors to detect abnormal heat patterns on the breast surface, which may indicate underlying tumor activity associated with increased metabolic demand and angiogenesis. While thermography alone has historically faced limitations related to subjective interpretation and environmental sensitivity, recent advances in AI-driven image analysis have significantly improved its potential reliability and consistency.

Machine learning–based interpretation of thermal images enables automated detection of subtle temperature asymmetries that may not be readily apparent through manual assessment. However, despite encouraging algorithmic performance reported in the literature, most AI-enhanced thermographic systems remain confined to controlled research environments or centralized computing platforms. There is a notable lack of integrated, edge-deployable screening systems that combine low-cost thermal sensing, robust AI analysis, and real-world usability tailored to resource-constrained settings.

Therefore, the central problem addressed by this project is the absence of a breast cancer screening system that is affordable, non-invasive, AI-assisted, and suitable for decentralized deployment within the Bangladeshi healthcare context. Existing screening technologies are either inaccessible due to cost and infrastructure requirements or insufficiently optimized for large-scale community-level use. Bridging this gap requires a system-level engineering solution that integrates non-invasive sensing, embedded intelligence, and ethical safeguards to support early-stage cancer risk identification and timely referral, without replacing established diagnostic procedures.

1.1.2 Background Study

Breast cancer remains the most prevalent malignancy among women globally, with an estimated incidence exceeding 2.8 million new cases annually and accounting for approximately 23% of all newly diagnosed oncology cases [4], [5]. The disease represents the second leading cause of cancer-related mortality among women worldwide, with more than 40,000 deaths occurring annually in the United States alone [5]. Early detection and timely intervention are critical factors in reducing breast cancer-related mortality, as approximately 95% of breast cancer cases diagnosed at early stages demonstrate significantly improved treatment outcomes and survival probabilities [4]. The exponential growth in oncology-related data has catalyzed substantial interest in machine learning (ML) techniques as powerful tools for addressing diverse clinical challenges in cancer detection and diagnosis [4].

Mammography has served as the gold standard for breast cancer screening for several decades, leading to a 42% reduction in breast cancer mortality since 1989 [4]. Screen-film mammography (SFM) and its digital counterpart, full-field digital mammography (FFDM), are the most widely employed diagnostic modalities [6]. However, these techniques exhibit several significant limitations that compromise their clinical efficacy.

Research demonstrates that mammography yields a substantial number of false positives, with rates ranging from 4% to 34% [6]. A longitudinal study revealed that women undergoing annual mammography examinations over 10 years experienced a cumulative false positive diagnosis rate of 49.1% [7]. Furthermore, mammography demonstrates reduced efficacy in patients with dense breast tissue, where the sensitivity of detection is significantly compromised [4], [6]. The invasive nature of the procedure, exposure to ionizing radiation, and associated patient discomfort represent additional limitations that have motivated the exploration of alternative diagnostic approaches [6].

Complementary diagnostic techniques include ultrasound imaging, magnetic resonance imaging (MRI), and biopsy procedures [4]. While MRI and computed tomography (CT) offer valuable diagnostic information, they exhibit low sensitivity for sub-centimeter lesions due to their limited spatial resolution [8]. Biopsy procedures, though definitive, are invasive and associated with patient discomfort and potential complications [4]. These limitations underscore the critical need for non-invasive, cost-effective, and highly accurate alternative screening methodologies.

Infrared thermography has emerged as a promising non-invasive alternative for breast cancer detection, based on the fundamental principle that metabolic activity and vascular circulation in precancerous tissues and areas surrounding developing breast cancer are substantially elevated compared to normal tissues [4], [6]. This increased metabolic activity results from the proliferation of cancerous cells and associated angiogenesis, leading to measurable temperature variations on the breast surface [5].

The technique utilizes infrared cameras capable of detecting radiation in the wavelength range of 2-20 μm, with modern systems achieving temperature sensitivities as low as 0.05°C [5], [9]. The United States Food and Drug Administration (FDA) approved thermography as a supplementary technique to mammography for breast cancer detection in 1982 [6]. Digital infrared thermal imaging (DITI) offers several distinct advantages: it requires no physical contact with the patient, avoids exposure to ionizing radiation, and can potentially detect thermal abnormalities 8-10 years before mammography can identify structural masses [6].

Several geometric models have been developed to correlate surface temperature distributions with tumor characteristics. Early rectangular domain models provided initial insights into predictive relationships between surface temperature and tumor size and location, though they failed to accurately represent the actual breast geometry [9]. Subsequently, hemispherical computational domains with concentric and non-concentric layers were introduced, demonstrating improved agreement with experimental data [7], [9].

The Penne bioheat equation serves as the fundamental mathematical framework for modeling heat transfer in breast tissue:

$$\rho c \frac{\partial T}{\partial t} = \nabla \cdot k \nabla T - w_b p_b c_b (T - T_b) + Q_m$$

where ρ, c, and k represent tissue density, specific heat, and thermal conductivity, respectively; w_b denotes blood perfusion rate; and Q_m represents metabolic heat generation [7]. This equation enables inverse modeling approaches to estimate tumor depth, diameter, and metabolic heat generation from surface temperature distributions [7], [9].

Despite its promise, thermographic imaging faces significant challenges. Studies have reported high false-positive rates, with one investigation of 126 breasts (63 patients) concluding that thermal diagnosis alone was insufficient for the initial evaluation of symptomatic patients [10]. The technique requires strict protocol adherence regarding room temperature maintenance (18-22°C), patient preparation, and image acquisition timing to ensure reliable results [7], [9]. Furthermore, the interpretation of thermal images requires sophisticated computational analysis, as manual interpretation is prone to subjective errors and inter-observer variability [4], [5].

Classical artificial intelligence methods including Support Vector Machines (SVM), Random Forest (RF), k-Nearest Neighbors (k-NN), Logistic Regression, Naïve Bayes, and Decision Trees, have demonstrated notable success in breast cancer classification tasks. Comparative analyses using the Wisconsin Breast Cancer dataset revealed that Logistic Regression achieved the highest classification accuracy among tested models, primarily due to its computational efficiency and ease of training [4].

Advanced ensemble learning algorithms such as Gradient Boosted Trees and eXtreme Gradient Boosting (XGBoost) have been effectively employed to predict metastasis in breast cancer and survival outcomes, achieving accuracies exceeding 96% [11]. Research utilizing

Gabor filters with different scales and directions achieved an area under the ROC curve of 0.98, while hybrid features based on statistical measures and local binary patterns achieved accuracy rates of 98.63% with SVM classifiers [12].

Convolutional neural networks (CNNs) have demonstrated exceptional capabilities in addressing complex challenges associated with medical image classification, including breast cancer detection from various imaging modalities [4], [5], [13]. CNNs offer the advantage of automated feature extraction through hierarchical learning, eliminating the need for manual feature engineering required by traditional ML approaches [5].

Research demonstrates that CNN-based models can effectively classify breast cancer as invasive or non-invasive from histopathological images [5]. Transfer learning approaches utilizing pre-trained architectures such as Inception V3, ResNet50, DenseNet121, and Vision Transformers (ViT) have shown recognition rates exceeding 97% [5], [14]. These models leverage knowledge acquired from large-scale image datasets and fine-tune final classification layers for specific breast cancer detection tasks [5].

Recent research has explored hybrid methodologies combining multiple algorithmic approaches. Studies have investigated the integration of Artificial Neural Networks (ANNs) with genetic algorithms and computer simulations to relate skin surface temperature to tumor depth, diameter, and heat generation [9]. The stacked-based ensemble learning framework (SELF) integrating Random Forest, Extra Tree, AdaBoost, k-NN, and Gradient Boosting classifiers with logistic regression as the final estimator demonstrated strong classification capabilities with accuracy exceeding 99% [4].

A critical challenge in deep learning model development is the optimization of hyperparameters, which significantly impacts model performance and generalization capability. Particle Swarm Optimization (PSO) has emerged as a prominent metaheuristic optimization technique for hyperparameter tuning due to its simplicity and effectiveness in navigating complex, high-dimensional search spaces [4].

Traditional PSO suffers from potential entrapment in local minima. Enhanced Particle Swarm Optimization (EPSO) addresses this limitation by incorporating adaptive velocity adjustments and enhanced inertia weight strategies. Research demonstrates that EPSO-optimized CNN models achieve superior performance compared to traditional grid search or random search approaches, with classification accuracies reaching 98.8%. The optimization of parameters, including learning rate, batch size, dropout rate, number of layers, convolutional kernel size, and pooling kernel size, directly contributes to improved model robustness [4].

Alternative optimization approaches include Artificial Bee Colony (ABC) optimization, which has demonstrated effectiveness in colorectal cancer polyp detection by enhancing accuracy and real-time performance [14]. Bayesian optimization and genetic algorithms have also been investigated for fine-tuning deep learning models, showing improved model robustness crucial for medical decision support systems. The Dragonfly Algorithm for feature selection combined with Grey Wolf Optimization for ANN parameter tuning has shown

promise, though more advanced classification techniques could potentially yield higher accuracy [4].

Edge detection is crucial in breast cancer tumor identification as it highlights boundaries of abnormal growth, enabling precise localization and measurement of tumors. Traditional edge detection techniques, including Sobel, Canny, and Laplacian of Gaussian methods, have been widely employed, though they demonstrate sensitivity to noise [4][13].

Fuzzy logic-based approaches have gained attention due to their robust noise-handling capabilities. Type-2 fuzzy logic systems, particularly those implementing Mamdani fuzzy inference, demonstrate superior performance in identifying weak edges in noisy environments [4], [16]. Research comparing Canny edge detection with Type-2 fuzzy edge detection on thermographic breast images revealed that fuzzy approaches achieve recognition rates of 98.8% compared to 96.6% for Canny-based methods [4][13][14].

Contrast-Limited Adaptive Histogram Equalization (CLAHE) has emerged as an effective technique for enhancing thermographic image quality [4]. PSO-based optimization of CLAHE enhancement parameters, incorporating Local Contrast Modification (LCM), significantly outperforms conventional enhancement techniques in producing superior-quality mammographic images [4][14].

Median filtering is commonly employed for noise suppression in medical imaging applications. The integration of these preprocessing techniques—Type-2 fuzzy edge detection, CLAHE contrast enhancement, and median filtering—creates a comprehensive image processing pipeline that substantially improves feature extraction quality and subsequent classification accuracy [4][13][16].

Independent Component Analysis (ICA) represents a subspace projection technique that has demonstrated effectiveness in tumor area segmentation from thermographic images [6]. The ICA-based analysis method comprises three phases: separation of chrominance and luminance components, extraction of image-independent components, and post-processing for tumor area segmentation [6]. This approach reveals features imperceptible in original images that are associated with high-risk tumor regions, due to the strong relationship between body temperature and tissue abnormalities [6][17].

Dataset imbalance and limited sample availability represent significant challenges in training robust deep learning models for medical image analysis. Generative Adversarial Networks (GANs) have emerged as powerful tools for synthetic data generation, comprising a Generator (G) and Discriminator (D) engaged in adversarial training [4].

The loss functions for the Generator and Discriminator are defined as:

$$L_G = E_{z \sim p_g}[log(1 - D(G(z)))]$$

$$L_D = -E_{y\sim p_r}[log(D(y))] \; - E_{y\sim p_g}[log(D(z))]$$

Where P_r and P_g represent real and generated data distributions, respectively [4].

Traditional GANs suffer from training instability due to gradient vanishing when the Discriminator accurately identifies generated samples. Wasserstein GAN with Gradient Penalty (WGAN-GP) addresses this limitation by utilizing Wasserstein distance to measure distribution similarity, incorporating a gradient penalty term in the Discriminator loss function [4]:

$$L_D = E_{\bar{y}\sim p_g}[f(\bar{y})] - E_{\bar{y}\sim p_r}[f(y)] + \lambda E_{\hat{y}\sim p_{\hat{y}}}[(||\nabla_y f(\bar{y})||_2 - 1)]^2$$

Conditional GAN (CGAN) enables conditional sample generation, allowing researchers to generate samples with specific characteristics. Research demonstrates that datasets augmented using WGAN-GP achieve superior classification performance compared to those generated by standard GAN, Auxiliary GAN, or CGAN architectures, with recognition rates reaching 98.8% [4].

Near-infrared fluorescence (NIRF) imaging has demonstrated significant potential as an intraoperative imaging modality for cancer detection [8], [17]. Indocyanine Green (ICG), a hydrophilic tricarbocyanine dye with a molecular weight of 776 Da, becomes fluorescent at specific wavelengths (820 nm) in the NIR spectrum and has been widely adopted for sentinel lymph node (SLN) detection [17].

The IR780 phospholipid micelle represents another promising agent capable of crossing natural tissue barriers and specifically localizing to tumor cells, producing strong NIRF signals suitable for precise tumor localization. Unlike computed tomography and MRI, which have low sensitivity for sub-centimeter lesions, NIRF imaging enables surgeons to identify small superficial tumors with high sensitivity and positive predictive values reaching 100% and 70.3%, respectively [8].

NIRF imaging using ICG has proven feasible and safe for intraoperative SLN detection, allowing real-time observation with high detection rates and low false-negative rates [17]. Systems such as the HyperEye Medical System (HEMS) enable simultaneous detection of NIR rays under room light, providing color imaging with significant benefits for surgical navigation [17]. Laparoscopic ultrasound paired with NIRF imaging achieves superior performance in detecting perioperative tumors compared to conventional imaging modalities alone [8].

Recent comparative studies demonstrate the superior performance of optimized CNN architectures for thermographic breast cancer detection. Research utilizing Enhanced PSO-CNN achieved recognition rates of 98.8%, significantly outperforming conventional PSO-CNN (96.5%), IntelliSwAS-CNN (93.5%), MBO-CNN (92.6%), BO-CNN (88.6%),

GA-CNN (88.0%), SVM with polynomial kernel (85.5%), and SVM with RBF kernel (88.0%) [4].

The integration of WGAN-GP for data augmentation with EPSO-optimized CNN architectures demonstrates the highest classification accuracy across 11 different breast cancer disease stages. K-fold cross-validation (k=15) ensures robust performance estimation with low variance, providing reliable measures of model generalization capability [4], [5].

Pre-trained models, including Inception V3, ResNet50, DenseNet121, and Vision Transformer,s have been successfully adapted for breast cancer classification tasks [5], [14]. A study utilizing the InceptionV3 architecture with transfer learning achieved 98.8% recognition rate when combined with LinearSVC for uncertain predictions (confidence between 0.5 and 0.6) [5]. The model demonstrated precision of 0.97, recall of 0.98, and F1-score of 0.975, with significantly reduced computation time compared to other state-of-the-art methods [14].

Meta-learning techniques have been applied to address the challenge of limited labeled data in breast cancer imaging. Few-shot learning methods enable model training with minimal data samples, achieving competitive performance in classifying ultrasound breast cancer images. This approach is particularly valuable in clinical settings where acquiring large labeled datasets is challenging due to privacy concerns, annotation costs, and data scarcity [18].

Genetic predisposition plays a significant role in breast cancer development, with BRCA1 and BRCA2 genes identified as major contributors in genetic testing for patients with suggestive family histories. Confirmation of genetic predisposition enables implementation of risk reduction strategies and informs treatment decisions [19]. Recent studies demonstrate that poly (ADP-ribose) polymerase inhibitors (PARPs) may be particularly useful in treating tumors harboring BRCA1/2 mutations [19].

Computer-based breast cancer modeling approaches have been developed to map features and phenotypes between mammographic abnormalities and their histopathological representation, incorporating biological aspects into diagnostic frameworks [13]. This multimodal integration of genetic, molecular, and imaging data represents a promising direction for comprehensive breast cancer risk assessment and early detection [13], [19].

The economic burden of breast cancer is substantial, with medical expenses and lost income estimated at 245 million USD over the lifetime of a cohort in one study [20]. Medical costs account for approximately 80% of the economic burden, while loss of income and caregiver opportunity costs represent 15% and 5%, respectively [20]. In Poland, productivity loss related to breast cancer amounted to 583.7-699.7 million EUR between 2010 and 2014, representing 0.162-0.171% of GDP [21].

Global oncology costs are projected to exceed $150 billion by 2020, with annual growth rates between 7.5% and 10.5% [22]. Standard chemotherapy costs approximately €200, while

biological treatments suitable for one-fifth of patients cost around €30,000 [22]. Emerging gene and epigenetic therapies are expected to be even more expensive, emphasizing the critical need for cost-effective early detection methods [22].

Despite technological advances, several barriers impede the clinical adoption of ML-based thermographic screening systems. These include: lack of standardized protocols for image acquisition and interpretation, insufficient validation on large-scale diverse populations, concerns regarding interpretability of deep learning models ("black-box" problem), regulatory approval requirements, and integration challenges with existing clinical workflows [5].

The shortage of qualified radiologists and specialized medical professionals has created urgent demand for computer-aided diagnostic (CAD) systems that can analyze and interpret thermal images using sophisticated algorithms [6]. However, current systems must demonstrate clinical utility through rigorous validation studies and receive regulatory approval before widespread deployment [6], [10].

Current research predominantly focuses on single imaging modalities. Future investigations should explore multimodal approaches combining thermographic imaging with mammography, ultrasound, MRI, and molecular imaging to leverage the unique strengths of each technique [4], [5]. Such integration could significantly improve diagnostic accuracy and provide complementary information for comprehensive breast cancer assessment.

The black-box nature of deep learning models limits their clinical acceptance and trustworthiness [5]. Integration of explainable AI (XAI) techniques such as Grad-CAM, SHAP values, or attention mechanisms could provide clinicians with insights into model decision-making processes, fostering greater trust and facilitating clinical validation. Research on attention-based methods demonstrates improved feature representation and interpretability in skin cancer classification, suggesting similar benefits for breast cancer detection [23].

Optimization of ML models for real-time performance in clinical environments through model compression, quantization, or edge computing deployment represents a critical area for future research [5]. Achieving faster inference without sacrificing accuracy would enable integration of these systems into routine clinical workflows and point-of-care screening programs.

Expanding training datasets to include larger and more diverse populations spanning various breast cancer stages, demographic variations, geographic diversity, and imaging protocols would significantly enhance model generalizability and robustness, [5]. Longitudinal studies monitoring system performance over time in real-world clinical settings would provide valuable evidence regarding reliability and clinical impact [4].

Future work should extend current supervised learning approaches to incorporate semi-supervised and unsupervised learning methodologies. These techniques would enable

models to leverage both labeled and unlabeled data more effectively, addressing the challenge of limited annotated medical imaging datasets while discovering novel patterns and structures in thermographic data [4].

The convergence of infrared thermography with advanced machine learning techniques represents a promising paradigm for non-invasive, early-stage breast cancer screening. Recent developments in deep learning architectures, particularly CNN-based models enhanced with sophisticated optimization algorithms such as EPSO, have demonstrated remarkable classification accuracies exceeding 98%. The integration of data augmentation strategies using WGAN-GP, advanced image preprocessing techniques including Type-2 fuzzy edge detection and CLAHE contrast enhancement, and ensemble classification approaches has substantially improved diagnostic performance.

However, significant challenges remain regarding clinical validation, standardization of protocols, interpretability of AI models, and integration with existing healthcare workflows. Addressing these challenges through multimodal integration, explainable AI techniques, real-time optimization, and expanded diverse datasets will be essential for translating these technological advances into clinical practice. The economic burden of breast cancer, coupled with limitations of conventional screening methods, provides strong motivation for continued research and development of ML-based thermographic screening systems. Future investigations should focus on longitudinal clinical validation studies, regulatory approval pathways, and seamless integration with existing breast cancer screening programs to realize the full potential of these innovative technologies in reducing breast cancer mortality worldwide.

1.1.3 Literature Gap

Although substantial progress has been made in AI-assisted thermography for breast cancer screening, the existing body of literature reveals several critical gaps that limit real-world applicability, particularly in low-resource settings. While commercial and research platforms such as Thermalytix have demonstrated encouraging sensitivity and overall diagnostic performance, the majority of large-scale clinical validations have been conducted within a narrow set of geographic and demographic contexts. Most studies are concentrated in India and other limited clinical environments, with relatively homogeneous patient populations and controlled acquisition conditions. Consequently, there is insufficient empirical evidence regarding the generalizability of these systems to regions such as Bangladesh, where differences in climate, physiology, healthcare access, and socioeconomic conditions may significantly influence screening performance.

A second major gap concerns diagnostic specificity and false-positive management. Although high sensitivity is consistently reported across studies, specificity varies considerably depending on population characteristics, acquisition protocols, and model design. Few works systematically address population-specific calibration, threshold optimization, or false-positive reduction strategies that are essential for large-scale screening programs. In resource-constrained healthcare systems, excessive false positives can lead to unnecessary

referrals, increased patient anxiety, and inefficient use of limited diagnostic resources. The lack of standardized approaches to managing this trade-off between sensitivity and specificity limits the scalability of AI-assisted thermographic screening.

Furthermore, most existing studies emphasize algorithmic accuracy in isolation, often evaluated on curated or retrospective datasets, with limited consideration of deployment constraints. There is a notable lack of end-to-end system-level research that integrates AI models with hardware selection, power management, real-time inference, and user interfaces suitable for non-specialist healthcare workers. Many proposed solutions rely on centralized or cloud-based computing infrastructures, which are impractical for community clinics, mobile screening units, or rural settings with unreliable connectivity. The absence of lightweight, edge-deployable implementations such as systems based on low-cost embedded platforms creates a significant gap between laboratory-level performance and practical field deployment.

Another limitation in the literature is the restricted scope of clinical populations included in validation studies. Several investigations exclude individuals with comorbid conditions, inflammatory diseases, prior cancer history, pregnancy, or fever, despite the likelihood that such individuals may present in real-world screening scenarios. This exclusion limits understanding of model robustness and generalization under realistic operating conditions, where physiological variability and confounding thermal patterns are common. The lack of inclusive evaluation frameworks raises concerns regarding reliability and clinical trust when these systems are deployed beyond controlled research settings.

Ethical, regulatory, and governance considerations represent an additional underexplored dimension. While AI-assisted screening systems inherently interact with sensitive health data, many studies provide only superficial treatment of informed consent procedures, data privacy, algorithmic transparency, and the distinction between screening support and diagnostic authority. These factors are critical for clinical adoption, particularly in regions with evolving regulatory frameworks and limited oversight capacity. The absence of explicit ethical integration into system design poses risks related to misuse, misinterpretation, and loss of stakeholder trust.

Finally, despite the demonstrated effectiveness of advanced deep learning approaches—including Mask R-CNN, multimodal convolutional neural networks, and self-supervised learning pipelines—there is limited research focused on developing localized, adaptive models trained on region-specific thermal datasets. Most existing models are static and trained on externally sourced data, without mechanisms for continuous learning or population-specific adaptation. The absence of Bangladesh-centric thermal imaging datasets and adaptive learning strategies represents a substantial gap in the development of culturally, biologically, and environmentally relevant screening tools.

In summary, the current literature demonstrates strong technical potential for AI-assisted thermography but falls short in addressing generalizability, deployment feasibility, system integration, ethical implementation, and localization. These gaps collectively highlight the

need for a system-level engineering approach that moves beyond algorithmic performance to deliver an affordable, portable, edge-deployable, and ethically grounded screening solution tailored to the Bangladeshi healthcare context. Addressing these deficiencies forms the central motivation for the proposed work.

1.1.4 Relevance to current and future Industry

The rapid integration of artificial intelligence (AI) into medical imaging and diagnostics has significantly reshaped the global healthcare technology industry, particularly in the domain of cancer screening and early detection. Within this evolving landscape, AI-assisted thermography has emerged as a viable complementary screening modality alongside established imaging techniques such as mammography and ultrasonography. Rather than competing directly with diagnostic imaging, AI-integrated thermographic systems are increasingly positioned as front-line screening and triage tools, especially for large-scale population screening and resource-constrained environments.

One of the most notable commercial implementations in this space is Thermalytix, developed by NIRAMAI, which represents a mature example of AI-powered thermal imaging applied to breast cancer screening. In a large-scale real-world evaluation conducted in Punjab, India, the system screened 15,069 women and achieved a recall rate of only 3.1%, while successfully identifying 27 confirmed breast cancer cases [24]. These results demonstrate the feasibility of deploying AI-assisted thermography at population scale, achieving meaningful cancer detection rates while minimizing unnecessary referrals. Importantly, the screening was performed without radiation exposure and without requiring specialized radiologists, underscoring its relevance for decentralized healthcare delivery.

Beyond standalone platforms, comparable innovations have emerged in the form of smartphone-integrated thermal AI systems and portable thermal screening devices. These solutions leverage compact infrared sensors coupled with on-device or edge-based AI inference, enabling non-specialist healthcare workers to conduct screening in community clinics, mobile health units, and remote settings [25]. Such developments reflect a broader industry trend toward task-shifting and decentralization, where advanced diagnostic support is brought closer to patients rather than confined to tertiary hospitals.

From a market perspective, the relevance of AI-assisted breast cancer screening is reinforced by strong growth projections in the global diagnostics and digital health sectors. The global breast cancer diagnostics market was valued at approximately USD 5.86 billion in 2025 and is projected to reach USD 11.36 billion by 2033, corresponding to a compound annual growth rate (CAGR) of approximately 8.8% [26]. This growth is driven by rising disease prevalence, increased emphasis on early detection, and the incorporation of AI technologies that enhance diagnostic accuracy and workflow efficiency. Within this market, non-invasive and AI-enabled screening tools represent a rapidly expanding subsegment, particularly in emerging economies where conventional infrastructure remains limited.

In low- and middle-income countries (LMICs), the relevance of AI-thermography is particularly pronounced. Delayed diagnosis remains a major contributor to elevated breast cancer mortality in these regions, largely due to inadequate screening coverage and limited access to diagnostic imaging facilities. AI-assisted thermographic systems offer a cost-effective alternative that can extend screening coverage without imposing substantial infrastructure or workforce requirements. Recent studies have demonstrated that lightweight convolutional neural network (CNN) architectures optimized for thermal image analysis can achieve classification accuracies as high as 98.88%, while maintaining low computational complexity suitable for edge-device deployment [27]. These characteristics align closely with the operational realities of LMIC healthcare systems.

Industry momentum is further evident in growing collaborations between medical device manufacturers, AI startups, academic institutions, and healthcare providers. Many of these partnerships focus on multimodal AI integration, combining thermal imaging with other data sources such as clinical history, ultrasound, or molecular biomarkers to enhance screening reliability and precision diagnostics [28]. This trend reflects a broader shift within the medical technology industry toward systems-based solutions rather than isolated algorithms, emphasizing interoperability, scalability, and clinical workflow integration.

Looking toward the future, AI's role in non-invasive cancer screening is expected to expand substantially as advances in machine learning architectures, computing hardware, and data availability continue to accelerate. Projections indicate that the global AI in healthcare market may exceed USD 110.61 billion by 2030, driven by increasing adoption of deep learning, predictive analytics, and multimodal data fusion [29]. Within oncology, AI-enabled screening tools are anticipated to play a central role in early risk stratification, personalized screening strategies, and decision support across the care continuum.

Emerging research directions suggest that future screening systems may integrate thermal imaging with multimodal AI frameworks, incorporating clinical metadata, genomic information, laboratory results, and imaging data within unified predictive models. Large language models (LLMs) and foundation models may further enhance interpretability and clinical usability by translating AI outputs into human-readable explanations and contextual risk assessments [30]. Such developments are expected to improve clinician trust and facilitate broader adoption of AI-assisted screening technologies.

Evidence from related domains supports the potential impact of AI integration on screening performance. Prospective studies on AI-supported mammography have demonstrated increases in cancer detection rates of up to 21.6%, while maintaining or improving radiologist workflow efficiency [31], [32]. Although thermography serves a different clinical role, these findings highlight the broader industry trend toward AI augmentation rather than replacement of existing diagnostic practices. For thermographic screening, similar gains are anticipated through improved pattern recognition, population-specific calibration, and multimodal fusion.

For resource-limited contexts, future industry development is likely to prioritize lightweight, energy-efficient AI models capable of operating on embedded platforms with minimal power

consumption. CNN architectures incorporating spatial attention mechanisms and efficient feature extraction have already demonstrated strong performance under constrained computational budgets [27]. Such designs enable real-time inference on edge devices, reducing reliance on cloud connectivity and addressing concerns related to data privacy and latency. These capabilities are particularly relevant for community-level screening initiatives and mobile health deployments.

Regulatory evolution represents another key factor shaping the future relevance of AI-assisted screening technologies. Emerging regulatory frameworks, including the European Union AI Act and updated guidelines from the United States Food and Drug Administration (FDA) on software as a medical device (SaMD), emphasize transparency, explainability, bias mitigation, and post-deployment monitoring [33], [34]. Compliance with these standards is expected to become a prerequisite for commercial adoption and large-scale deployment. Consequently, industry solutions that integrate ethical safeguards, explainable AI mechanisms, and robust validation protocols will be better positioned for regulatory approval and clinical acceptance.

Within this regulatory context, screening tools that clearly define their role as decision-support or risk-assessment systems—rather than diagnostic authorities—are likely to face fewer adoption barriers. The distinction between screening and diagnosis is particularly important for AI-assisted thermography, as it aligns with regulatory expectations and mitigates risks associated with over-reliance on automated outputs. Industry solutions that incorporate clear referral pathways and clinician-in-the-loop designs are therefore expected to gain greater traction.

From a global health perspective, AI-assisted non-invasive screening technologies align closely with international development priorities, including the United Nations Sustainable Development Goal 3 (SDG 3), which emphasizes ensuring healthy lives and promoting well-being for all at all ages. By enabling early risk identification, reducing dependence on centralized infrastructure, and expanding screening access in underserved populations, AI-thermography systems contribute directly to reducing health disparities and improving equity in cancer care.

In this broader industrial and technological context, the relevance of the present project becomes evident. The proposed AI-assisted thermography system aligns with current industry trends toward decentralized, affordable, and ethically deployable screening solutions. By emphasizing edge-based deployment, system-level integration, and adaptability to low-resource settings, the project addresses both immediate healthcare needs and long-term industry trajectories. Rather than focusing solely on algorithmic performance, the system is designed with practical deployment, scalability, and regulatory alignment in mind.

Ultimately, this work positions itself within an ongoing industry transition toward equitable, AI-augmented diagnostics. As healthcare systems worldwide increasingly adopt AI-driven tools to enhance early detection and preventive care, solutions that combine technical rigor with real-world deployability will play a critical role. By addressing unmet needs in breast

cancer screening for resource-constrained environments, this project contributes to a future in which advanced diagnostic support is accessible beyond traditional hospital settings, supporting timely intervention and improved survival outcomes.

1.2 Objectives, Requirements, Specification and constant

1.2.1. Objectives

1. To design a system that can help detect cancer at an early stage.
2. Reducing the screening costs compared to other traditional methods.
3. To create a solution that does not require invasive testing, which causes distress in patients' conditions by increasing the risk of infection.
4. To focus on common cancers like breast cancer, which are often diagnosed too late.
5. To make the system affordable and easy to use, especially in rural or low-resource areas.
6. To support early detection so that people can get treatment sooner and have better chances of recovery.
7. To use modern technology like AI to make the detection process faster and smarter.
8. To help doctors and healthcare workers with a tool that can screen patients quickly.
9. Create a simple user guide so healthcare workers and patients can understand how the system works.
10. Ensure the system works in different environments, including hospitals, clinics, and mobile health camps.

1.2.2 Functional and Nonfunctional Requirements

1.2.2.1 Functional Requirements

- Input data (e.g., imaging, VOCs, audio, vitals) that is relevant for cancer screening must be collected.
- Have to process collected data through a trained ML model.
- Have to provide a clear diagnostic signal or indicate the associated risk level.
- ML models must achieve ≥ 80% classification accuracy.
- Compact and lightweight, suitable for mobile or rural deployment.
- The system must have Portable battery support.
- Have to output a clear diagnostic signal or risk level.

- Have to be operable with minimal training.
- Results must be provided quickly to support rapid screening.

1.2.2.2 Non-Functional Requirements

- It shall be portable, affordable, and usable in rural, low-resource environments.
- It shall feature a user-friendly interface for healthcare workers and community use.
- Shall comply with ethical standards on patient privacy and data handling.
- Shall function reliably under varying environmental conditions.
- The total component cost should not exceed $1100.

1.2.3 Specifications

The suggested diagnostic system creates a non-invasive, AI-based approach for early-stage cancer detection by fusing thermography.

- To detect heat anomalies that are usually linked to cancerous activity, a thermal camera that has a resolution of at least 160×120 pixels and a thermal sensitivity of less than 0.1°C can record surface temperature variations across specific body regions.
- The Raspberry Pi 5 serves as the central processor for running a CNN processing model on collected data.
- Our AI-ML model subsequently processed the data gathered from the camera to identify the cancer.
- Python, OpenCV, and TensorFlow Lite are the software that enable real-time processing and control local encrypted data storage with an optional cloud synchronization feature.
- The system can be used in clinics, mobile screening units, and rural areas without sufficient medical facilities because it is reasonably priced at $1000 (৳122381.00).

1.2.4 Technical and Non-technical Considerations and Constraints in the Design Process

1.2.3.1 Technical Considerations & Constraints

- **Sensing accuracy:**
  Thermal camera resolution is limited to **≥160×120** and sensitivity is **<0.1 °C**, which constrains fine-grained anomaly detection.
- **Environmental sensitivity:**
  Thermal readings are affected by **ambient temperature**, **humidity**, **patient posture**, and **distance**, requiring strict capture protocols.
- **Data variability:**
  Thermal patterns vary across individuals due to **age**, **body composition**, **vascular differences**, and **climate**.

- **Model performance threshold:**
  ML models must maintain **≥80% classification accuracy**, balancing sensitivity and specificity to reduce false positives.

- **Edge computation limits:**
  Deployment on **Raspberry Pi 5** restricts model size, memory usage, and inference speed.
- **Real-time processing:**
  The system must process images and output results quickly for **rapid screening**, limiting computational complexity.
- **Dataset limitations:**
  Limited availability of **Bangladesh-specific thermal datasets** requires reliance on public datasets and localized retraining.
- **Explainability requirement:**
  AI decisions must be interpretable (e.g., heatmaps) to support clinical trust and review.
- **Power constraints:**
  Battery operation limits processing duration and requires energy-efficient hardware and software optimization.
- **System integration:**
  Ensuring reliable communication between the camera, processor, UI, and storage under portable conditions.

1.2.3.2 Non-Technical Considerations & Constraints

- **Cost ceiling:**
  Total system cost must remain **≤ $1100**, limiting hardware choices and scalability options.
- **Accessibility:**
  Design must be usable in **rural and low-resource settings** with minimal infrastructure.
- **Ease of use:**
  Healthcare workers with **minimal technical training** must be able to operate the system reliably.
- **Non-invasive requirement:**
  Screening must be **pain-free**, **radiation-free**, and psychologically comfortable for patients.
- **Ethical compliance:**
  Must follow **IRB guidelines**, informed consent, and ethical screening practices.
- **Data privacy & security:**
  Patient data must be **anonymized**, **encrypted**, and stored securely (GDPR-aligned).
- **Clinical scope limitation:**
  The system is a **screening support tool**, not a diagnostic replacement, requiring clear communication to users.

- **Population diversity:**
  Must perform across **urban and rural populations**, varying socioeconomic and climatic conditions.
- **Regulatory readiness:**
  Design must align with evolving standards for **AI-based medical devices**.
- **Adoption barriers:**
  Fear, lack of awareness, and trust in AI-based screening can affect real-world acceptance.

1.2.4 Applicable compliance, standards, and codes

Table- 1: Standard Codes and Description

Standard Code	Description	Relevance to Project
ISO 13485	Management system to ensure the quality of medical devices	Ensures the regulatory requirements for the efficacy and safety of the devices
IEC 62304	Software lifecycle processes for medical devices	Safe integration of AI/ML into the system
WHO Guidelines on using AI in healthcare	Using AI in medical diagnostics ethically	Following the ethical guidelines in using AI prioritizes the safety of the patients.
ISO 9001	An internationally recognized standard for quality management systems (QMS).	Ensuring the benchmarks in the manufacturing and testing of the devices.
Digital Security Act 2018	Laws on cybersecurity and data protection in Bangladesh	Ensure the privacy of the data collected from the volunteers for this project

1.3 Systematic Overview/summary of the proposed project

The proposed project presents the systematic design and development of a portable, non-invasive, and artificial-intelligence–assisted cancer screening system, with an initial focus on early-stage breast cancer detection. The system is conceived as a screening and triage support tool intended to operate in resource-constrained and decentralized healthcare environments, where access to conventional diagnostic infrastructure is limited. By integrating thermal imaging, machine learning–based analysis, and embedded edge computing within a unified framework, the project seeks to address the practical and technical limitations associated with existing screening modalities.

At a system level, the proposed solution is designed to overcome key barriers of traditional breast cancer screening approaches, including high cost, dependence on specialized clinical facilities, geographic inaccessibility, and limited scalability in rural and community-based settings. Rather than replacing established diagnostic procedures, the system is explicitly

positioned as a preliminary screening mechanism that supports early risk identification and timely referral. This distinction ensures alignment with ethical, clinical, and regulatory expectations while enhancing accessibility to early-stage screening.

The core sensing modality employed in the system is infrared thermography, which enables non-contact and radiation-free acquisition of surface temperature distributions of the breast. Thermal imaging captures physiological signatures associated with abnormal metabolic activity and vascularization, which are commonly linked to malignant tissue growth. To improve robustness and reduce sensitivity to acquisition artifacts, the system captures thermal images from multiple viewpoints, including frontal, left, and right orientations. This multi-view acquisition strategy enhances spatial coverage and allows the system to better account for anatomical asymmetry and positional variability during screening.

Following image acquisition, the thermal data undergoes a structured preprocessing pipeline designed to mitigate noise and environmental variability. Preprocessing steps include normalization, contrast enhancement, and artifact suppression, ensuring consistent input quality for downstream analysis. These steps are critical for maintaining reliability in real-world deployment scenarios, where ambient temperature, humidity, and patient posture may vary significantly. By standardizing the thermal inputs prior to analysis, the system reduces the influence of non-physiological factors on screening outcomes.

The analytical core of the proposed system is a convolutional neural network (CNN) trained to identify abnormal thermal patterns indicative of potential malignancy. The CNN architecture is selected and optimized to balance diagnostic performance with computational efficiency, enabling deployment on embedded hardware. Model training is initially conducted using publicly available thermal imaging datasets to establish baseline performance and generalizability. To enhance population-specific relevance, the system architecture supports the incorporation of locally acquired clinical data, allowing for future refinement and calibration tailored to the Bangladeshi population.

The use of machine learning enables automated, objective, and reproducible interpretation of thermographic data, addressing limitations associated with subjective visual assessment. The CNN learns discriminative features related to thermal asymmetry, localized hotspots, and spatial temperature gradients, which may not be readily apparent to human observers. The output of the model is a binary screening decision—classified as *Normal* or *Abnormal*—intended to guide healthcare practitioners in determining whether further diagnostic evaluation is warranted. Importantly, the system output is designed as a risk indication rather than a definitive diagnosis, preserving appropriate clinical boundaries.

To support real-time operation and independence from centralized infrastructure, the trained AI model is deployed on an embedded edge-computing platform based on the Raspberry Pi 5. This design choice enables on-device inference, eliminating reliance on cloud connectivity and reducing latency, data transmission requirements, and privacy risks. Edge deployment also enhances suitability for rural and mobile screening environments, where internet access may be unreliable or unavailable. The hardware platform is selected to balance processing

capability, power efficiency, and cost, ensuring that the overall system remains affordable and portable.

The system architecture incorporates user-centred design principles to facilitate ease of use by non-specialist healthcare workers. The screening workflow is designed to be intuitive, minimizing training requirements and operational complexity. Visual outputs and system prompts are structured to clearly communicate screening results and recommended next steps, supporting informed decision-making without overwhelming users with technical details. This emphasis on usability is essential for deployment in primary healthcare settings, community clinics, and outreach programs.

From an ethical and regulatory standpoint, the proposed framework is designed to support validation and oversight under Institutional Review Board (IRB) protocols. The system architecture accommodates informed consent procedures, anonymized data handling, and secure local storage, ensuring alignment with ethical guidelines for human-centered screening research. By maintaining transparency in system functionality and clearly defining the scope of use, the project addresses key concerns related to AI-driven healthcare technologies.

In addition to its immediate application in breast cancer screening, the proposed system is designed with scalability and extensibility in mind. The modular architecture allows for future expansion to other oncological indicators or non-invasive screening applications by adapting the sensing modality, data acquisition protocol, or machine learning model. This flexibility supports long-term relevance and potential translation beyond the initial use case, aligning with evolving industry and healthcare needs.

Overall, the proposed project represents a system-level engineering solution that integrates hardware design, artificial intelligence, and user-focused workflow development within a single, deployable platform. By emphasizing affordability, portability, and ethical deployment, the system aims to bridge the gap between advanced screening technologies and real-world healthcare constraints. The framework supports early risk identification, community-level screening initiatives, and future clinical validation, contributing to improved accessibility and equity in cancer screening for low-resource settings.

1.4 Conclusion

This chapter has established the motivation, context, and technical foundation for the proposed AI-assisted, non-invasive breast cancer screening system. By critically examining existing screening practices, emerging AI-based solutions, and their limitations within low-resource healthcare settings, the chapter has identified a clear and unresolved gap in early-stage cancer screening accessibility in Bangladesh. The proposed project directly addresses this gap by introducing a portable, low-cost, and ethically deployable screening framework designed to operate beyond conventional hospital environments.

The system leverages infrared thermography, machine learning–based pattern recognition, and embedded edge computing to provide a practical alternative to infrastructure-intensive screening modalities. By prioritizing affordability, portability, and non-invasive operation, the proposed solution aligns with the operational realities of rural clinics, community health programs, and decentralized healthcare delivery models. Importantly, the system is positioned as a screening and triage support tool rather than a diagnostic replacement, ensuring appropriate clinical use and regulatory alignment.

Through a system-level engineering approach, the project integrates hardware selection, data acquisition protocols, AI model development, and user-centred workflow design within a unified architecture. Attention to both technical and non-technical constraints including environmental variability, usability by non-specialist healthcare workers, ethical compliance, and data governance strengthens the feasibility of real-world deployment. The framework is designed to support validation under Institutional Review Board (IRB) oversight and provides a structured pathway for future clinical evaluation and refinement.

In summary, this project establishes a robust foundation for the development and assessment of AI-based, non-invasive screening technologies tailored to resource-constrained settings. By enabling early risk identification and facilitating timely referral, the proposed system has the potential to reduce diagnostic delays and support improved breast cancer outcomes. The chapter concludes by positioning the work as a scalable and adaptable screening framework that contributes to ongoing efforts to improve equity, accessibility, and effectiveness in cancer screening within Bangladesh and comparable low- and middle-income contexts.

Chapter 2: Project Design Approach [CO5, CO6]

2.1 Introduction

The development of an effective early-stage cancer screening system requires a systematic exploration of alternative design approaches before converging on a final solution. In complex biomedical engineering problems, particularly those involving artificial intelligence (AI) and healthcare applications, multiple design pathways may satisfy the primary functional objective yet differ substantially in performance, cost, safety, scalability, and suitability for real-world deployment. A structured design approach is therefore essential to ensure that the selected solution is not only technically feasible but also economically viable, ethically responsible, and aligned with the constraints of the target deployment environment.

Early-stage cancer screening presents a multidimensional design challenge. The system must achieve sufficient sensitivity to identify potential malignancies at an early phase, while maintaining acceptable specificity to avoid unnecessary referrals and patient anxiety. Simultaneously, the design must account for practical considerations such as portability, power consumption, ease of use, and compatibility with low-resource healthcare settings. These requirements often impose conflicting constraints, requiring trade-offs between diagnostic depth, system complexity, and cost.

In the context of low- and middle-income countries such as Bangladesh, these constraints are particularly pronounced. Healthcare infrastructure is unevenly distributed, with advanced diagnostic facilities concentrated in urban centers, while rural and community-level healthcare settings often lack access to sophisticated imaging equipment and trained specialists. As a result, a screening system optimized solely for clinical accuracy but requiring high-cost infrastructure may be impractical for large-scale deployment. Conversely, an overly simplified system may compromise reliability and clinical relevance.

To address these challenges, this chapter adopts a comparative design approach. Multiple candidate screening methodologies are identified, analyzed, and evaluated based on engineering, clinical, and deployment-oriented criteria. The objective of this analysis is to justify the selection of the final system architecture through transparent and systematic reasoning. By examining alternative design pathways, this chapter ensures that the chosen solution represents an optimal balance between technical performance, affordability, safety, and scalability.

The design approaches explored in this chapter are evaluated in terms of their sensing modality, AI integration strategy, operational requirements, deployment feasibility, and alignment with the project's stated objectives. This structured evaluation forms the basis for subsequent optimization, system integration, and validation stages presented in later chapters.

2.2 Identify multiple design approaches

Cancer detection and screening using artificial intelligence can be approached through a variety of sensing modalities and analytical frameworks. Advances in machine learning have enabled the extraction of clinically relevant patterns from diverse data sources, including medical images, physiological signals, biochemical markers, and multimodal combinations thereof. However, the suitability of each approach depends heavily on the intended application context, particularly when the goal is early-stage, non-invasive screening rather than definitive diagnosis.

In the proposed design project, two primary screening approaches were identified as potential candidates for addressing early, non-invasive cancer detection:

1. Thermography combined with breath analysis, and AI
2. Ultrasonography combined with AI

Both approaches leverage AI-based models to identify patterns associated with malignancy, yet they differ fundamentally in their sensing mechanisms, infrastructural requirements, operational complexity, and suitability for decentralized deployment.

The first approach focuses on physiological and metabolic signatures of cancer. Infrared thermography captures surface temperature variations related to abnormal blood flow and metabolic activity, while breath analysis targets volatile organic compounds (VOCs) produced by cancerous cells. Together, these modalities provide indirect yet potentially powerful indicators of early malignancy without requiring invasive procedures or exposure to ionizing radiation.

The second approach relies on conventional anatomical imaging techniques. Ultrasonography provides real-time visualization of soft tissue structures,. When combined with AI-based image analysis, these modalities can achieve high diagnostic accuracy but at the cost of increased infrastructure, operational complexity, and reduced portability.

The identification of these two approaches enables a comparative analysis that reflects a broader trade-off between physiological screening versus anatomical imaging, and between community-level screening versus hospital-based diagnostics. The following sections describe each approach in detail, laying the groundwork for subsequent evaluation and optimization.

2.3 Describe multiple design approaches

2.3.1 Approach 1: Thermography and Breath Analysis

The first proposed design approach integrates infrared thermography and breath analysis to enable non-invasive, AI-assisted early cancer screening. This approach is grounded in the

physiological and biochemical characteristics of cancer development, which manifest as measurable changes in body temperature distribution and metabolic byproducts.

Infrared thermography is a non-contact imaging technique that captures the natural thermal radiation emitted by the human body. In the context of cancer screening, thermography exploits the fact that malignant tumors often exhibit increased metabolic activity and angiogenesis. These processes result in elevated blood perfusion and localized heat generation, which may appear as asymmetrical or abnormal temperature patterns on the skin surface.

For breast cancer screening, thermography offers several advantages. It is radiation-free, painless, and does not require physical compression or contact, making it suitable for repeated screening and for asymptomatic individuals. Thermal cameras can capture temperature distributions across the breast surface from multiple viewpoints, enabling spatial analysis of thermal asymmetry and localized hotspots. AI models, particularly convolutional neural networks (CNNs), are then employed to analyze these thermograms and identify patterns associated with potential malignancy [35].

Thermography is particularly attractive for deployment in low-resource settings due to its portability and relatively low hardware cost compared to conventional imaging systems. However, raw thermal images are sensitive to environmental factors such as ambient temperature, humidity, patient posture, and acquisition distance. As a result, effective thermographic screening requires robust preprocessing and AI-based interpretation to distinguish physiological signals from environmental noise.

Breath analysis complements thermography by targeting biochemical signatures of cancer. Cancerous cells are known to alter cellular metabolism, producing distinctive volatile organic compounds (VOCs) that can be detected in exhaled breath. Compounds such as toluene, benzene, acetone, and other hydrocarbons have been associated with various malignancies, including lung, gastric, liver, and breast cancers [36].

Breath analysis typically employs gas sensors to measure VOC concentrations, generating time-series or spectral data that reflect metabolic activity. Machine learning models are then used to classify these patterns and distinguish between healthy and potentially cancerous states. When integrated with thermography, breath analysis provides an additional layer of physiological information, increasing the robustness of early screening by combining independent biomarkers.

Like thermography, breath analysis is non-invasive, radiation-free, and relatively low-cost. The sensing hardware can be miniaturized and integrated into portable devices, making it suitable for community-level screening. However, VOC detection is influenced by factors such as diet, smoking status, environmental exposure, and sensor drift, necessitating careful calibration and AI model training.

The combination of thermography and breath analysis offers a multimodal screening framework that leverages both thermal and biochemical indicators of cancer. By fusing data from these complementary modalities, AI models can improve screening sensitivity and reduce false positives. This integrated approach aligns well with the objectives of early-stage screening, where the goal is to identify individuals who may require further diagnostic evaluation rather than to provide definitive diagnosis.

From an engineering perspective, this approach emphasizes portability, affordability, and scalability. The absence of ionizing radiation and invasive procedures enhances patient acceptance, while the use of AI-driven interpretation reduces reliance on specialist expertise. However, achieving reliable performance requires careful system design, including standardized acquisition protocols, robust preprocessing pipelines, and well-trained machine learning models capable of handling real-world variability.

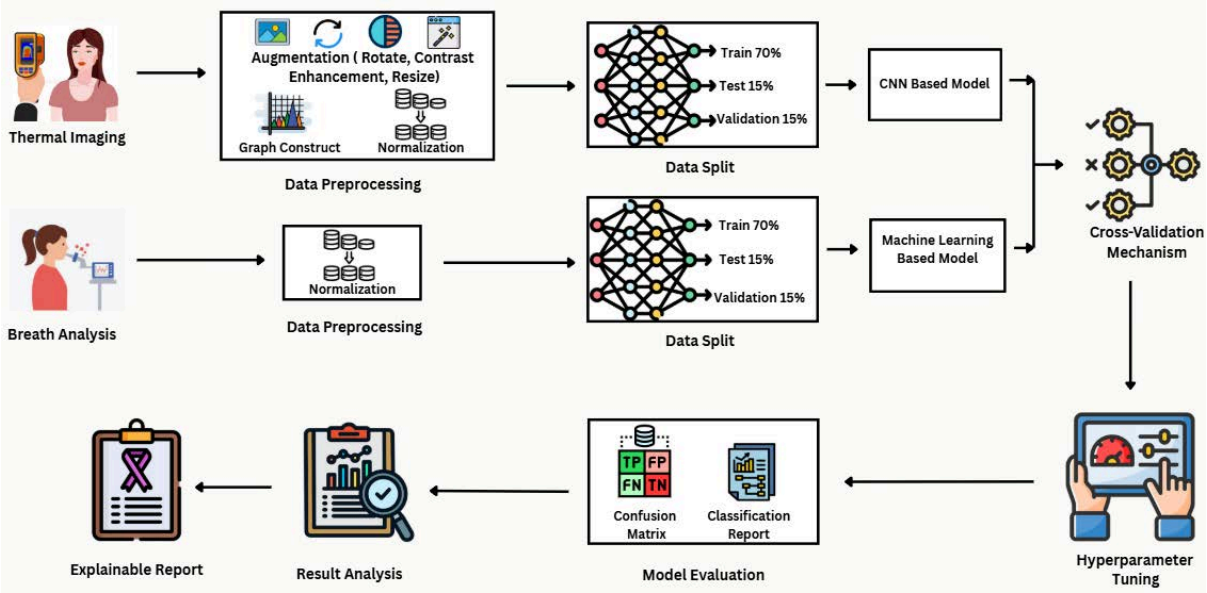

Figure 1: Workflow diagram of approach 1

2.3.1.1 Budget for Approach 1:

Table - 2 :Budget for thermography and breath analysis

Product Name	Price (USD)	Price (BDT)
TGS822	$26.00	৳3,159.00
TGS2620	$6.30	৳765.45
TGS2602	$7.32	৳889.38
MQ-135	$1.43	৳173.75
MQ-136	$22.95	৳2,788.43

MQ-138	$43.00	৳5,224.50
Thermal camera	$250.00	৳30,375.00
Raspberry Pi 4 (4GB)	$55.00	৳6,682.50
Custom 3D Printed Case + Hardware	$100.00	৳12,150.00
Display	$100.00	৳12,150.00
Total	**$612.00**	**৳74,358.00**

2.3.2 Approach 2: Ultrasonography

The second design approach explored in this project is based exclusively on ultrasonography, a well-established anatomical imaging modality widely used in clinical cancer detection and diagnosis. Unlike thermography and breath analysis, which rely on indirect physiological or biochemical signatures, ultrasonography enables direct visualization of internal soft tissue structures. When combined with artificial intelligence (AI)–based image analysis, ultrasonography can achieve high diagnostic accuracy and is routinely employed in hospital-based breast cancer screening and diagnostic workflows.

Ultrasonography is a non-ionizing imaging technique that utilizes high-frequency acoustic waves to generate real-time cross-sectional images of soft tissues. In breast cancer screening and diagnosis, ultrasound is commonly used as an adjunct modality, particularly in patients with dense breast tissue where other imaging techniques may exhibit reduced sensitivity. Ultrasound imaging allows clinicians to assess lesion morphology, size, shape, margins, orientation, and internal echogenicity, all of which are important indicators for differentiating benign from malignant tumors.

From a clinical perspective, ultrasonography offers several advantages. It is radiation-free, relatively safe for repeated use, and capable of providing real-time imaging, which makes it suitable for follow-up examinations and targeted evaluation of suspicious regions. Ultrasound is also widely accepted in clinical practice and is familiar to healthcare professionals, contributing to its credibility as a diagnostic tool. These characteristics make ultrasonography a strong candidate for cancer detection in controlled clinical environments.

However, traditional ultrasound-based screening suffers from significant limitations related to operator dependency. The quality and diagnostic utility of ultrasound images are heavily influenced by probe positioning, scanning angle, pressure applied during acquisition, and the experience of the operator. Variations in acquisition technique can lead to inconsistent image quality, reduced reproducibility, and inter-observer variability. These factors pose challenges for standardization, particularly in large-scale screening programs or decentralized healthcare settings where operator expertise may vary.

The integration of AI with ultrasonography has been proposed as a solution to mitigate these limitations. Deep learning models, particularly convolutional neural networks (CNNs), have demonstrated strong capability in automatically detecting and segmenting tumor regions in ultrasound images. By learning hierarchical feature representations from raw imaging data,

these models reduce reliance on subjective human interpretation and improve consistency across operators and clinical sites.

Ding et al. [37] introduced an Attention-Gated Multi-ResU-Net architecture for breast cancer detection using ultrasound images. This model incorporates attention mechanisms that enable the network to focus selectively on salient regions of interest, while multiresolution feature extraction captures both fine-grained texture details and global structural patterns. The proposed architecture demonstrated superior performance in identifying malignant lesions compared to conventional CNN-based segmentation models, highlighting the effectiveness of attention-based deep learning in ultrasound image analysis.

Similarly, MDA-Net employs dual attention mechanisms and multiscale fusion blocks to enhance lesion detection and reduce false-positive rates [38]. By integrating spatial and channel-wise attention with multiscale feature fusion, the network improves discrimination between malignant tumors and benign tissue structures. These architectural innovations allow AI systems to better handle the inherent noise and variability present in ultrasound images, improving robustness and diagnostic reliability.

AI-enhanced ultrasonography systems align well with modern trends in clinical decision support, where AI functions as an assistive tool rather than a replacement for clinicians. Automated lesion detection, segmentation, and risk scoring can support radiologists and clinicians by highlighting regions of interest, standardizing interpretation, and reducing cognitive workload. In controlled hospital environments, such systems have demonstrated strong performance and clinical utility

Despite these advances, ultrasound-based screening systems impose several engineering and deployment constraints that are particularly relevant when considering early-stage, community-level screening. Ultrasound machines require specialized probes, coupling gel, and controlled physical contact with the patient to ensure proper acoustic coupling and image quality. The need for trained operators remains a significant limitation, as improper acquisition can degrade both image quality and AI inference performance.

From a hardware perspective, ultrasound systems are relatively expensive compared to thermal cameras or gas sensors. Even portable ultrasound devices involve higher capital costs, greater power consumption, and more complex maintenance requirements. These factors reduce their affordability and scalability for widespread deployment in low-resource environments. Additionally, enforcing standardized acquisition protocols across decentralized screening sites can be challenging, which may compromise the reliability of AI-assisted interpretation.

Portability is another important consideration. While handheld and portable ultrasound devices exist, their effective use still requires stable power supply, trained operators, and appropriate infection control measures. These requirements limit flexibility for deployment in mobile screening units, rural clinics, or community outreach programs, where infrastructure and trained personnel may be limited.

From a systems engineering standpoint, integrating ultrasonography with AI for early-stage screening necessitates careful consideration of workflow design, user training, and quality control mechanisms. Unlike fully non-contact modalities, ultrasound requires direct interaction with the patient, increasing operational complexity and reducing throughput in mass screening scenarios. These factors make ultrasound-based screening more suitable for secondary or confirmatory evaluation rather than primary, large-scale screening.

In the context of this project's objectives—namely the development of an early-stage, non-invasive, low-cost screening system suitable for rural and resource-constrained environments—ultrasonography represents a clinically robust but infrastructure-dependent solution. While it offers superior anatomical detail and strong diagnostic accuracy in hospital settings, its reliance on specialized equipment, trained operators, and controlled acquisition conditions constrains its applicability for decentralized screening initiatives.

Nevertheless, evaluating ultrasonography as a candidate design approach is essential for establishing a meaningful baseline. Ultrasound represents the current standard for soft tissue imaging and provides a reference point against which alternative screening modalities can be compared. By analyzing both its strengths and limitations, this project gains valuable insight into the trade-offs between diagnostic depth and deployment feasibility.

These insights inform subsequent design decisions by clarifying why anatomically detailed imaging, while effective in clinical diagnosis, may not be optimal for early-stage, population-level screening in low-resource contexts. The evaluation of ultrasonography therefore plays a critical role in justifying the selection of alternative screening approaches that better balance accessibility, affordability, and scalability while still providing clinically meaningful risk assessment.

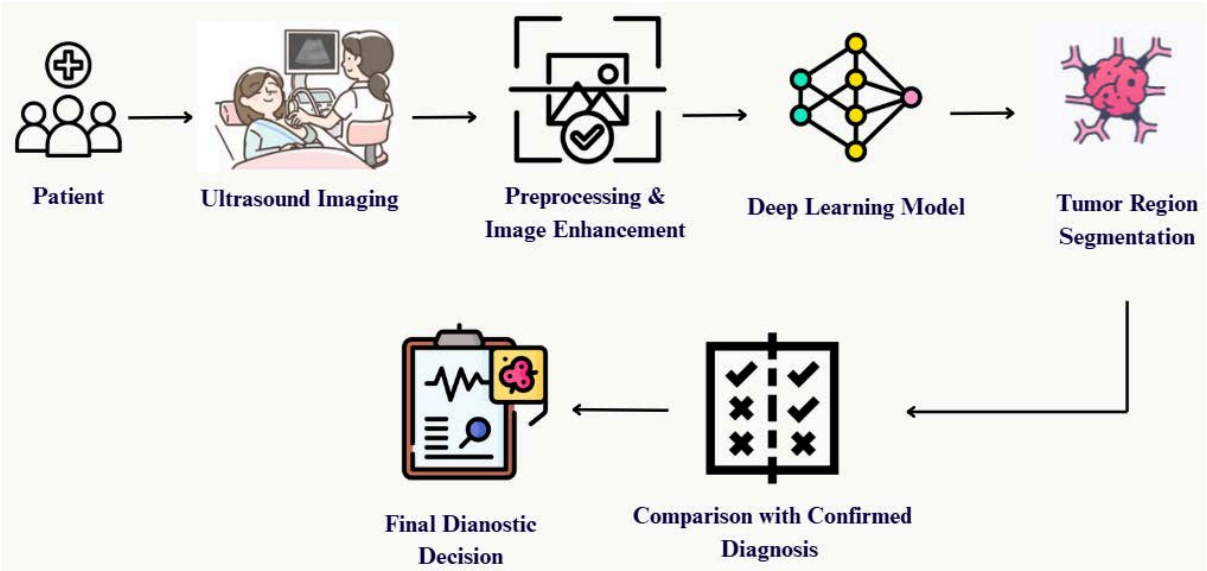

Figure 2 : Workflow diagram of approach 2

2.3.2.1 Budget for Approach 2:

Table - 3 : Budget for Ultrasonography Imaging

Product Name	Price (USD)	Price (BDT)
Ultrasonography machine	$1,152.26	৳140,000.00
Raspberry Pi 4 (4GB)	$55.00	৳6,682.50
Ultrasound Gel (consumables)	$10.00	৳1,215.00
Misc. Hardware (Cables, SD cards, Mounts, Spares)	$12.00	৳1,458.00
Total	$1,229.26	৳149,355.50

2.4 Analysis of multiple design approaches

Following the identification and detailed description of the two candidate design approaches namely (i) thermography combined with breath analysis and (ii) ultrasonography a qualitative engineering analysis was conducted to evaluate their suitability for early-stage cancer screening within the context of Bangladesh's healthcare infrastructure. The objective of this analysis is to assess each approach against practical design criteria that govern feasibility, scalability, and real-world deployment, rather than to optimize isolated performance metrics. Accordingly, the evaluation emphasizes invasiveness, safety, cost, portability, operational complexity, and long-term sustainability.

From a patient safety and interaction perspective, the thermography and breath analysis approach offers a fully non-invasive and contactless screening pathway. Infrared thermography captures surface temperature distributions without physical contact, while breath analysis relies on passive sampling of exhaled air. Neither modality involves ionizing radiation, mechanical compression, or invasive procedures. This design significantly enhances patient comfort and reduces health risks, particularly for repeated screening and asymptomatic populations. From an engineering standpoint, the absence of direct physical interaction simplifies system design, reduces sterilization requirements, and lowers operational risk.

In comparison, ultrasonography, although radiation-free, requires direct physical contact between the probe and the patient, as well as the use of coupling gel to ensure adequate acoustic transmission. Image quality is highly sensitive to probe positioning, contact pressure, and scanning technique. These factors introduce operator dependence and variability, which can compromise reproducibility across different screening locations. While ultrasonography is safe and clinically accepted, its reliance on contact-based acquisition imposes additional operational complexity relative to fully non-contact screening modalities.

Cost and resource requirements further differentiate the two approaches. Thermographic cameras and gas sensors used for breath analysis are comparatively low-cost and can be integrated with embedded computing platforms to form compact screening systems. These components typically require minimal consumables and maintenance, resulting in lower total cost of ownership. Such characteristics are particularly advantageous for large-scale

deployment in low-resource and rural settings, where healthcare budgets and infrastructure are constrained.

By contrast, ultrasonography systems involve higher hardware costs, including specialized probes, signal processing units, and display systems. Even portable ultrasound devices require greater initial investment, ongoing maintenance, and trained personnel for operation. These factors increase both capital and operational expenditure, limiting the feasibility of widespread deployment at the community level. From an engineering design perspective, higher system cost directly impacts scalability and sustainability in resource-constrained environments.

Portability and deployment flexibility represent another critical axis of comparison. Thermography and breath analysis systems can be designed as lightweight, battery-powered units that operate independently of fixed infrastructure. Their compatibility with edge-based computing enables real-time inference without reliance on cloud connectivity, supporting deployment in rural clinics, mobile screening units, and temporary outreach programs. This flexibility aligns well with decentralized healthcare delivery models.

Ultrasonography, although available in portable formats, remains less adaptable to highly decentralized deployment. Effective operation requires stable power supply, trained operators, controlled acquisition conditions, and consistent quality assurance. These requirements constrain portability and limit usability in mobile or minimally equipped settings. Additionally, the need for physical contact and longer acquisition times reduces throughput in mass screening scenarios.

Operational complexity and ease of use further highlight the contrast between the two approaches. Thermography and breath analysis can be supported by standardized acquisition protocols and AI-driven interpretation, enabling screening to be conducted by non-specialist healthcare workers with minimal training. Automated preprocessing and inference pipelines reduce user-dependent variability and support consistent screening outcomes across different sites.

In contrast, ultrasonography remains inherently operator-dependent despite AI assistance. While AI models can enhance interpretation, they cannot fully compensate for poor-quality image acquisition. This dependence on skilled operators introduces variability and increases training requirements, which pose challenges for scaling screening programs in underserved regions.

Scalability and long-term sustainability are central considerations for early-stage screening systems. Thermography and breath analysis support a scalable screening model that can be expanded geographically with relatively low marginal cost. The modular nature of the system allows incremental upgrades to sensors or AI models without significant infrastructural changes. This adaptability supports continuous improvement and long-term relevance.

Ultrasonography-based screening, on the other hand, scales less efficiently due to its dependence on specialized equipment and personnel. Expanding coverage requires proportional increases in hardware, training, and maintenance, which may not be feasible within limited healthcare budgets. These scalability constraints are particularly significant in countries with large rural populations and uneven healthcare access.

From a design trade-off perspective, the two approaches represent distinct philosophies. The thermography and breath analysis approach prioritizes accessibility, affordability, safety, and deployment feasibility, relying on AI-driven interpretation to extract clinically relevant information from indirect physiological signals. Ultrasonography prioritizes anatomical detail and diagnostic depth but at the cost of increased system complexity, reduced portability, and higher resource requirements.

In the context of this project's objectives early-stage, non-invasive, low-cost screening suitable for rural and resource-constrained environments the thermography and breath analysis approach demonstrates closer alignment with engineering and deployment requirements. Ultrasonography remains clinically valuable for targeted evaluation and confirmatory assessment in controlled healthcare settings, but its constraints limit its effectiveness as a primary screening tool at scale.

This qualitative analysis establishes a clear engineering rationale for prioritizing non-contact, AI-assisted screening modalities over contact-based anatomical imaging for early-stage screening. The insights derived from this comparison guide the selection and optimization of the final system design, ensuring that the proposed solution balances clinical relevance with practical deployability and long-term sustainability.

2.5 Conclusion

This chapter presented a structured evaluation of multiple design approaches for early-stage cancer screening, with particular emphasis on a comparative analysis between a non-contact, physiology-driven screening approach (thermography combined with breath analysis) and an anatomically focused, contact-based imaging approach based solely on ultrasonography. By systematically identifying, describing, and qualitatively analyzing these two alternatives, the chapter demonstrated how differing sensing modalities and system architectures influence feasibility, scalability, and real-world deployability.

The ultrasound-based approach was shown to offer strong anatomical visualization and high diagnostic reliability within controlled clinical environments. Its established role in breast cancer assessment and compatibility with AI-assisted interpretation make it a valuable tool for confirmatory evaluation and secondary screening. However, the analysis highlighted that ultrasonography remains highly dependent on trained operators, specialized hardware, controlled acquisition conditions, and sustained infrastructural support. These requirements introduce operational complexity, increase costs, and constrain portability, limiting its effectiveness as a primary screening solution in decentralized and resource-limited settings.

In contrast, the thermography and breath analysis approach demonstrated closer alignment with the project's design objectives of non-invasiveness, affordability, portability, and suitability for community-level deployment. The absence of physical contact, reliance on low-cost sensors, and compatibility with embedded edge-computing platforms enable scalable screening without dependence on specialized personnel or hospital-based infrastructure. While this approach requires robust AI-driven interpretation to compensate for indirect sensing and environmental variability, its engineering characteristics support wider screening coverage and repeated use in rural contexts.

Importantly, the comparative analysis emphasized that the selection of an early-stage screening system must extend beyond diagnostic accuracy alone. Factors such as patient safety, ease of deployment, operational simplicity, and long-term sustainability play a decisive role in determining real-world impact. Through the ultrasound-only comparison, this chapter established a defensible engineering rationale for prioritizing non-contact, AI-assisted screening modalities over contact-based anatomical imaging for large-scale, early-stage screening applications.

The conclusions drawn from this chapter provide a clear foundation for the subsequent optimization and system integration stages. Building on the insights gained from the ultrasound-only comparative analysis, the next chapter focuses on refining the selected screening approach through detailed system architecture, component selection, and performance optimization, ensuring that the final proposed system meets both technical requirements and real-world deployment constraints.

Chapter 3: Use of Modern Engineering and IT Tool. [CO9]

3.1 Introduction

The development of a reliable, non-invasive, and portable breast cancer screening system based on machine learning requires the systematic application of modern engineering and information technology tools across multiple stages of the design lifecycle. These tools play a critical role in transforming conceptual system requirements into a functional, validated prototype capable of operating under real-world constraints. In this project, contemporary software and hardware tools were strategically selected to support electronic system design, thermal imaging integration, machine learning model development, embedded deployment, and system-level validation.

Modern engineering tools enable an iterative and modular development workflow, allowing individual subsystems to be designed, tested, and refined before full system integration. In the early stages, circuit simulation and power-stage validation tools are employed to ensure electrical safety, stability, and energy efficiency—key requirements for a portable screening device. These tools reduce hardware development risk by enabling virtual testing of power regulation, component selection, and fault conditions prior to physical implementation.

On the data and intelligence layer, advanced machine learning and data science frameworks are utilized to develop, train, and evaluate convolutional neural network (CNN) models for thermographic image analysis. These tools support large-scale data handling, preprocessing, model optimization, and performance evaluation, enabling reproducible and transparent experimentation. The use of established ML frameworks ensures compatibility with state-of-the-art research practices and facilitates future model extension or retraining using locally acquired datasets.

For system deployment, embedded computing and edge AI tools are employed to integrate the trained machine learning model with the physical screening device. The selection of a Raspberry Pi–based platform enables on-device inference, eliminating reliance on cloud infrastructure and ensuring data privacy, low latency, and operational independence. Supporting development tools allow cross-platform integration, performance profiling, and optimization to meet the computational and power constraints of embedded hardware.

Priority was given to tools that are industry-relevant, widely adopted in academic research, accessible to student developers, and suitable for rapid prototyping. The combined use of simulation software, machine learning frameworks, and embedded development environments ensures that the proposed system is not only technically sound but also verifiable, scalable, and deployable in low-resource healthcare settings.

Overall, the effective use of modern engineering and IT tools underpins the reliability, safety, and feasibility of the proposed screening system. This chapter details the specific tools employed throughout the project and explains their role in enabling an integrated, low-cost, and AI-driven breast cancer screening solution aligned with contemporary engineering practice and clinical deployment requirements.

3.2 Selection of Engineering and IT Tools

The successful development of the proposed AI-based, non-invasive breast cancer screening system required the careful selection of modern engineering and information technology tools that support the full system lifecycle—from conceptual design and simulation to implementation, validation, and deployment. Given the multidisciplinary nature of the project, tools were selected to address electronic design, power-system modeling, machine learning development, embedded deployment, and system integration.

The selection process was guided by the following key criteria:

- Ability to support **rapid prototyping and iterative design**
- Relevance to **current industry practices and academic research**
- Compatibility with **embedded and edge-computing platforms**
- Robust support for **AI/ML model development, training, and validation**
- Accessibility and suitability for **student-led engineering projects**
- Capability to ensure **system safety, reliability, and manufacturability**

Based on these criteria, a combination of **software tools** and **hardware platforms** was selected to enable end-to-end system development and validation prior to physical deployment. The chosen tools collectively reduce development risk, improve design confidence, and ensure that the final system meets functional, safety, and deployment requirements.

3.2.1 Software Tools

Table - 4 :Software tools and Corresponding Description.

Tool name	Description
 **Proteus**	We use Proteus to model and simulate the breath-mask sensor electronics. Proteus enables circuit-level simulation of heater-driven gas sensors (MQ/TGS family), ADC front-ends, and microcontroller interfaces. This allows you to verify signal conditioning, ADC ranges, and timing (preheat, sampling), as well as compare multiple front-end designs quickly without having to build physical prototypes. Proteus' virtual instruments accelerate early iterations and reduce parts waste. Rapid circuit iteration, virtual verification of sensor interface timing, and analog conditioning; ideal for student prototyping.
 **Altium Designer**	Altium is used to create the final schematics and PCB layouts for the mouth/sensor unit and the primary electronics. Altium can handle multi-sheet schematics, design rule checks, component libraries, and high-quality GERBER output for fabrication. Altium ensures the proper routing of high-current traces (buck converter, battery), the placement of decoupling capacitors, and an EMC-aware layout for the thermal camera interface and sensor lines. An industry-standard PCB tool for dependable layouts, DRC, and manufacturable output; essential for a safe, compact portable device.

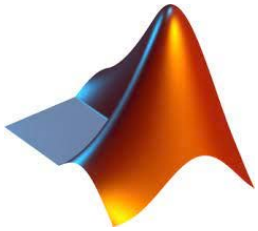 **MATLAB / Simulink**	Simulink is used to model and validate the buck converter, input/output filtering, control-loop dynamics, and transient behavior. Using the continuous-time and switch-mode simulation blocks, we can calculate the required inductance and capacitance, investigate inductor current ripple, validate CCM operation, and test worst-case startup/short-circuit scenarios. These simulations reduce risk before component selection and PCB layout. System-level power simulation and control-loop validation; rapid iteration on L, C, control strategy, and thermal/efficiency trade-offs.
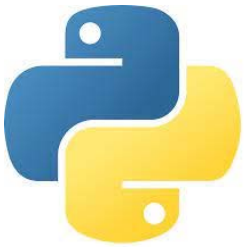 **Python**	All AI/ML model development is done in Python, with Visual Studio Code as the development environment. To build and train models, we use widely adopted machine learning libraries (TensorFlow or PyTorch, scikit-learn, XGBoost) as well as image/vision tools (OpenCV, Pillow). Typical flow: 1. Data load and augmentation (thermal images). 2. CNN model design and training (segmentation, classification). 3. VOC feature processing (1D-CNN/XGBoost) for breath sensor data. 4. Cross-validation, hyperparameter selection, and performance metrics (accuracy, sensitivity, specificity, and AUC). VS Code provides integrated debugging, Git support, and plugin-based environment management to enable reproducible development. Python has the most robust ML ecosystem; VS Code is lightweight and ideal for student teams.

3.2.2 Hardware and Embedded Platforms

In addition to software tools, selected hardware platforms enable embedded deployment and real-time system operation:

- **Raspberry Pi 5** serves as the primary embedded edge-computing platform. Its processing capability supports on-device inference of trained machine learning models, eliminating reliance on cloud infrastructure and ensuring low-latency, privacy-preserving operation.
- **Thermal Imaging Camera Module** (e.g., FLIR-based sensor) is used to acquire infrared thermograms of the breast surface from multiple viewpoints. The camera is selected for its resolution, accuracy, and compatibility with embedded Linux environments.
- **Gas Sensor Modules (MQ/TGS family)** are employed for breath analysis to detect volatile organic compounds associated with cancer metabolism. These sensors are integrated with analog front-end circuitry and ADCs to enable digital feature extraction.

- **Power Electronics Components** (buck converter ICs, inductors, capacitors, batteries) are selected based on simulated performance to ensure stable, efficient, and safe power delivery for portable operation.

The integration of these hardware platforms with the selected software tools enables a complete embedded AI system capable of real-time screening, data acquisition, and decision support.

3.2.3 End-to-End Validation Capability

The combined use of modern engineering and IT tools allows validation at multiple levels:

- Circuit- and system-level electrical validation through simulation
- AI model validation using established performance metrics
- Embedded deployment testing under computational and power constraints
- System integration testing prior to physical prototyping

This toolchain ensures that the proposed screening system is technically reliable, manufacturable, and deployable in real-world, low-resource healthcare environments.

3.4 Conclusion

This chapter has demonstrated the critical role of modern engineering and information technology tools in the systematic development of the proposed AI-assisted, non-invasive breast cancer screening system. The deliberate selection and effective application of simulation, design, and computational tools enabled a structured and low-risk engineering workflow, spanning electronic design, power system validation, machine learning development, and embedded deployment.

Electronic and power-stage simulation tools ensured that circuit behavior, power efficiency, and safety constraints were thoroughly validated prior to physical implementation, thereby reducing design uncertainty and component-level risks. Similarly, industry-standard PCB design tools supported the creation of compact, manufacturable, and reliable hardware layouts suitable for portable medical applications. These tools collectively strengthened the robustness, safety, and manufacturability of the system.

On the computational side, modern AI development environments and programming frameworks facilitated efficient training, validation, and optimization of machine learning models using thermal imaging data. The use of widely adopted ML libraries ensured reproducibility, performance benchmarking, and compatibility with embedded inference pipelines. Furthermore, the deployment of trained models on an edge-computing platform demonstrated the feasibility of real-time, on-device screening without reliance on cloud infrastructure, addressing latency, privacy, and connectivity constraints relevant to low-resource settings.

Overall, the integrated use of modern engineering and IT tools enabled a cohesive system-level design approach rather than isolated component development. This tool-driven methodology aligns with current industry practices in medical device engineering and AI-enabled healthcare systems. By supporting rapid prototyping, validation, and deployment readiness, the selected tools contributed directly to the realization of a portable, affordable, and ethically deployable screening solution. The outcomes of this chapter establish a strong technical foundation for subsequent optimization, system integration, and performance evaluation stages of the project.

Chapter 4: Optimization of Multiple Design and Finding the Optimal Solution. [CO7]

4.1 Introduction

The selection of an optimal design solution for an early-stage, AI-based, non-invasive breast cancer screening system requires a structured and evidence-driven optimization framework. Given the multidisciplinary nature of the problem—spanning biomedical sensing, electronics, power systems, machine learning, and real-world healthcare deployment—design selection cannot rely on conceptual feasibility alone. Instead, it must be supported by systematic verification across multiple engineering domains to ensure both technical validity and practical deployability.

In this project, two competing design approaches were identified and carried forward from the earlier chapters:
Approach 1, which integrates thermography with breath-based volatile organic compound (VOC) analysis, and
Approach 2, which relies on AI-assisted ultrasonography.
While both approaches are scientifically sound and clinically motivated, they exhibit fundamentally different sensing principles, hardware requirements, and operational constraints. As a result, a formal optimization process was required to determine which approach best satisfies the project objectives and contextual constraints.

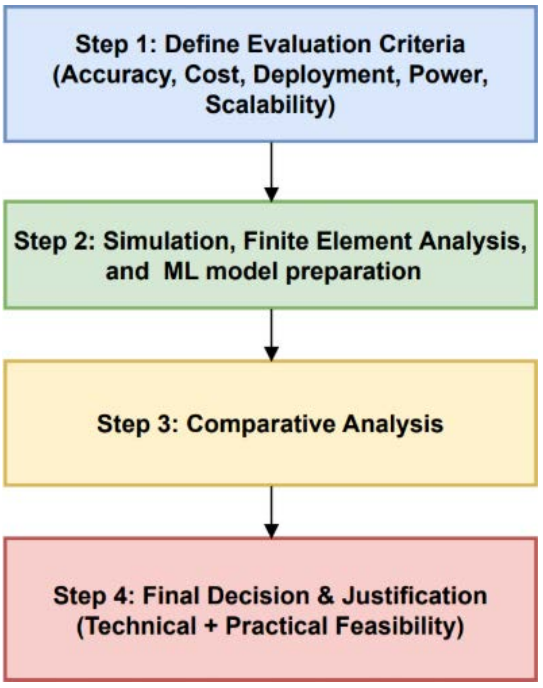

Figure 3 : Flowchart of AI-assisted ultrasonography process.

The first step in the optimization process was the definition of clear and quantifiable evaluation criteria. These criteria were selected to reflect both engineering performance and real-world deployment requirements. Specifically, each design approach was evaluated based on:

- **Diagnostic accuracy and reliability**, assessing the ability of the system to consistently identify abnormal patterns associated with early-stage malignancy;
- **Cost effectiveness**, including hardware cost, maintenance requirements, and total cost of ownership;
- **Ease of deployment**, particularly in decentralized, rural, and low-resource healthcare environments;
- **Power consumption and energy efficiency**, which directly affect portability and battery-powered operation;
- **Scalability and extensibility**, considering the feasibility of large-scale screening and future system upgrades.

These criteria ensure a balanced evaluation that extends beyond algorithmic performance to include engineering feasibility, sustainability, and societal impact. By applying the same criteria uniformly to both approaches, a fair and objective comparison was achieved.

To rigorously validate each design approach, a three-level engineering verification framework was adopted. This framework ensures that every design is tested from fundamental physical principles through to system-level intelligence, reducing uncertainty and development risk at each stage.

At the first level, physics-based simulations were conducted to verify the scientific foundations of each sensing modality. Finite Element Analysis (FEA) was employed to model the interaction between biological tissue and the respective sensing mechanisms.

For **Approach 1**, FEA simulations were performed to analyze **thermal diffusion and heat transfer within breast tissue**. These simulations modeled how localized metabolic activity and angiogenesis associated with malignant growth influence surface temperature distributions. The results confirmed that temperature variations produced by early-stage tumors are theoretically detectable through infrared thermography, thereby validating the feasibility of thermal-based screening.

For **Approach 2**, FEA was used to study **ultrasound wave propagation through heterogeneous breast tissue**. The simulations examined acoustic impedance mismatches, reflection coefficients, and signal attenuation across different tissue layers. These results verified that ultrasound waves can reliably interact with and reflect from internal tissue structures, supporting the scientific basis of ultrasound imaging for lesion detection.

This level of analysis established that both design approaches are grounded in valid physical principles and warranted further system-level evaluation.

At the second level, each design was evaluated from an electronic and power-system engineering perspective to assess feasibility, reliability, and suitability for portable operation.

For **Approach 1**, detailed circuit-level simulations were conducted using **Proteus** to model the VOC sensor interface, including sensor preheating cycles, analog signal conditioning, ADC interfacing, and timing behavior. In parallel, the portable power subsystem was modeled in **MATLAB/Simulink**, focusing on the buck converter's stability, transient response, voltage regulation, and efficiency under varying load conditions. This stage ensured that the sensor electronics and power delivery system could operate reliably in real-world scenarios.

For **Approach 2**, circuit-level analysis primarily focused on **power-system simulation**, as ultrasound probes and front-end electronics are typically standardized. Simulink-based models were used to assess voltage stability and energy consumption. The simulations revealed higher power demand and stronger dependence on stable power infrastructure, highlighting limitations in portability and battery-based operation.

This verification level demonstrated that while both designs are electronically feasible, **Approach 1 offers a significantly lower-power and more portable implementation**.

At the third level, both approaches were evaluated based on their ability to support robust and reliable machine learning inference.

For **Approach 1**, multiple AI models were developed and tested for:

- Thermal image analysis using convolutional neural networks (CNNs), and
- VOC pattern classification using statistical and machine learning techniques.

Model training and evaluation were conducted using real medical datasets, with performance assessed using metrics such as accuracy, sensitivity, specificity, and robustness across different conditions.

For **Approach 2**, deep learning models were trained on breast ultrasound datasets to classify benign and malignant tissue patterns. While these models achieved strong classification performance, their effectiveness remained sensitive to image quality and acquisition consistency, which are influenced by operator expertise.

Through this AI evaluation stage, the most effective model architectures for each approach were identified, and their real-world robustness was assessed.

In summary, the optimization and verification strategy employed in this chapter was comprehensive and engineering-driven. By validating each design at the scientific, electronic, and intelligence levels, the project ensured that both approaches were not merely conceptually attractive but also practically viable and evidence-backed.

This structured framework provides a strong foundation for the objective comparison and final design selection presented in the subsequent sections of this chapter. The results of this optimization process directly inform the identification of the optimal solution that best balances accuracy, cost, portability, and scalability for early-stage breast cancer screening in low-resource environments.

4.2 Optimization of multiple design approaches

4.2.1 Finite Element Analysis (FEA) Simulation

Finite Element Analysis (FEA) is a computational modeling technique widely used in engineering to predict the physical behavior of complex systems under realistic operating conditions. The method works by discretizing a complex geometry into a large number of small, finite elements interconnected at nodes. Governing physical equations such as heat transfer, wave propagation, or stress–strain relationships are then solved numerically over these elements to estimate the system's global response. This approach enables accurate analysis of systems whose analytical solutions are otherwise intractable due to geometric complexity or material heterogeneity.

In the context of this project, FEA serves as a critical optimization and verification tool, allowing early-stage evaluation of competing design approaches before committing to physical prototyping. By simulating the underlying physical phenomena that drive each sensing modality, FEA reduces development uncertainty, minimizes trial-and-error experimentation, and lowers overall design cost and time. More importantly, it provides quantitative evidence that each approach is scientifically feasible and capable of producing measurable signals suitable for AI-based interpretation.

One of the primary advantages of FEA is its ability to provide internal insight into system behavior—often referred to as a virtual or digital twin of the physical system. Through simulation, it becomes possible to visualize how heat diffuses through biological tissue, how acoustic waves propagate and reflect at tissue boundaries, and how these effects vary with changes in geometry, material properties, or operating conditions. This level of insight is difficult, costly, or ethically impractical to obtain through direct experimentation alone, particularly in biomedical applications.

For Approach 1, FEA was employed to model heat transfer within breast tissue arising from abnormal metabolic activity associated with malignant tumors. Cancerous tissue typically exhibits increased blood perfusion and metabolic rate, resulting in localized heat generation. The FEA model simulates this heat source within multilayer breast tissue and analyzes how thermal energy diffuses toward the skin surface.

By varying parameters such as tumor depth, size, and thermal conductivity of surrounding tissues, the simulation enables evaluation of how subsurface abnormalities influence surface temperature distributions. This analysis helps determine whether the resulting thermal contrast is sufficiently pronounced to be detected by an infrared thermal camera under

realistic conditions. Additionally, the simulations provide insight into how environmental factors and tissue heterogeneity may affect detection sensitivity.

These results directly inform system optimization by identifying detection limits, such as the maximum tumor depth that remains thermographically observable, and by guiding sensor resolution and preprocessing requirements. In this way, FEA validates the scientific foundation of thermography as a viable early-stage screening modality rather than relying solely on empirical assumptions.

For Approach 2, FEA was applied to simulate ultrasound wave propagation through heterogeneous breast tissue. The simulation models the interaction of acoustic waves with tissues of varying density and acoustic impedance, including reflections, scattering, and attenuation effects. This allows analysis of how internal structures, such as tumors, influence received ultrasound signals.

Through these simulations, it becomes possible to assess how factors such as tissue composition, lesion geometry, and depth affect echo strength and image quality. The FEA results provide a theoretical basis for understanding the strengths and limitations of ultrasound-based detection, particularly with respect to spatial resolution and contrast.

This modeling also highlights the dependence of ultrasound performance on consistent probe positioning and tissue contact, factors that later influence the evaluation of deployment feasibility and operator dependency. Thus, FEA not only confirms physical feasibility but also reveals practical constraints that impact system optimization.

Beyond feasibility verification, FEA plays a central role in design optimization. By enabling rapid evaluation of multiple scenarios and parameter variations, it supports informed decision-making without repeated physical experimentation. The simulations help identify operating ranges where each approach performs optimally and reveal conditions under which performance degrades.

In this project, FEA acts as a bridge between theoretical principles and real-world implementation. It provides scientific justification for advancing both design approaches to subsequent stages of electronic, power-system, and AI-level evaluation. Furthermore, the insights gained from FEA contribute to selecting appropriate sensors, defining acquisition protocols, and setting realistic performance expectations for the overall system.

In summary, Finite Element Analysis is a foundational component of the optimization framework employed in this project. By modeling heat transfer and acoustic wave propagation within biological tissue, FEA establishes the physical validity of both thermography-based and ultrasound-based screening approaches. It enables early detection of design limitations, guides system parameter selection, and significantly reduces development risk.

The use of FEA ensures that subsequent optimization steps are grounded in scientifically verified behavior rather than assumptions. As such, it strengthens confidence that the

proposed screening system can operate reliably under real-world conditions and supports the objective comparison and selection of the optimal design solution presented in the following sections.

4.2.2 Approach 1

To understand heat transfer patterns associated with early-stage breast cancer, we performed a Finite Element Analysis (FEA) of the breast using both 2D and 3D computational models. The goal was to simulate how the presence of a tumor alters the thermal distribution on the skin's surface, thereby justifying the use of thermal imaging as part of our non-invasive detection system.

The mathematical foundation for our modeling is Pennes' Bioheat Equation, which predicts how heat generated in biological tissues spreads through conduction, blood perfusion, and metabolic activity:

$$\rho c \frac{\partial T}{\partial t} = \nabla \cdot (k \nabla T) + \omega_b c_b (T_a - T) + Q$$

Where

- T is the tissue temperature(℃)
- k is thermal conductivity (W/m·K)
- ω_b is the blood perfusion rate (1/s)
- c_b and c are the specific heat capacities of blood and tissue,
- Q is the local metabolic heat generation (W/m³)
- T_a is arterial blood temperature
- ρ is tissue density

In our breast model, we distinguish two domains: healthy tissue and tumor tissue. Tumors typically have:

- increased metabolic heat production (up to 70 times higher than healthy tissue),
- greater blood perfusion (about 50 times higher),
- slightly higher thermal conductivity,
- a well-defined geometric location (e.g., 3 cm lateral, 2 cm anterior, 4 cm deep from the breast reference point).

We also account for boundary conditions (convection at the skin-air interface) and the ambient temperature. We created two simulation scripts—one for a simplified 2D cross-section and another for a full 3D approximation.

- 2D Model:
    - We started by constructing a semicircular mesh representing the breast. Points were placed evenly along the arc and within the interior.
    - We inserted additional points to represent the tumor, using a smaller circular region (center at radius 1 cm).
    - A Delaunay triangulation meshed the geometry for finite element computation.
- 3D Model:
    - For realism, a 3D hemisphere was created with uniformly sampled points for the volume of the breast, and a smaller spherical region for the tumor (at radius 1.5 cm).
    - Delaunay triangulation was again used to structure the mesh for the volume.

We differentiated the thermal properties of healthy tissue and tumor tissue in each mesh element:

- Healthy tissue:
    - Thermal conductivity = 0.50 W/m·K
    - Blood perfusion = 0.00018 1/s
    - Metabolic heat = 400 W/m³
- Tumor tissue:
    - Thermal conductivity = 0.55 W/m·K
    - Blood perfusion = 0.009 1/s
    - Metabolic heat = 29,000 W/m³

We calculated perfusion energy contributions using blood density and specific heat. For our FEA, we adopted an iterative finite difference method across the mesh nodes:

- At each iteration, every mesh point updates its temperature based on:
    - Neighboring node temperatures (heat diffusion),
    - Local material properties (healthy/tumor),
    - Blood perfusion and metabolic heat,
    - Boundary conditions (surface nodes fixed to ambient temperature).

- The process repeats until the solution converges (temperature changes below a threshold).
- For boundary nodes (on the surface), convective heat loss to the ambient (e.g., 25°C) is enforced.

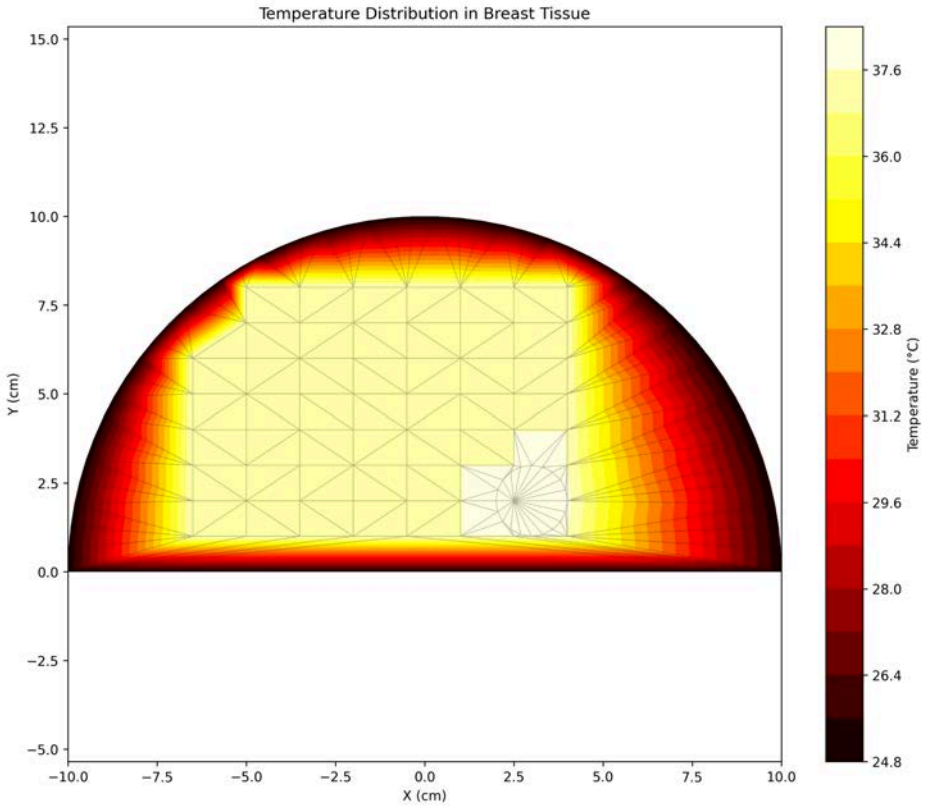

Figure 4: Temperature Distribution in Breast Tissue in 2D

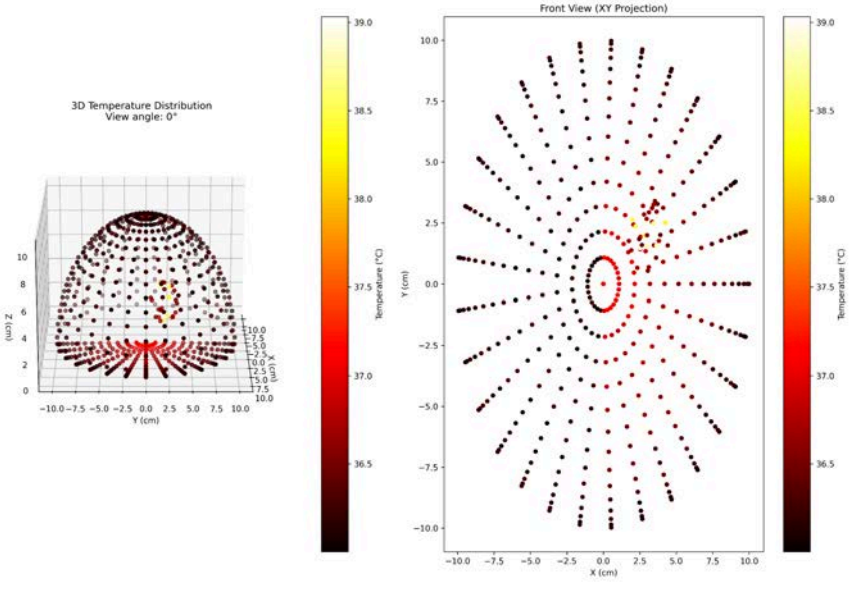

Figure 5 : 3D temperature distribution with view angle 0°

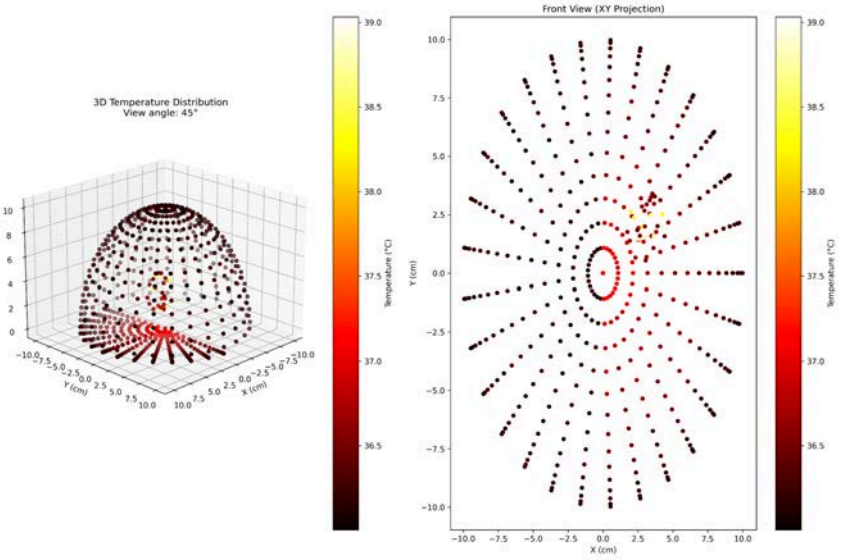

Figure 6 : 3D temperature distribution with view angle 45°

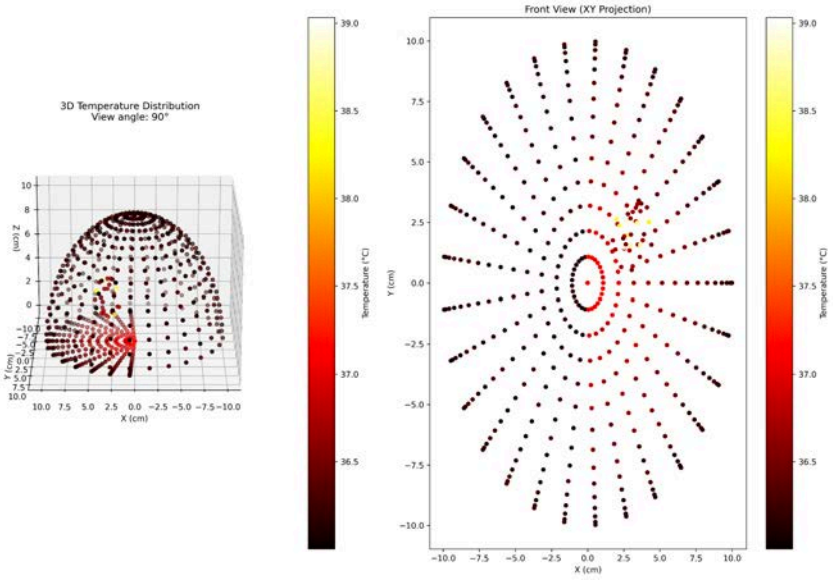

Figure 7 : 3D temperature distribution with view angle 90°

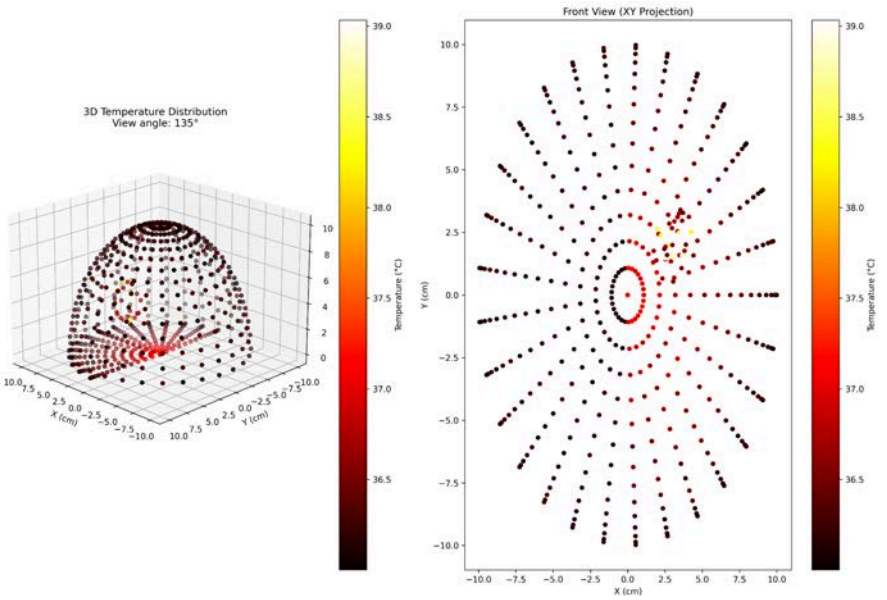

Figure 8 : 3D temperature distribution with view angle 125°

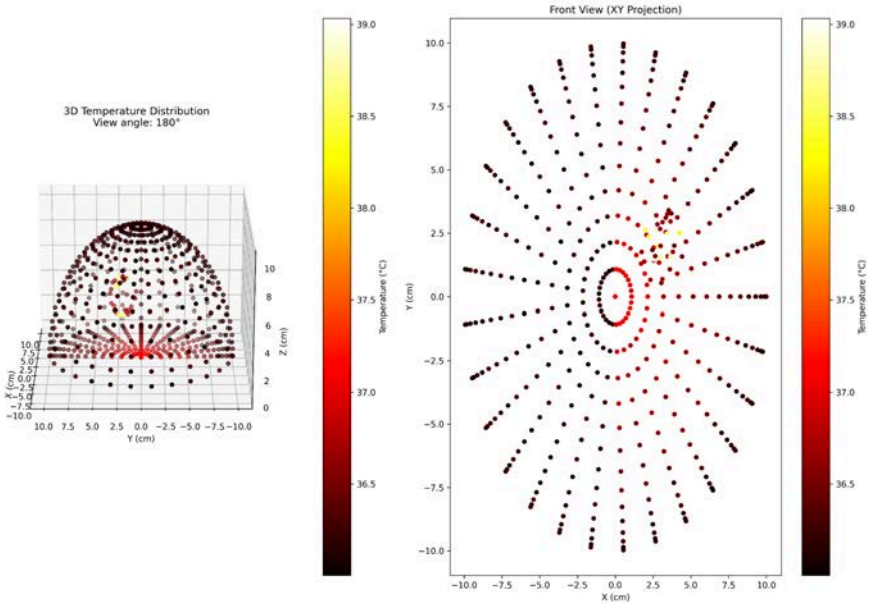

Figure 9 : 3D temperature distribution with view angle 180°

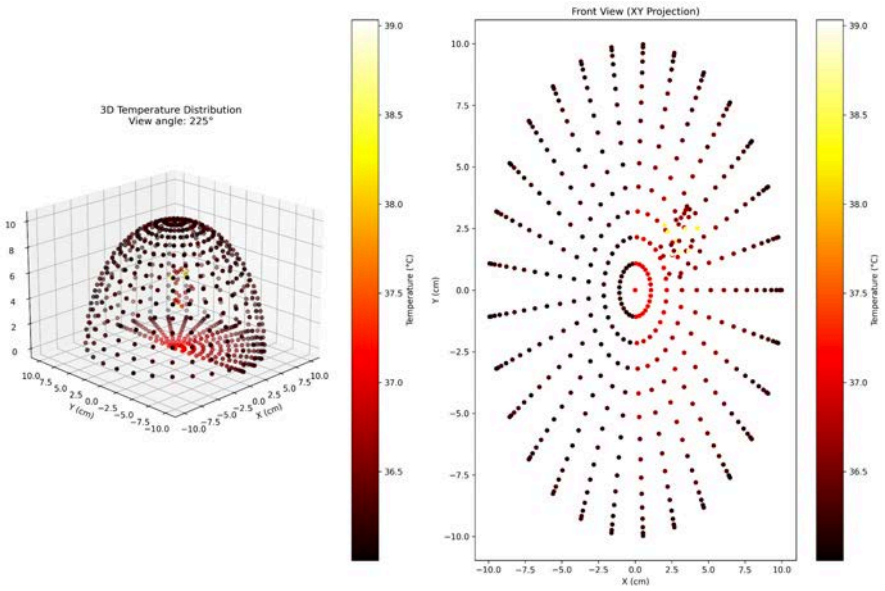

Figure 10 : 3D temperature distribution with view angle 225°

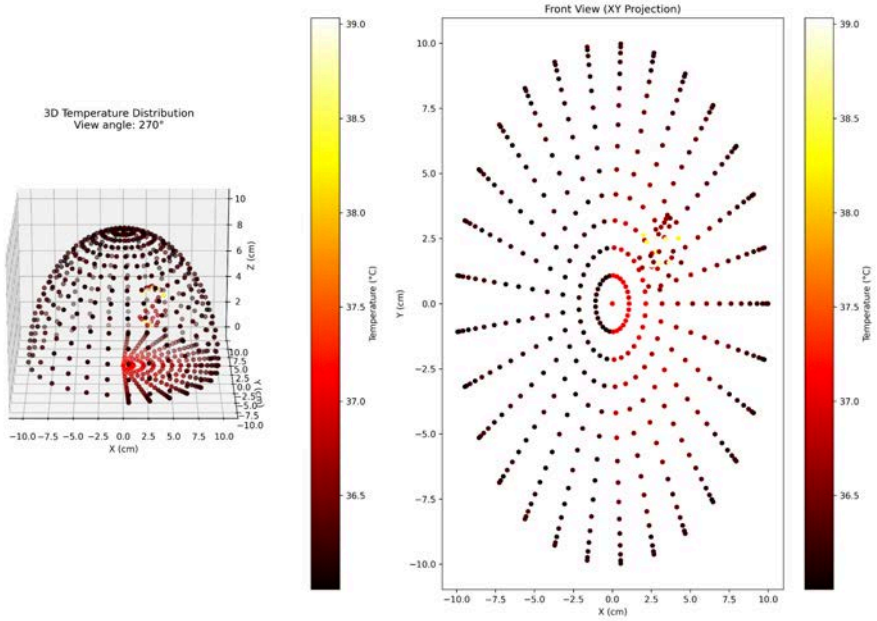

Figure 11 : 3D temperature distribution with view angle 270°

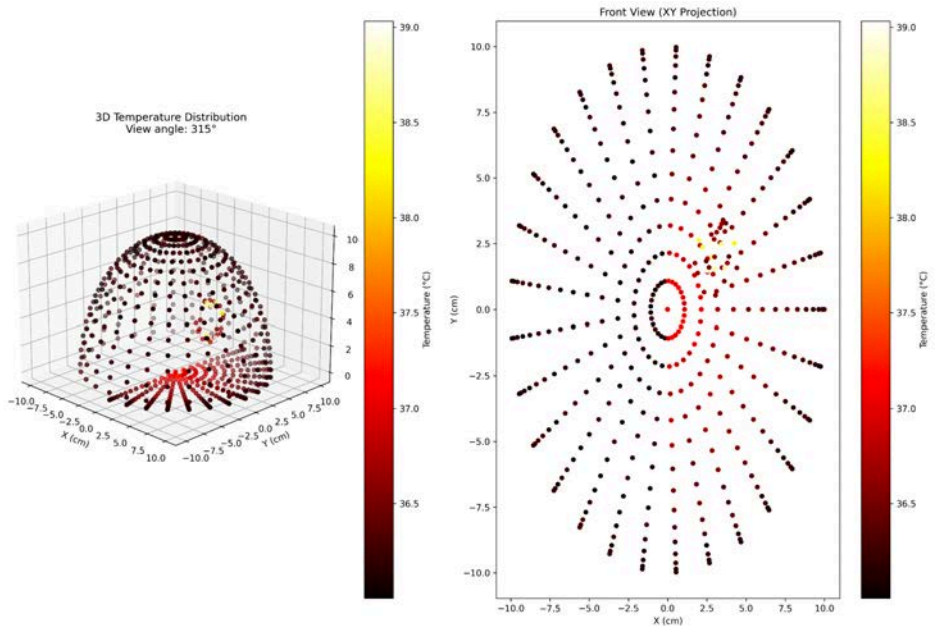

Figure 12 : 3D temperature distribution with view angle 315°

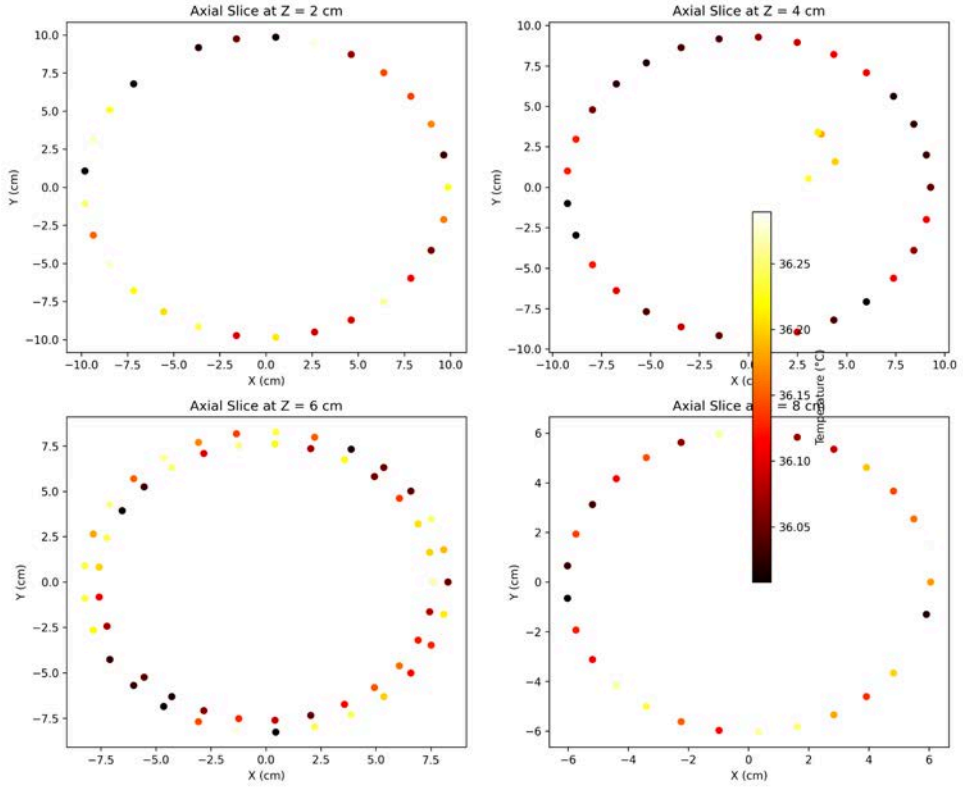

Figure 13 : 3D temperature distribution axial slice

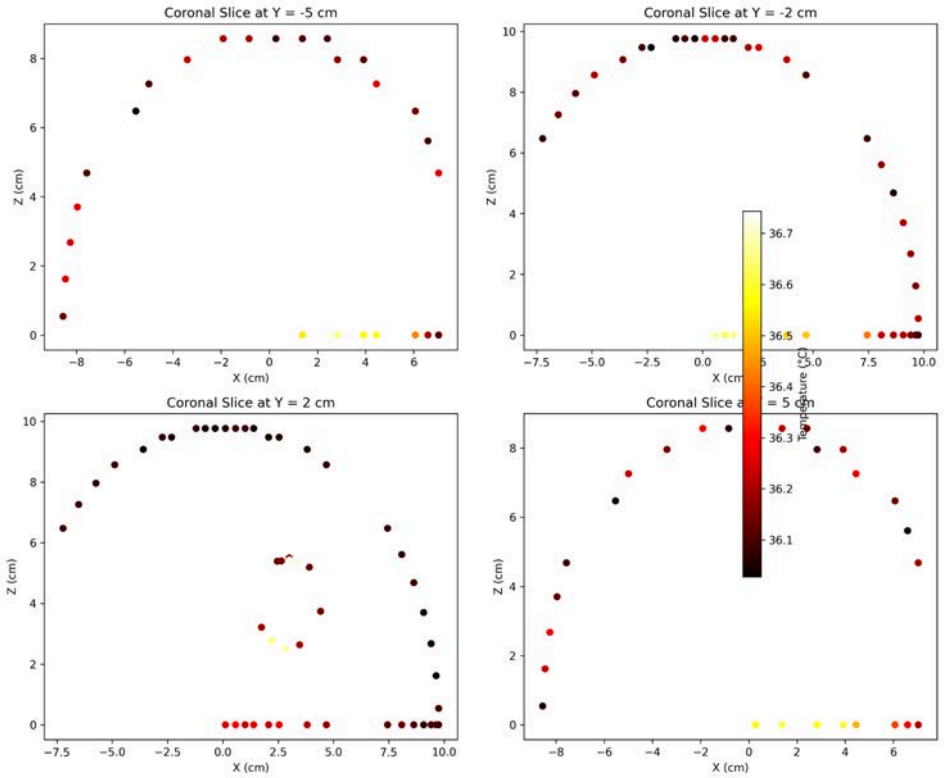

Figure 14 : 3D temperature distribution conical slice

Result Visualization and Analysis:

2D Results:

We visualized the temperature field as a color-mapped contour plot over the breast cross-section, overlaid on the mesh. The contours clearly show a "hot spot" in the tumor region, about 1.5–2.0°C higher than the surrounding tissue, illustrating the physiological signature targeted by thermography.

3D Results:

Our 3D simulations produced both volumetric and plan-view (XY-projection) plots, rotating the view angle to mimic different camera placements during actual screening. Within the tumor, the interior registers as much as 1.5°C above the average core temperature even after accounting for depth-dependent cooling—from interior to surface.

Additionally, we extracted 2D slices (axial, sagittal, coronal) from the 3D data to simulate what a thermal camera might "see" on different breast planes. These slices confirmed that the abnormal temperature zone persists on the skin's surface directly above the simulated tumor.

Statistically, the model outputs typical max-to-min temperature differences of nearly 2°C, which matches observed values in published infrared thermography studies.

Achievements and Impact

- Validation for Imaging: The FEA demonstrates—mathematically and visually—that tumors do create surface temperature differences that non-invasive thermal cameras can detect, especially when processed by AI algorithms trained to recognize small, localized hot spots.
- Multi-Angle Assessment: By simulating multi-view and multi-slice imaging, we ensured our approach remains robust regardless of how the breast is oriented during scanning—a crucial design consideration for real-world, portable devices.
- Parameter Sensitivity: The model highlights the dependence of thermal contrast on tumor size, location, and physiological properties, which guides hardware selection (camera sensitivity) and the necessary training for our AI models.
- Justification for Approach 1: The results support our decision to combine thermal imaging with breath analysis for a cost-effective, safe, and accessible early-screening tool, appropriate for resource-limited settings and field deployment.

In summary, our FEA work provided critical quantitative and visual evidence that underpins the technical feasibility and diagnostic power of the thermography component in our ML-based, non-invasive multi-cancer screening system. This forms the analytic backbone for device design, clinical training, and AI model development as detailed throughout our project deliverables.

4.2.3 Approach 2

For Approach 2, our focus was on the simulation of ultrasound waves interacting with both healthy breast tissue and a modeled tumor. This analysis is crucial to demonstrate how the presence of a tumor alters the wave field, providing measurable signals for AI-powered cancer diagnostics. Our simulation is based on the discrete 2D Finite Difference Time Domain (FDTD) method a widely used approach for modeling acoustic wave propagation in tissue.

The primary governing equation for wave propagation in a lossless and homogeneous (but spatially variable) medium is the 2D scalar wave equation:

$$\frac{\partial^2 p}{\partial t^2} = c(x,y)^2\left(\frac{\partial^2 p}{\partial x^2} + \frac{\partial^2 p}{\partial y^2}\right)$$

where:

- $p(x,y,t)$ is the acoustic pressure at position (x,y) and time t;
- $c(x,y)$ is the local speed of sound, determined by tissue type (healthy or tumor).

We set up a 2D simulation grid representing a cross-section of the breast, with each grid cell specifying the local speed of sound. Most of the domain uses a typical sound speed for soft

tissue (e.g., 1.0 arbitrary units), but inside a centrally placed circular region (the tumor), the speed is increased by 10% (to 1.1 units). This difference reflects known physical properties of tumors, which have slightly higher density, elasticity, and therefore a higher speed of sound.

The domain was large enough (200×200 points) to capture wave reflections and scattering, and the tumor radius was selected to be noticeable but realistic relative to typical breast anatomy.

The wave field is advanced in discrete time steps using the following finite-difference scheme:

$$p_{new}[i,j] = 2p[i,j] - p_{old}[i,j] + (c[i,j]^2 dt^2)\Delta^2 p[i,j]$$

- $\Delta^2 p[i,j]$ is the discrete Laplacian (sum of four neighboring values minus four times the center).
- Boundary conditions were implicitly set by the grid size (no explicit absorption in this basic model).
- A stable time step (dt=0.2) was chosen to satisfy the Courant stability condition for wave propagation.

The simulation starts with an initial pulse at a fixed location (representing an ultrasound transducer emitting a wave). As the wave propagates, it interacts with the inhomogeneous medium, scattering, reflecting, and refracting at tissue-tumor interfaces.

Visualization: 3D Mapping and Multi-View Analysis

To better match real-device operation, we mapped the 2D simulation results (pressure field) onto the surface of a 3D hemispherical breast model. The hemisphere was constructed using mesh grids representing the breast curvature. The coloring of the 3D surface directly encodes the simulated pressure amplitude at every (x, y) point, using a continuous "coolwarm" color map to indicate phase and amplitude (positive and negative pressures).

With matplotlib's 3D plotting tools, we animated the time evolution of the wave field:

- Surface Waves: The simulation clearly shows wave propagation across the curved breast surface, with wavefronts originating from the source.
- Tumor Signatures: As the wave strikes the tumor, part of the energy is scattered and transmitted differently compared to the surrounding tissue. This is visible as distinct patterns—localized rings and distortions—around the tumor zone.
- Multiple Views: To help with spatial intuition, the visualization can be rotated to various angles (elevation and azimuth), mimicking different ultrasound probe orientations.

This setup closely mimics what would be seen by a real ultrasound imager: echoes and interference patterns caused by the contrast in acoustic properties between normal and tumorous tissue.

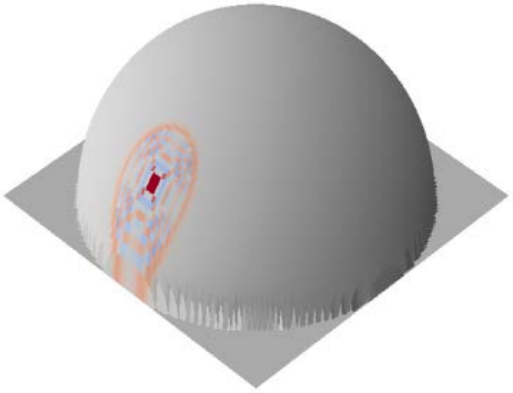

Figure 15 : Ultrasound Simulation on 3D Shape (Time Step: 116)

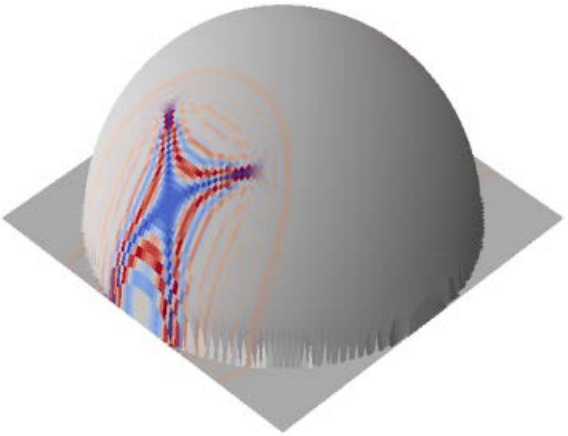

Figure 16 : Ultrasound Simulation on 3D Shape (Time Step: 291)

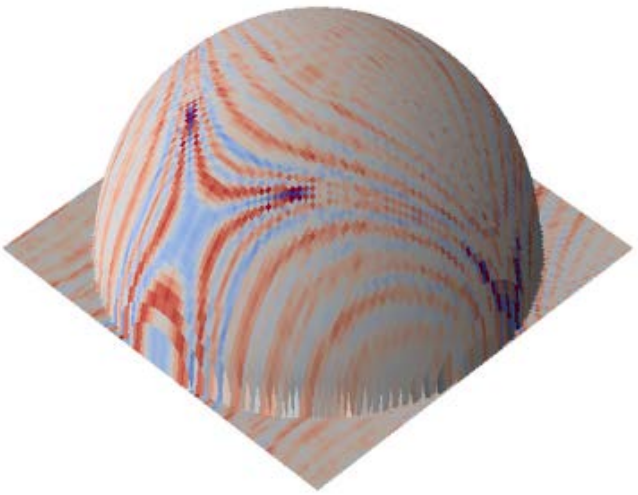

Figure 17 : Ultrasound Simulation on 3D Shape (Time Step: 371)

Through this simulation, we achieve several important outcomes:

- Proof of Detectability: The simulation demonstrates that an acoustic wave encounters a measurable change when passing through a tumor, providing a solid physical basis for using ultrasound and AI algorithms for early cancer diagnostics.
- Multi-View Understanding: The ability to rotate the 3D surface and observe the pressure/echo pattern from multiple viewpoints helps us understand where the best detection spots are, which has implications for both probe design and AI model input strategies.
- Parameter Sensitivity: By varying properties like tumor size, sound speed contrast, and the location of the emitter, we can test the robustness of the diagnostic approach under realistic variances. This helps optimize both the design and deployment procedure.
- Basis for AI Training: The raw pressure map provides a simulated dataset for developing and validating machine learning models, which will learn to classify tumorous vs. healthy signatures even in the presence of noise and artifacts.

In summary, our FDTD-based ultrasound simulation offers critical, physics-based validation for Approach 2, showing that ultrasonic imaging—enhanced with deep learning—has the potential to detect early-stage tumors via their unique effect on wave propagation. This analysis is directly aligned with the clinical motivation for expanding affordable, high-accuracy diagnostics in resource-constrained environments, supporting the engineering choices in our system design.

4.2.3 Machine Learning Model Analysis and Simulation

Machine learning (ML) constitutes a core analytical component of the proposed screening system, enabling the automated interpretation of complex biomedical data generated by non-invasive sensing modalities. In early-stage breast cancer screening, subtle spatial, thermal, or structural patterns often remain indistinguishable through manual observation or traditional threshold-based techniques. ML models, particularly those based on deep learning, are capable of learning high-dimensional feature representations and identifying latent correlations within data, thereby significantly enhancing detection sensitivity and consistency.

In this project, ML is employed as a decision-support and pattern-recognition layer rather than a standalone diagnostic authority. Its primary role is to analyze sensor-derived data such as thermal images, ultrasound images, and breath-based features and generate reliable screening-level predictions while minimizing false positives and false negatives. This automated interpretation reduces dependence on operator expertise and improves reproducibility across different screening environments.

For the purpose of validation and proof-of-concept development, the ML models were trained and evaluated using publicly available, peer-reviewed datasets related to breast cancer detection. Although the long-term objective of the project is to develop a localized dataset tailored to the proposed hardware system and population demographics, the use of established datasets enables early verification of model feasibility, performance trends, and architectural suitability. This approach accelerates development while maintaining scientific rigor and comparability with existing research.

The ML analysis followed a structured workflow comprising data preprocessing, feature enhancement, model training, performance evaluation, and robustness assessment. Different model architectures were explored and compared to identify configurations that provide optimal trade-offs between accuracy, computational efficiency, and deployment feasibility on embedded edge platforms. Performance was evaluated using standard medical AI metrics, including accuracy, sensitivity, specificity, and area under the ROC curve (AUC), ensuring clinical relevance and interpretability.

By validating the ML pipeline on real medical datasets, this stage confirms that the proposed screening framework is not merely theoretical but capable of producing meaningful predictions under realistic conditions. Furthermore, the simulation results inform subsequent optimization decisions regarding model complexity, inference latency, and suitability for on-device deployment.

4.2.4 Machine Learning Analysis for Approach 1 (Thermography-Based)

Approach 1 adopts an ML-driven framework centered on the analysis of infrared thermal breast images (thermograms) for early-stage cancer screening. Thermographic imaging captures spatial temperature distributions across the breast surface, reflecting underlying physiological processes such as increased blood perfusion and metabolic activity associated

with malignant growth. However, these thermal variations are often subtle and spatially complex, necessitating advanced computational analysis for reliable interpretation.

To address this challenge, the proposed ML pipeline integrates image preprocessing, feature enhancement, and deep learning–based classification to detect abnormal thermal patterns indicative of potential malignancy. Edge detection and contrast enhancement techniques are applied during preprocessing to amplify thermal asymmetries and localized hotspots, improving the discriminative capability of the learning models. These enhanced representations are then processed by convolutional neural networks (CNNs), which automatically learn hierarchical spatial features relevant to screening-level decision-making.

This approach emphasizes non-invasive, contactless screening, making it well suited for large-scale and community-level deployment. From an optimization perspective, ML analysis allows the system to compensate for environmental variability and sensor noise, which are inherent challenges in thermographic imaging. The evaluation of different model architectures enables identification of configurations that balance predictive performance with computational efficiency, a critical requirement for embedded edge deployment.

4.2.4.1 Dataset Description

The thermography-based ML models were trained and validated using the Database for Mastology Research InfraRed (DMR-IR) dataset, a publicly available and widely referenced thermal imaging dataset for breast cancer research. The DMR-IR dataset consists of infrared thermograms captured under controlled conditions, representing surface temperature distributions of the breast.

Each image in the dataset is a grayscale thermogram, where pixel intensity corresponds to localized temperature variation. These temperature maps contain subtle spatial patterns such as asymmetry between breasts or localized hotspots—that may correlate with underlying pathological changes. The dataset includes labeled samples indicating the presence or absence of breast cancer, enabling supervised learning and quantitative performance evaluation.

The use of the DMR-IR dataset provides a realistic benchmark for assessing the capability of ML models to detect early signs of malignancy using non-invasive thermal imaging. Its structured labeling allows objective comparison between predicted outcomes and ground truth, supporting rigorous validation of model accuracy, sensitivity, and robustness.

From an optimization standpoint, training on this dataset enables systematic evaluation of preprocessing strategies, network depth, and feature extraction techniques. The insights gained from this analysis inform decisions regarding model selection and parameter tuning, ensuring that the final system configuration is both scientifically grounded and practically deployable.

In summary, the machine learning analysis and simulation conducted in this section establish the computational feasibility of thermography-based breast cancer screening within the proposed framework. By validating model performance on established medical datasets, this stage confirms that AI can reliably extract clinically meaningful information from thermal images and support early-stage risk identification.

The results of this ML optimization phase directly contribute to the comparative evaluation of design approaches and play a decisive role in identifying the optimal screening solution. Furthermore, the validated ML pipeline provides a scalable foundation for future enhancement using locally collected datasets, supporting continuous learning and population-specific adaptation.

4.2.4.2 Methodology and Model Architecture

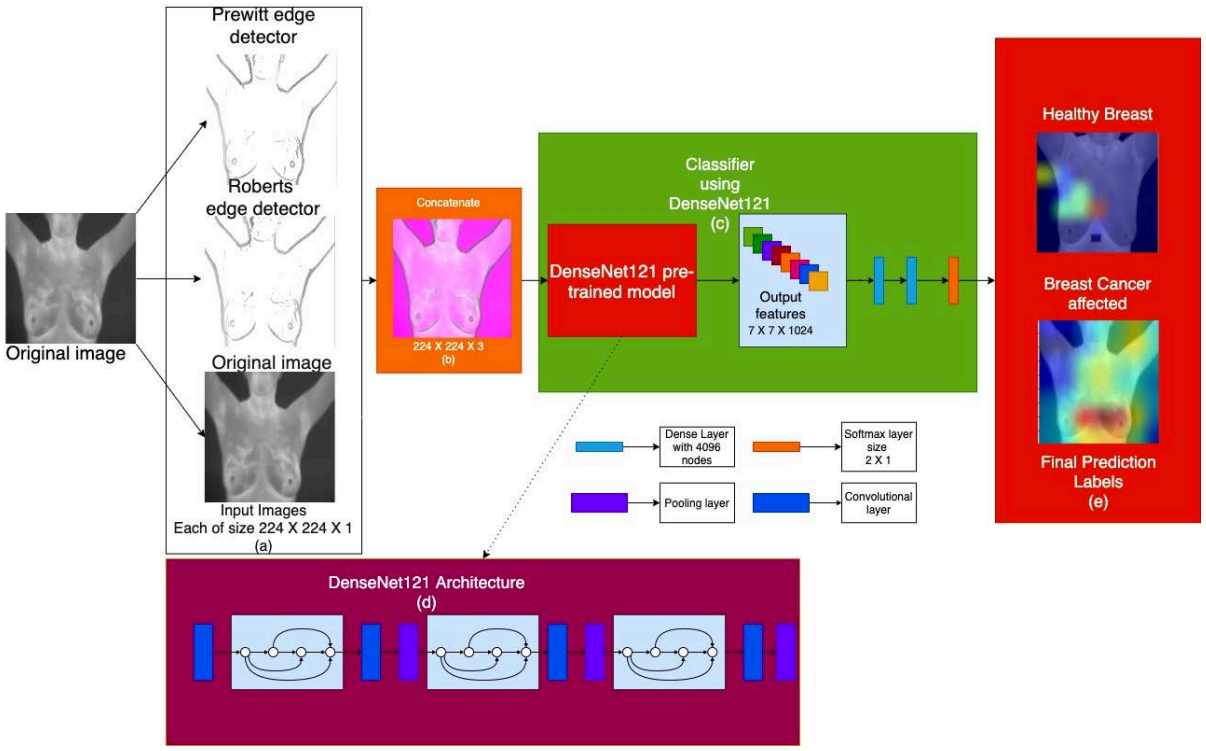

Figure 18 : ML workflow diagram

4.2.4.3 Input Enhancement via Edge Detection

Thermal images alone may lack sufficient detail for precise feature extraction. To address this, we enhanced the input data by applying two well-known edge detection algorithms:

- **Prewitt Edge Detector**
- **Roberts Edge Detector**

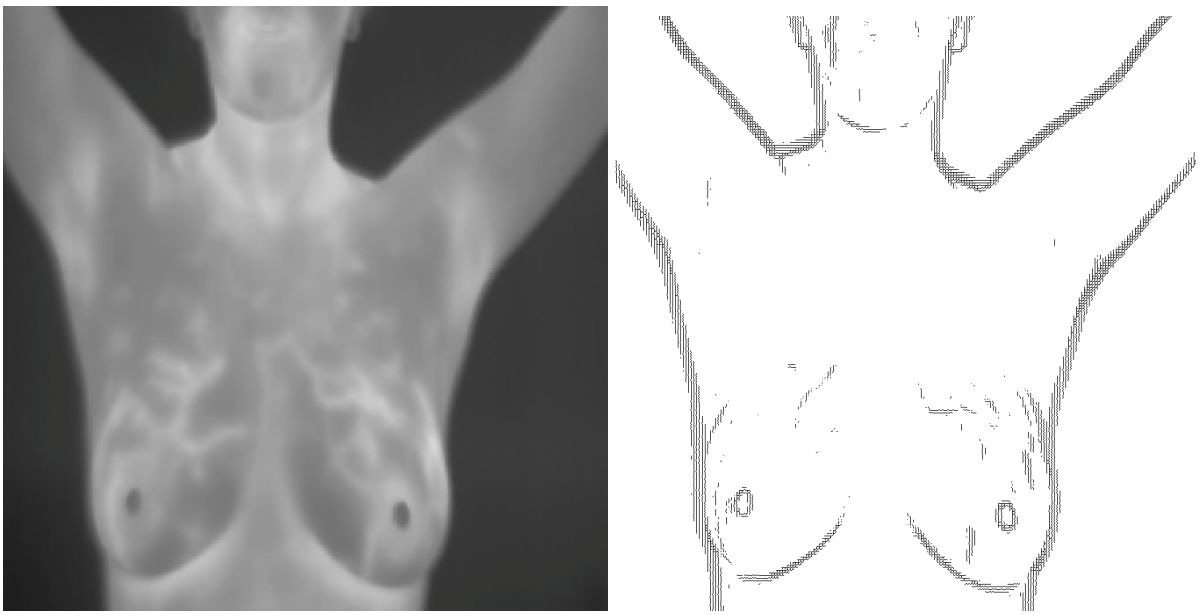

Figure 19 : Prewitt and Roberts edge-detected maps

Both perform gradient-based detection of subtle edges, highlighting minute features such as blood vessels and tissue deformations critical for cancer classification. The outputs of these edge detectors are combined with the original grayscale thermal image to form a 3-channel composite image suitable as input for the deep learning model.

4.2.4.4 Transfer Learning Model Selection and Comparative Evaluation

To identify which model performs the best we created a shared classification head (global average pooling, batch normalization, dense layers with dropout) attached to multiple pretrained CNN backbones (MobileNet, DenseNet121, ResNet50, VGG16, InceptionV3, EfficientNetB0, Xception), with most backbone layers initially frozen.

Employed a two-stage training strategy:

- Stage 1: trained the classification head using binary cross-entropy (Adam, learning rate 1e-3) with early stopping based on validation AUC.
- Stage 2: unfroze the backbone and fine-tuned the entire network using focal loss (gamma=2.0, alpha=0.75) with a reduced learning rate (Adam, 1e-5).
- Optimized the decision threshold by sweeping 0.2–0.7 to maximize the F1 score, then generated final predictions using the optimal threshold.
- Conducted comprehensive evaluation: accuracy, balanced accuracy, precision, recall, F1-score, AUC, sensitivity, specificity, confusion matrix, and ROC curves.

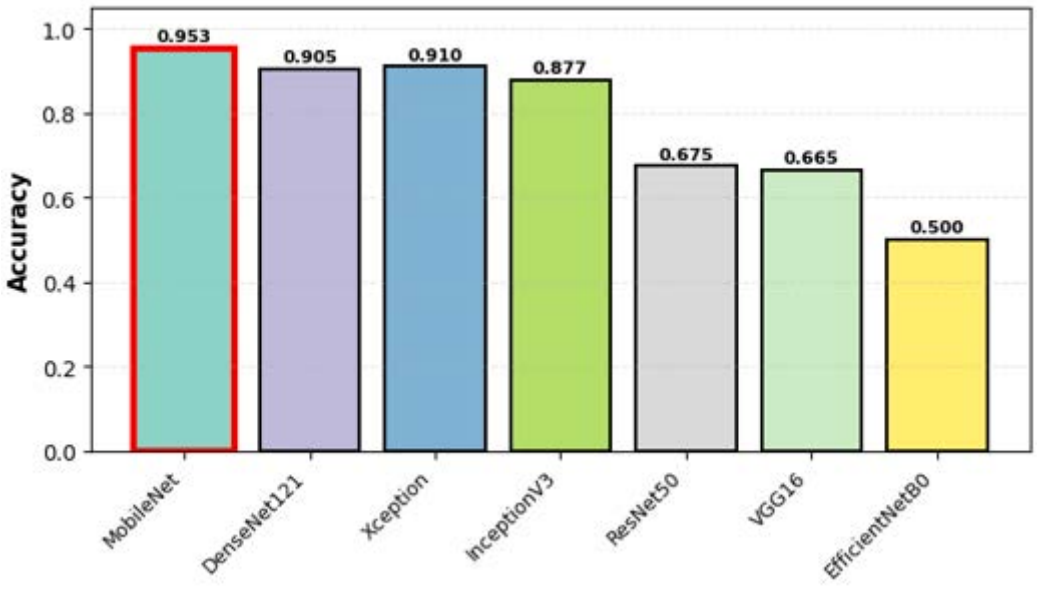

Figure 20 : Transfer Learning model Accuracy Comparison

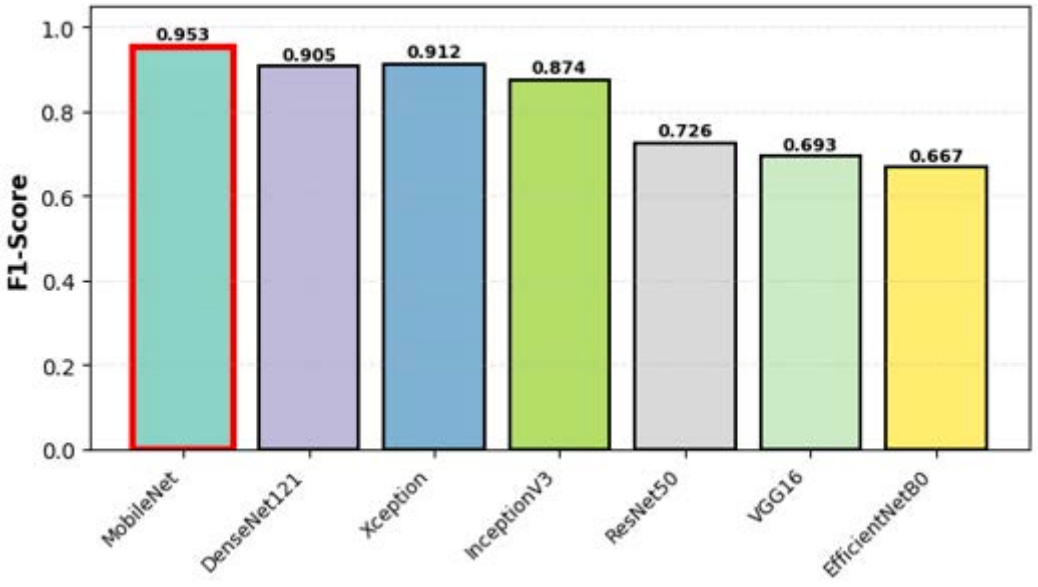

Figure 21 : Transfer Learning Model F1-Score Comparison

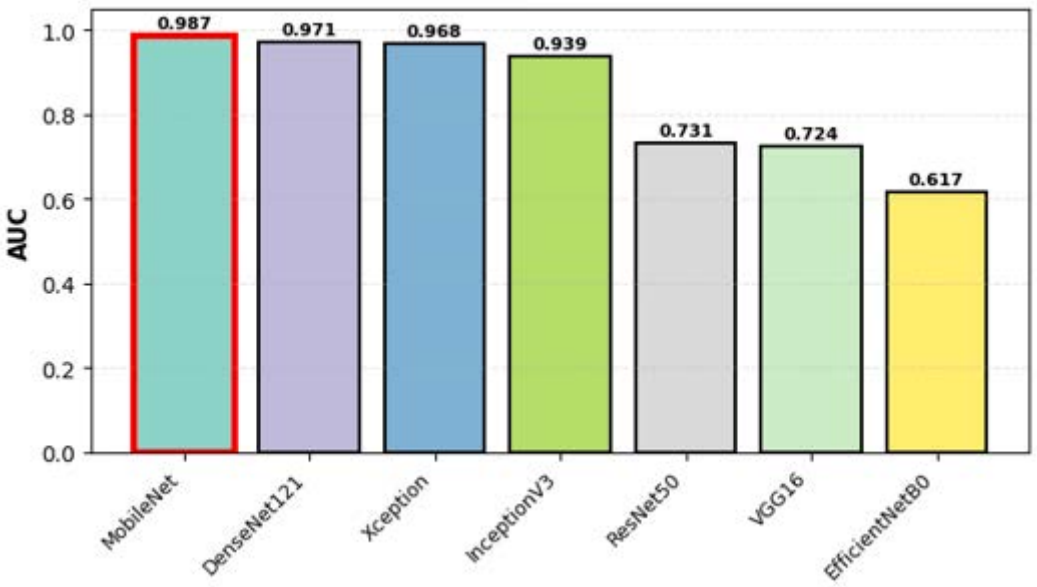

Figure 22 : Transfer Learning Model AUC Comparison

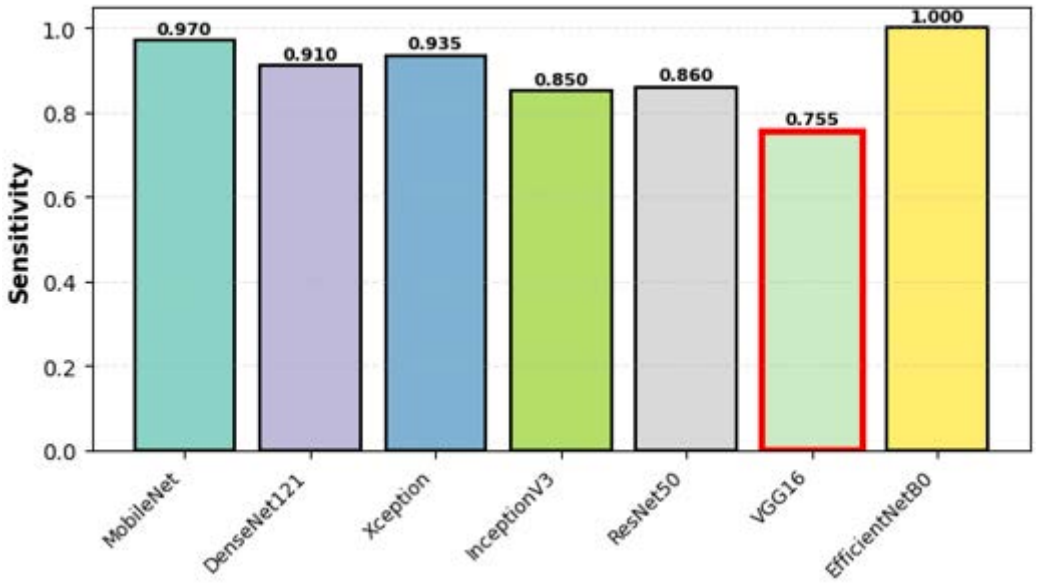

Figure 23: Transfer Learning Model Sensitivity Comparison

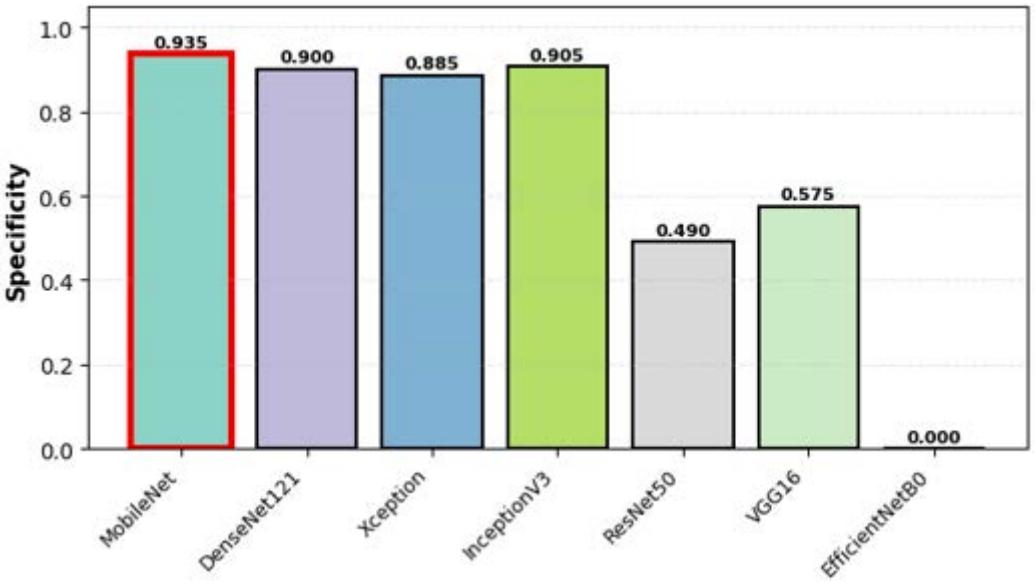

Figure 24 : Transfer Learning Model Specificity Comparison

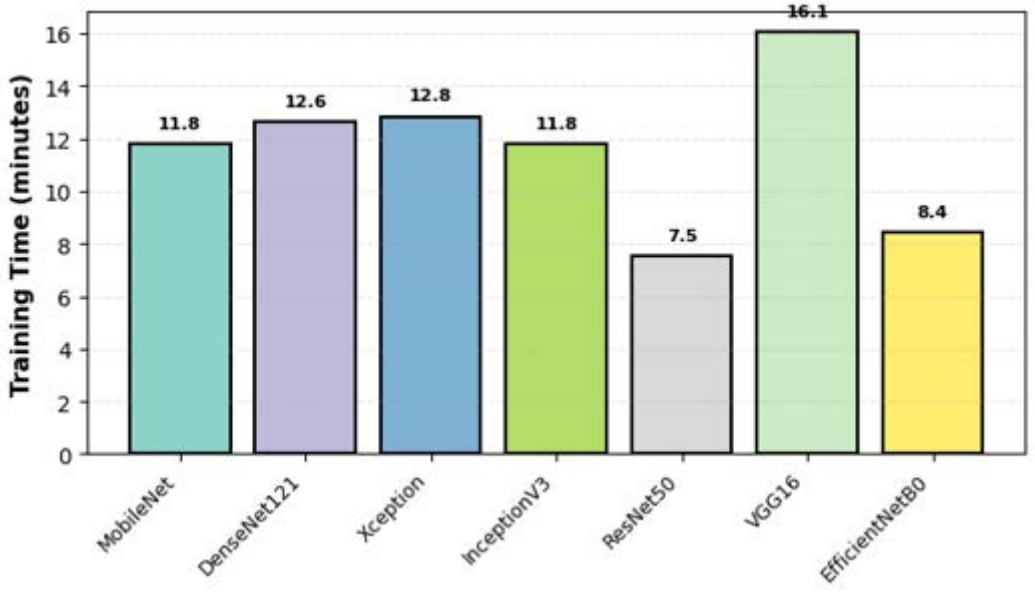

Figure 25 : Transfer Learning Model Training Time Comparison

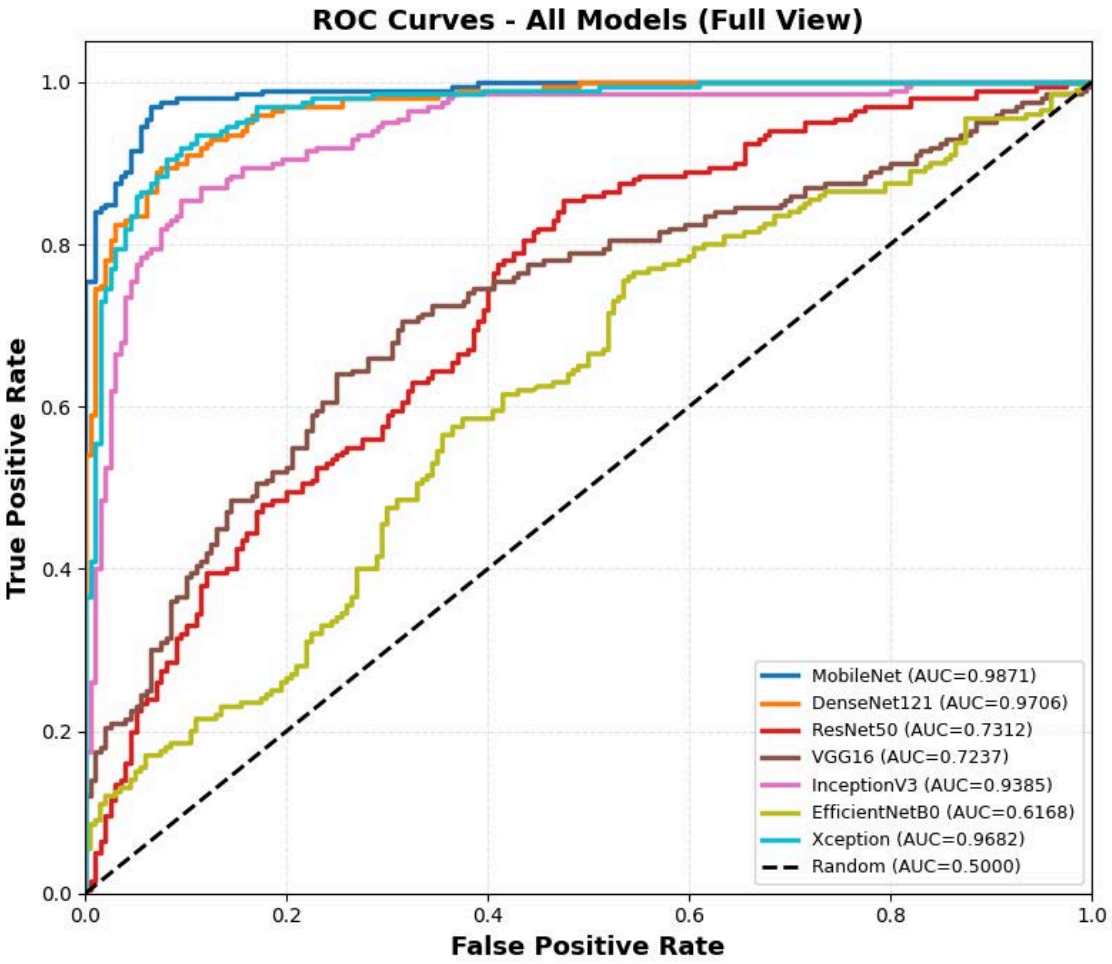

Figure 26 : Transfer Learning Model ROC comparison

In a summary

Table -5 : Different Models and their performances

Model	Training Time (min)	Accuracy	F1-Score	AUC	Sensitivity	Specificity
MobileNet	11.767047	0.9525	0.953317	0.98710	0.970	0.935
DenseNet121	12.634171	0.9650	0.905473	0.97662	0.910	0.900
Xception	12.834676	0.9100	0.912195	0.96817	0.935	0.885
InceptionV3	11.789789	0.8775	0.874036	0.93850	0.850	0.905
ResNet50	7.527671	0.6750	0.725738	0.73120	0.860	0.490
VGG16	16.057580	0.6650	0.692661	0.72367	0.755	0.575
EfficientNetB0	8.429806	0.5000	0.666667	0.61683	1.000	0.000

MobileNet was selected as the primary model based on its consistent superiority across all evaluation criteria and its computational efficiency. It achieved the highest AUC (0.9871), accuracy (0.9525), F1-score (0.9533), and balanced accuracy (0.9525), outperforming DenseNet121 (AUC 0.9706; accuracy 0.9050; F1 0.9055) and Xception (AUC 0.9682; accuracy 0.9100; F1 0.9122). The alignment between accuracy and balanced accuracy indicates stable performance across classes after threshold optimization, while the top AUC reflects strong ranking ability independent of threshold choice. From an efficiency perspective, MobileNet's 3.89M parameters and 11.77-minute training time offer a favorable accuracy–complexity trade-off, reducing overfitting risk and enabling faster, resource-light training and deployment. Given its dominance in both discriminative performance and model compactness, MobileNet provides the most reliable and practical choice for the final system and for reporting in the thesis.

4.2.4.5 Model Training

The model was trained using transfer learning with a MobileNet backbone (ImageNet weights, include_top disabled) and a compact classification head. The dataset was prepared with an 80/20 train–validation split, extensive image augmentations (rotation, translation, zoom, horizontal flip, brightness), and rescaling to [0,1]. Class imbalance was addressed through balanced class weights.

Training proceeded in two stages. In Stage 1, most backbone layers were frozen, and only the head was trained using binary cross-entropy with Adam (learning rate 1e-3). Early stopping

and learning rate reduction (on validation AUC) were applied to stabilize convergence. In Stage 2, the entire backbone was unfrozen and fine-tuned with focal loss (gamma=2.0, alpha=0.75) and a reduced learning rate (Adam 1e-5), again with early stopping and learning rate scheduling based on validation AUC. After training, the decision threshold was optimized by sweeping 0.2–0.6 to maximize the F1-score on the validation set.

Performance was reported using accuracy, balanced accuracy, F1-score, AUC, sensitivity, specificity, and the confusion matrix. ROC curve was generated for interpretability, and the final trained model and figures were saved for reproducibility. Hyperparameters were fixed (image size 224×224, batch size 32, EPOCHS 10+20, SEED=42) to ensure consistent results.

In the evaluation phase, validation probabilities were generated, and the decision threshold was optimized to maximize both accuracy and F1, yielding an operating point at 0.524. At this threshold, the model achieved an accuracy of 0.9300, balanced accuracy of 0.9300, F1-score of 0.9289, AUC of 0.9699, sensitivity of 0.9150, specificity of 0.9450, and precision of 0.9433 on a balanced validation set (n=400). Compared with the default threshold (0.5), the optimized threshold improved accuracy (+0.005), precision (+0.0096), and specificity (+0.010) while maintaining the same sensitivity, indicating fewer false positives without reducing the true-positive rate. Class-wise, benign cases reached a precision of 0.9175 and a recall of 0.9450 (F1 0.9310), and malignant cases reached a precision of 0.9433 and a recall of 0.9150 (F1 0.9289). The high AUC confirms strong separability, and the close match between accuracy and balanced accuracy indicates consistent performance across classes.

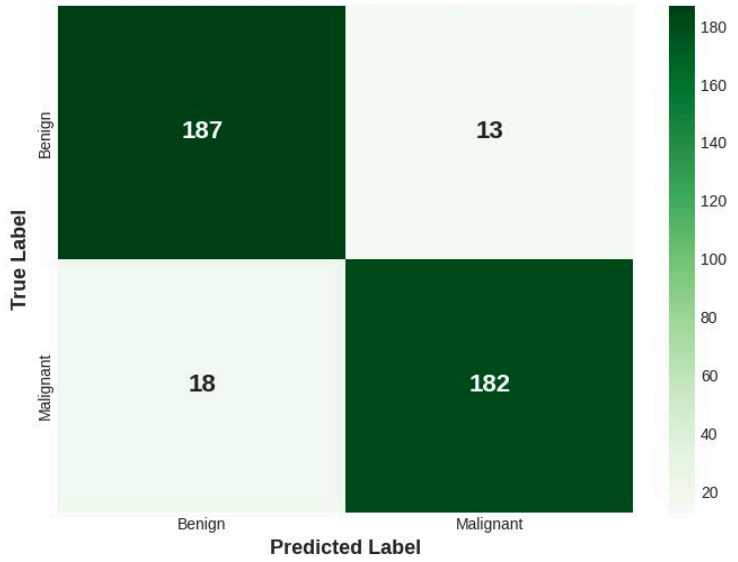

Figure 27 : Confusion matrix

Table -6 : MobileNet Model and performance

Metric	Default Threshold (0.5)	Optimal Threshold (0.52)
Accuracy	0.925000	0.930000
Balanced Accuracy	0.925000	0.930000
Precision	0.933673	0.943299
Recall	0.915000	0.915000
F1-Score	0.924242	0.928934
AUC	0.969875	0.969875
Sensitivity	0.915000	0.915000
Specificity	0.935000	0.945000

Approach 1 demonstrates that non-invasive breast cancer detection can be significantly enhanced by preprocessing thermal images through edge detection and deep learning with MobileNet. The high classification accuracy validates this combined method as an effective solution for accessible and affordable cancer screening, especially in low-resource settings. This work lays a strong foundation for developing portable thermal imaging devices integrated with AI-driven diagnostics.

4.2.5 Approach 2

Approach 2 employs a machine learning–driven framework for automated breast cancer detection using ultrasound imaging, leveraging recent advances in deep learning and transfer learning. The primary objective of this approach is to enable reliable identification, classification, and localization of breast lesions from ultrasound images by distinguishing between normal tissue, benign tumors, and malignant tumors. By automating image interpretation, this approach aims to reduce inter-operator variability and support faster, data-driven decision-making in clinical workflows.

Ultrasound imaging presents a unique set of challenges for machine learning analysis due to inherent noise, speckle artifacts, and variability introduced by probe positioning and tissue heterogeneity. To address these challenges, deep learning models particularly convolutional neural networks (CNNs) are employed to learn hierarchical spatial features directly from raw image data. Transfer learning techniques are incorporated to improve model convergence and performance by leveraging pretrained feature extractors, thereby reducing the dependency on extremely large, task-specific datasets.

From an optimization perspective, the ML models in this approach are evaluated not only for classification accuracy but also for robustness, generalization capability, and sensitivity to image quality variations. These factors are critical in assessing whether ultrasound-based AI systems can function reliably across different clinical environments and acquisition conditions.

4.2.5.1 Dataset Used: BUS-BRA and Public Breast Ultrasound Images

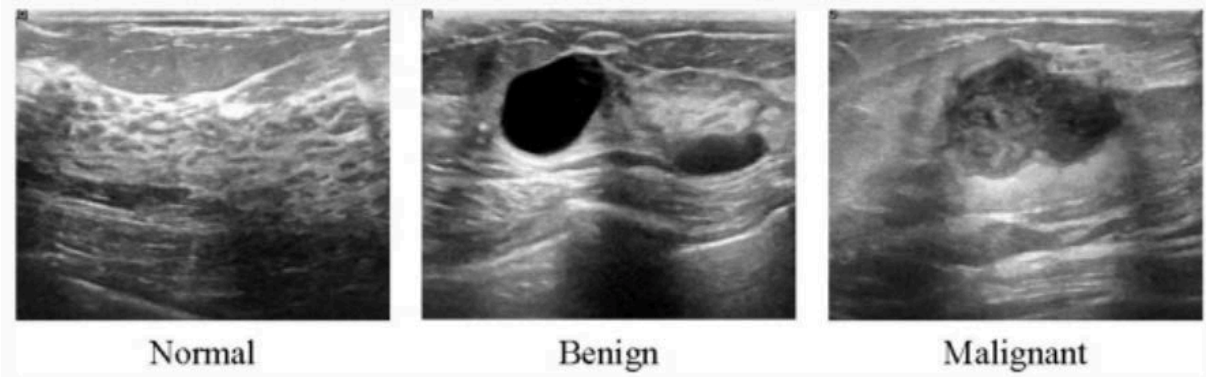

Figure 28 : Different Cases of Data Images

Figure: Dataset view

To validate the feasibility and performance of the ultrasound-based ML pipeline, two well-established and publicly available datasets were utilized. These datasets were selected due to their credibility, extensive use in peer-reviewed research, and suitability for multiclass classification and segmentation tasks.

The **BUS-BRA dataset** is a comprehensive breast ultrasound image repository that includes cases annotated with benign and malignant tumor labels, along with corresponding BI-RADS categories. The dataset comprises ultrasound images collected from **1,064 patients** who underwent routine breast imaging studies. A key strength of BUS-BRA is the availability of **ground truth segmentation masks**, which delineate tumor regions within each image. This enables both lesion classification and pixel-level segmentation, supporting detailed evaluation of deep learning models.

In this project, the BUS-BRA dataset was used to assess the capability of ML models to detect and localize suspicious regions within ultrasound images. The availability of standardized annotations allows objective comparison between predicted outputs and clinically validated ground truth. All relevant preprocessing routines, segmentation pipelines, and baseline model implementations were adapted from the publicly available source code provided by the dataset maintainers, ensuring reproducibility and methodological consistency.

The second dataset, commonly referred to as the **Breast Ultrasound Images Dataset**, contains **1,578 grayscale ultrasound images** with a spatial resolution of **500 × 500 pixels**, collected from **600 female patients** aged between **25 and 75 years**. The dataset categorizes images into three clinically relevant classes: normal, benign, and malignant. Each image is provided in PNG format with corresponding labels validated through clinical diagnosis and peer-reviewed studies.

This dataset is widely used in academic research as a benchmark for evaluating ultrasound-based breast cancer detection systems. Its multiclass structure allows comprehensive evaluation of classification performance, particularly the model's ability to distinguish malignant lesions from benign conditions and normal tissue. The diversity in patient age and imaging conditions further supports assessment of model generalization.

Together, these two datasets provide a robust experimental foundation for validating the ultrasound-based ML approach. They enable systematic evaluation of model accuracy, sensitivity, specificity, and segmentation performance under realistic conditions. From an optimization standpoint, training and testing on these datasets allow assessment of how well ultrasound-based models perform relative to thermography-based approaches when subjected to real clinical variability.

In summary, the machine learning analysis for Approach 2 demonstrates that AI-enhanced ultrasonography is a technically capable and clinically relevant solution for breast cancer detection. The use of high-quality public datasets such as BUS-BRA and the Breast Ultrasound Images Dataset enables rigorous validation of deep learning models for both classification and segmentation tasks. However, the insights gained from this analysis also reveal practical constraints related to data acquisition and operational complexity, which are considered in the final optimization and design selection process presented in the following section.

4.2.5.2 Deep Learning Model: DenseNet121 and Transfer Learning

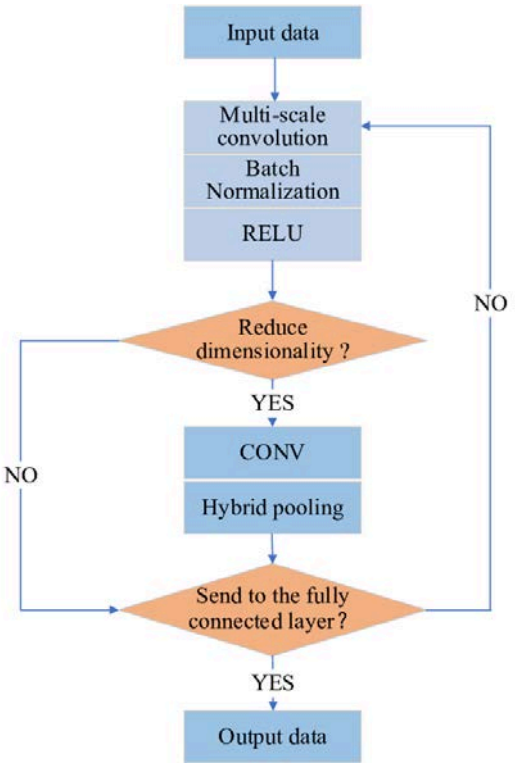

Figure 29 : Flowchart of DenseNet121

For classification, we relied on DenseNet121, a state-of-the-art Convolutional Neural Network (CNN) architecture widely known for its superior performance in medical image analysis. The workflow involved transfer learning, which adapts a powerful pre-trained base model to our specific breast ultrasound task:

- Initial layers of DenseNet121, trained on large generic datasets, remain frozen to preserve general feature extraction capabilities.
- The final layers are fine-tuned using our labeled BUS-BRA and public ultrasound images, optimizing the model for breast cancer-specific patterns.
- The classification problem is handled as multiclass learning, where the goal is to sort images into one of three categories: normal, benign, or malignant.

This methodology allows us to benefit from powerful deep learning features without needing millions of custom-labeled images, a critical advantage for applied research in medical settings.

4.2.5.3 Model Workflow and Evaluation

The model pipeline consists of these key stages:

- Data preprocessing: Images are resized, normalized, and split into training, validation, and test sets.
- Training: The fine-tuned DenseNet121 model learns discriminative features for each tumor class using the annotated images and ground truth segmentations.
- Validation: Model performance is monitored on a separate validation set to avoid overfitting.
- Testing: Final accuracy and robustness are measured using a held-out test set. The pipeline also includes semantic segmentation using DeepLabV3+ (with ResNet backbones) for precise lesion localization, further supporting the multiclass classification framework.

4.2.5.4 Results Achieved

Table -7 : Experimental results

Set	Loss	Accuracy
Train	0.038702	99.04%
Validation	0.188313	90.97%
Test	0.136501	94.94%

The experimental results validate our approach:

- Model accuracy on the test set reached 94.94%, confirming robust generalization to unseen cases.
- Loss values (ranging from 0.038 on training to 0.136 on test) indicate good convergence and predictive stability.
- The classification report from the test set shows macro-averaged precision, recall, and F1 scores all above 0.93, and high per-class performance. Malignant cases (critical for diagnosis) registered a recall of 1.00 and a precision of 0.88.

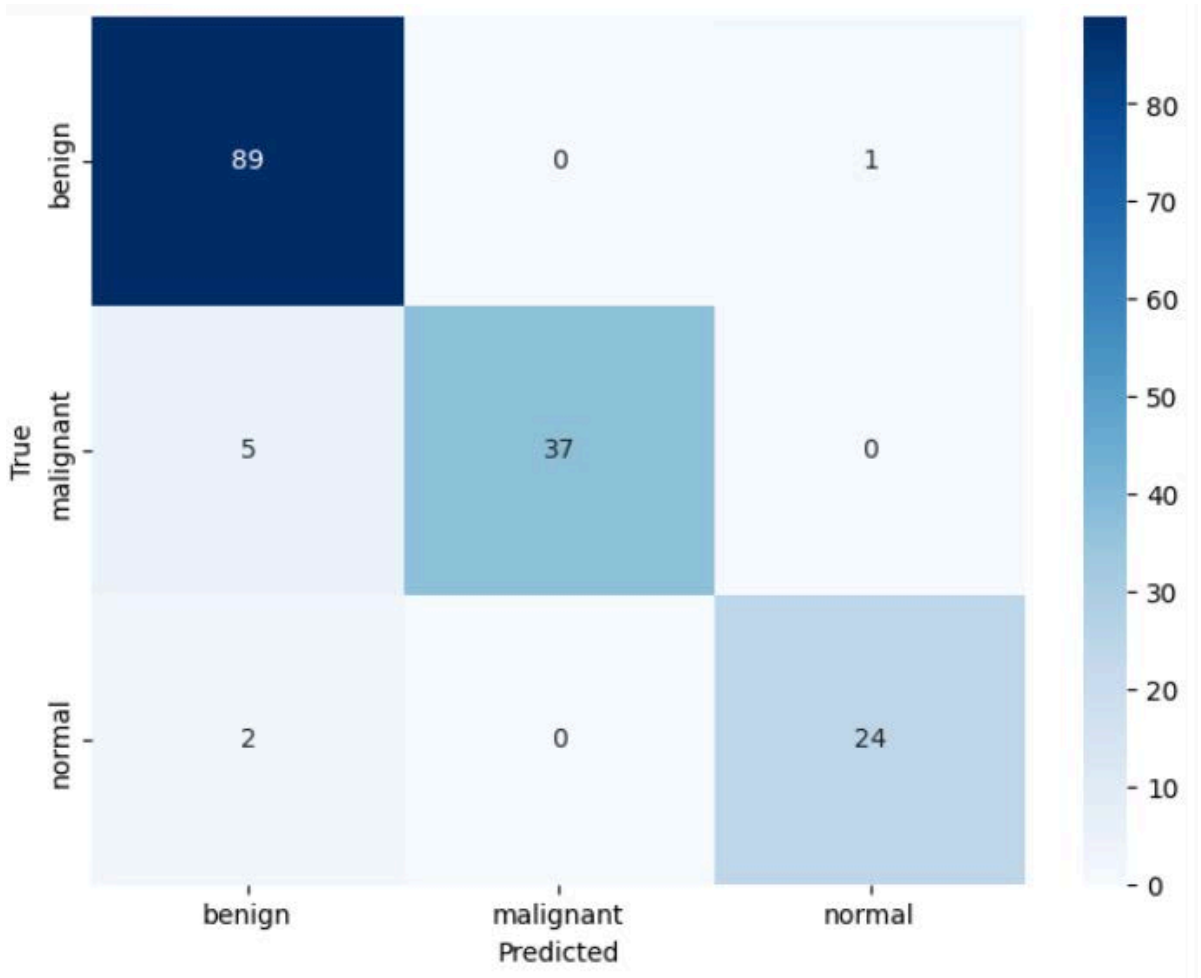

Figure 30 : Confusion matrix of DenseNet121

- The confusion matrix demonstrates the model's ability to differentiate correctly between benign, malignant, and normal tissue.

This level of performance is in line with leading academic benchmarks and shows the practical effectiveness of our method using real, diverse patient data.

Table -8: :Performance Table

Precision	Recall	F1-Score	Support	
Benign	0.93	0.99	0.96	90
Malignant	1.00	0.88	0.94	42
Normal	0.96	0.92	0.94	26
----------	----------	--------	----------	---------
Accuracy			0.95	158
Macro Avg	0.96	0.93	0.94	158
Weighted Avg	0.95	0.95	0.95	158

Our ML pipeline for Approach 2 uses public datasets and proven architectures to deliver high-accuracy, automated cancer detection from ultrasound images. All model training and experiments were transparently reproduced using the open-source BUS-BRA codes and datasets, ensuring reliability and reproducibility. As our next step, we plan to curate our own dataset tailored to the local healthcare context, which will enable additional fine-tuning and eventually deployment of an optimized, field-ready cancer screening solution.

4.2.6 VOC Justification

Table 9: Characteristics of breast-derived cell lines.

Cell line	Isolated from	Histology	CDT (h)	ER	PgR	HER2	Molecular Subtype
MCF-10a	BT	FD	96	-	-	-	-
MDA-231	PE	ADC	24	-	-	-	Triple negative
MCF-7	PE	IDC	24	+	+	-	Lumina A
SKBR-3	PE	ADC	36	-	-	+	ERB type
BT-474	PT	IDC	48	-	+	+	Luminal B
BT-474	PE	IDC	80	+	+	+	Luminal B

BT, non-malignant breast tissue;

FD, fibrocystic disease;

PE, pleural effusion;

PT, primary tumor;

ADC, adenocarcinoma;

IDC, intraductal carcinoma.

The results of the IHC characterization of the breast cell lines are indicated. ER/PgR/HER2 status: ER/PgR positivity, HER2 overexpression. The molecular classification of the breast cancer cell lines subtypes according to WHO guidelines is reported.

ER (Estrogen Receptor): This indicates the presence or absence of estrogen receptors on the surface of breast cancer cells.

ER positivity (+) suggests that the cancer cells may grow in response to estrogen, and these tumors are often treated with hormone therapies (e.g., tamoxifen). ER negativity (-) means the cancer is not driven by estrogen.

PgR (Progesterone Receptor): This indicates the presence or absence of progesterone receptors. Like ER, PgR positivity (+) implies that the cancer may be influenced by progesterone, and it often correlates with ER positivity. PgR negativity (-) indicates no significant progesterone receptor activity.

HER2 (Human Epidermal Growth Factor Receptor 2): This refers to the overexpression or amplification of the HER2 gene, which promotes cell growth. HER2 positivity (+) indicates an aggressive form of breast cancer that may respond to targeted therapies like trastuzumab (Herceptin). HER2 negativity (-) means the HER2 gene is not overexpressed.

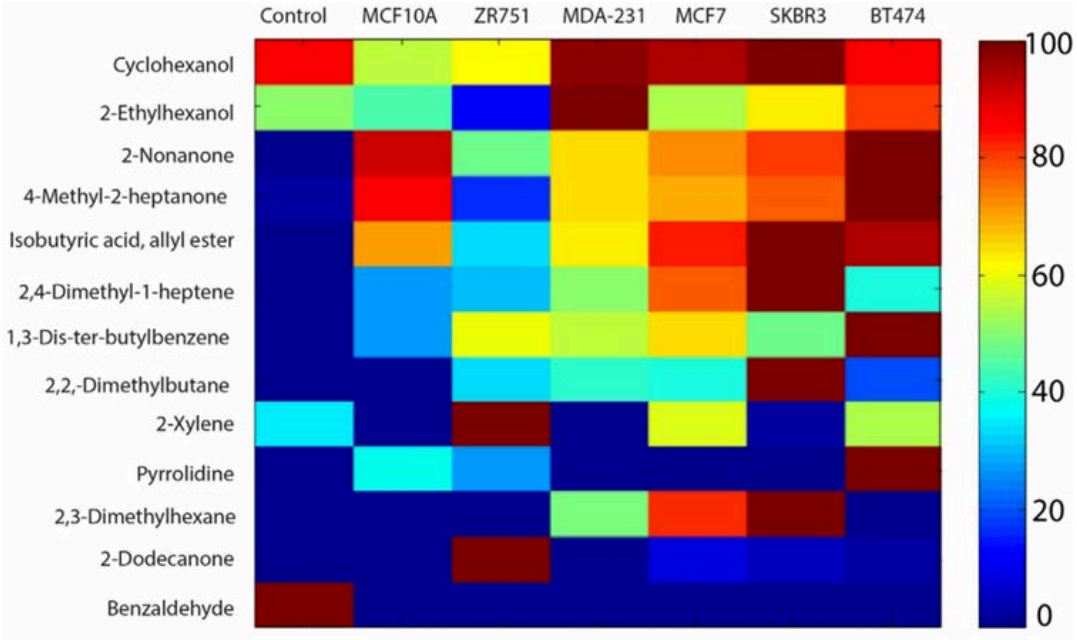

Figure 31 : Fingerprint patterns of VOCs detected in headspace of breast-derived cell lines.

The heatmap shows the abundance of selected volatile organic compounds (VOCs) detected in the headspace of breast-derived cell lines (Control, MCF10A, ZR75-1, MDA-231, MCF7, SKBR3, BT474). The color-coding, normalized to the maximum abundance across all

samples, indicates the relative concentration of each VOC, with red representing high abundance and blue representing low abundance.

Table 10 : VOCs discriminating the headspace of breast-derived cell lines.

Trend	Class	Compound	CAS number	P value
Increase	Aromatic Amines	Pyrrolidine	123-75-1	0.02
	Hydrocarbons	2,3-Dimethylhexane	584-94-1	1.8 × 10^−4
		2,4-Dimethyl-1-heptene	19549-87-2	1.3 × 10^−9
		2,2-Dimethylbutane	75-83-2	8.1 × 10^−5
		1,3-Di-tert-butylbenzene	1014-60-4	1.8 × 10^−9
		2-Xylene	95-47-6	0.77
	Ketons	2-Nonanone	821-55-6	6.5 × 10^−21
		4-Methyl-2-heptanone	6137-06-0	5.8 × 10^−11
		2-Dodecanone	6175-49-1	3.6 × 10^−3
	Carboxylic acid	Isobutyric acid, allyl ester	15727-77-2	3.6 × 10^−10
	Fatty alcohol	2-Ethylhexanol	104-76-7	0.41
Decrease	Aromatic aldehyde	Benzaldehyde	100-52-7	0.013
	Secondary alcohol	Cyclohexanol	108-93-0	0.92
Manova				1.6 × 10^−16

VOCs released (increase) or consumed/degraded (decrease) by breast cell lines are reported with respect to the control medium. The p-values obtained by t-test analysis for each compound and by MANOVA analysis (MANOVA is Multivariate Analysis of Variance) for all compounds are shown. A p-value < 0.05 (the statistical significance of the difference in the concentration or presence of each compound between the compared groups) has been considered statistically significant.

Table 11 : VOCs discriminating breast non-transformed from cancer-derived cell lines.

Trend	Class	Compound	CAS number	p value
Increase	Hydrocarbons	2,4-Dimethyl-1-heptene	19549-87-2	3.0 × 10^−4
		2-Xylene	95-47-6	1.0 × 10^−4
		2,3-Dimethylhexane	584-94-1	1.0 × 10−4
		2,2-Dimethylbutane	75-83-2	1.0 × 10^−4
	Secondary Alcohol	Cyclohexanol	108–93-0	2.0 × 10^−5
	Ketons	2-Dodecanone	6175-49-1	0.003
Decrease	Ketons	2-Nonanone	821-55-6	0.03
		4-Methyl-2-heptanone	6137-06-0	0.04
Manova*				7.7 × 10^−3

A p-value < 0.05 has been considered statistically significant. *considering all the VOCs of the previous Table

Increase (9 VOCs): These compounds are higher in cell-exposed media than in the control, likely produced by cell metabolism.

What it means: Out of the 13 VOCs in the table, 9 have higher concentrations in the air (headspace) above media that have cells in them, compared to the control media (which has no cells). This suggests the cells are actively creating or releasing these VOCs as part of their normal life processes (metabolism), like waste products or byproducts from breaking down food.

Why it's important: It points to VOCs that cells "make," which could be signs of cell activity—useful for detecting cancer-related changes. Thus, p-values are low here.

Example: 2,4-Dimethyl-1-heptene ($p = 1.3 \times 10^{-9}$)

Decrease (2 VOCs): These are lower in cell-exposed media than in the control, suggesting cells use them up.

What it means: For these 2 VOCs, the levels drop in the headspace when cells are present, compared to the control. This implies the cells are absorbing, consuming, or breaking down these compounds for energy or other needs, reducing what's left in the air.

Why it's important: It highlights VOCs that cells "take in" or destroy, which might indicate specific metabolic needs in breast cells, helping identify differences in healthy vs. cancerous states.

Example: Benzaldehyde (p = 0.013)

Table 12 : Correlation of VOCs with replication time and molecular markers of breast-derived cell lines.

Class	Compound	CDT	ER status	PgR status	HER2 status
		>48 h vs ≤48 h	(−) vs (+)	(−) vs (+)	(−) vs (+)
Hydrocarbons	2,4-Dimethyl-1-heptene	2.9×10^{-4}↑	0.78	0.30	0.89
	1,3-Di-tert-butylbenzene	0.29	0.88	0.049↑	0.25
	2-Xylene	0.14	6.2×10^{-4}↑	2.5×10^{-5}↑	0.08
	2,3-Dimethylhexane	8.4×10^{-5}↑	0.98	0.15	0.41
Secondary alcohol	Cyclohexanol	0.001↑	0.42	0.51	0.78
Fatty alcohol	2-Ethylhexanol	1.9×10^{-6}↑	9.1×10^{-5}↓	0.046↓	0.16
Carboxylic acid	Isobutyric acid, allyl ester	0.04↑	0.12	0.59	0.86
Ketons	2-Dodecanone	0.009↓	0.003↑	0.005↑	0.01↑
	2-Nonanone	0.11	0.001↓	0.58	0.85
	4-Methyl-2-heptanone	0.023↑	6.4×10^{-4}↓	0.18	0.48
Manova		5×10^{-4}	3.5×10^{-5}	7.4×10^{-4}	0.03

The arrows in this table indicate the trend (direction of change) for the concentration or presence of each volatile organic compound (VOC) in the specified groups

↑ (Upward arrow): Indicates an increase in the compound's abundance or concentration in the first group compared to the second group (e.g., >48h vs. ≤48h for CDT, (-) vs. (+) for ER, PgR, or HER2 status).

↓ (Downward arrow): Indicates a decrease in the compound's abundance or concentration in the first group compared to the second group.

Example:

2,4-Dimethyl-1-heptene: The ↑ p-value of 2.9×10^{-4} for CDT (>48h vs. ≤48h) means its concentration increases significantly in cell lines with a doubling time >48h compared to ≤48h.

2-Ethylhexanol: The ↓ with a p-value of 9.1×10^{-5} for ER status (-) vs. (+) means its concentration decreases significantly in ER-negative (-) cell lines compared to ER-positive (+) cell lines.

Table 13 : Confusion Matrix of self-modulation sensor outputs.

		predicted	
		Cancer	**No cancer**
measured	Cancer	29	4
	No cancer	3	12
	Sensitivity (%)	88	
	Specificity (%)	80	
	Accuracy (%)	85	

Classification success of the PLS-DA (Partial Least Squares Discriminant Analysis: a statistical method used in this context to classify and predict breast cancer cell line-derived samples from other samples based on the confusion matrix data) classification model to predict breast cancer cell line-derived samples from all other. samples Sensitivity = TP/ (TP + FN); specificity = TN/(TN + FP); accuracy = (TP + TN)/(TP + TN + FP + FN). Where TP = True Positive; TN = True Negative; FP = False Positive; FN = False Negative.

Table 14 : VOC detection with the proposed sensors

Compound	CAS Number	Chemical Class	Sensors Likely to Detect	Notes
Pyrrolidine	123-75-1	Aromatic Amine	TGS2602, MQ-135	TGS2602 and MQ-135 are sensitive to ammonia and amines.
2,3-Dimethylhexane	584-94-1	Hydrocarbon	TGS2620, MQ-138	Similar to toluene/xylene; detected by TGS2620 (organic solvents) and MQ-138.
2,4-Dimethyl-1-heptene	19549-87-2	Hydrocarbon	TGS2620, MQ-138	Alkene, similar to toluene; detected by TGS2620 and MQ-138.
2,2-Dimethylbutane	75-83-2	Hydrocarbon	TGS2620, MQ-138	Alkane, similar to toluene; detected by TGS2620 and MQ-138.
1,3-Di-tert-butylbenzene	1014-60-4	Hydrocarbon (Aromatic)	TGS2620, TGS2602, MQ-138	Aromatic, similar to toluene/xylene;

				detected by TGS2620, TGS2602, MQ-138.
2-Xylene	95-47-6	Hydrocarbon (Aromatic)	TGS822, TGS2620, TGS2602, MQ-138	Xylene is explicitly detected by these sensors.
2-Nonanone	821-55-6	Ketone	TGS2602, MQ-135, MQ-138	Ketone; TGS2602 (VOCs), MQ-135 (ketones), MQ-138 (acetone-like).
4-Methyl-2-heptanone	6137-06-0	Ketone	TGS2602, MQ-135, MQ-138	Ketone; similar to 2-nonanone, detected by the same sensors.
2-Dodecanone	6175-49-1	Ketone	TGS2602, MQ-135, MQ-138	Long-chain ketone; detected by TGS2602, MQ-135, MQ-138.
2-Ethylhexanol	104-76-7	Fatty Alcohol	TGS822, TGS2620, MQ-135, MQ-138	Alcohol; detected by TGS822 (ethanol), TGS2620, MQ-135, MQ-138.
Benzaldehyde	100-52-7	Aromatic Aldehyde	TGS2602	Aldehyde; TGS2602 is explicitly sensitive to benzaldehyde.
Cyclohexanol	108-93-0	Secondary Alcohol	TGS822, TGS2620, MQ-135, MQ-138	Alcohol; detected by TGS822, TGS2620, MQ-135, MQ-138.
Isobutyric acid, allyl ester	15727-77-2	Carboxylic Acid/Ester	TGS2602, MQ-135	Ester; TGS2602 (VOCs) and MQ-135 (organic compounds) likely to detect.

4.2.6 Circuit Simulation

Both approaches incorporate specific hardware components. In Approach 1, the system features a sensor array consisting of multiple gas sensors, which is powered by a buck converter to ensure a stable power supply. In Approach 2, the hardware requirements are simpler, with the buck converter acting as the primary power regulation unit.

4.2.6.1 Approach 1:

4.2.6.1.2 Sensor simulation:

We used **Proteus** software to simulate the sensors. Knowing that we will be using the Raspberry Pi 4 Model B 8GB version, we chose the same model to simulate our system. The Raspberry Pi does not have dedicated analog pins. We used an analog-to-digital converter to read the values because the majority of the sensors we use are analog and only produce analog output. So, the components we are simulating include:

Table 15 :Components name and type

Component name	Type
Raspberry Pi 4	On board computer
MQ-3	Gas sensor
MQ-4	Gas sensor
MQ-135	Gas sensor
LM35	Temperature sensor
MCP3008	Analog-to-digital converter

4.2.6.1.3 Simulation Proteus:

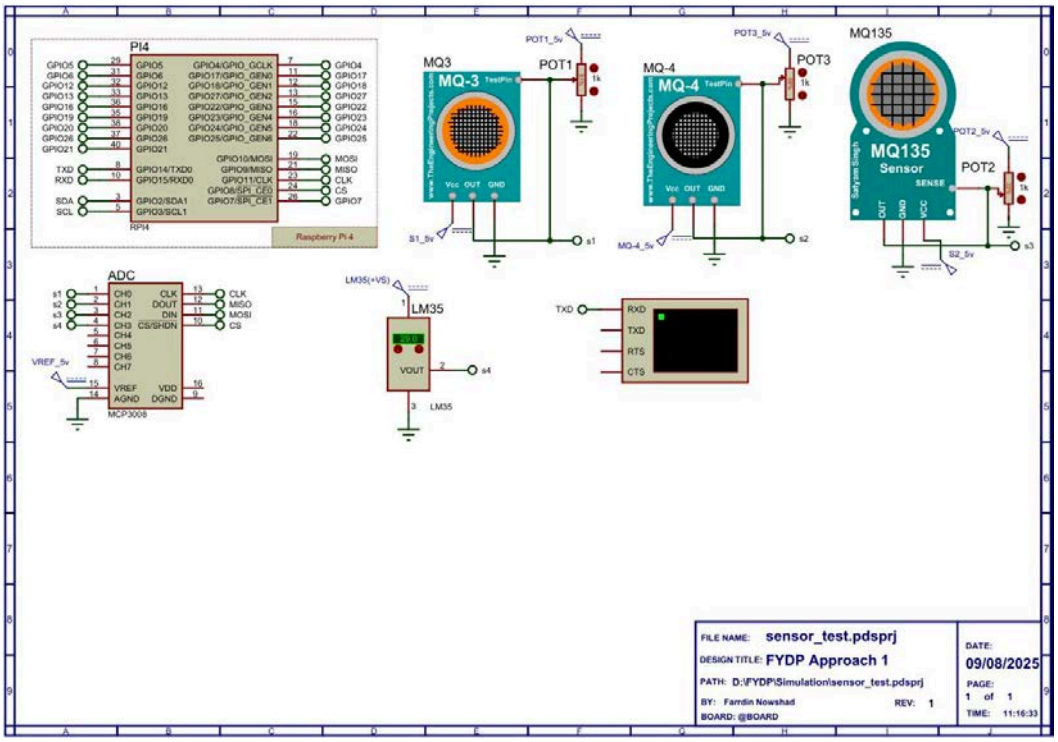

Figure 32 : Sensor simulation in Proteus.

After making this, we wrote a code in *Python 3* and did our simulation.

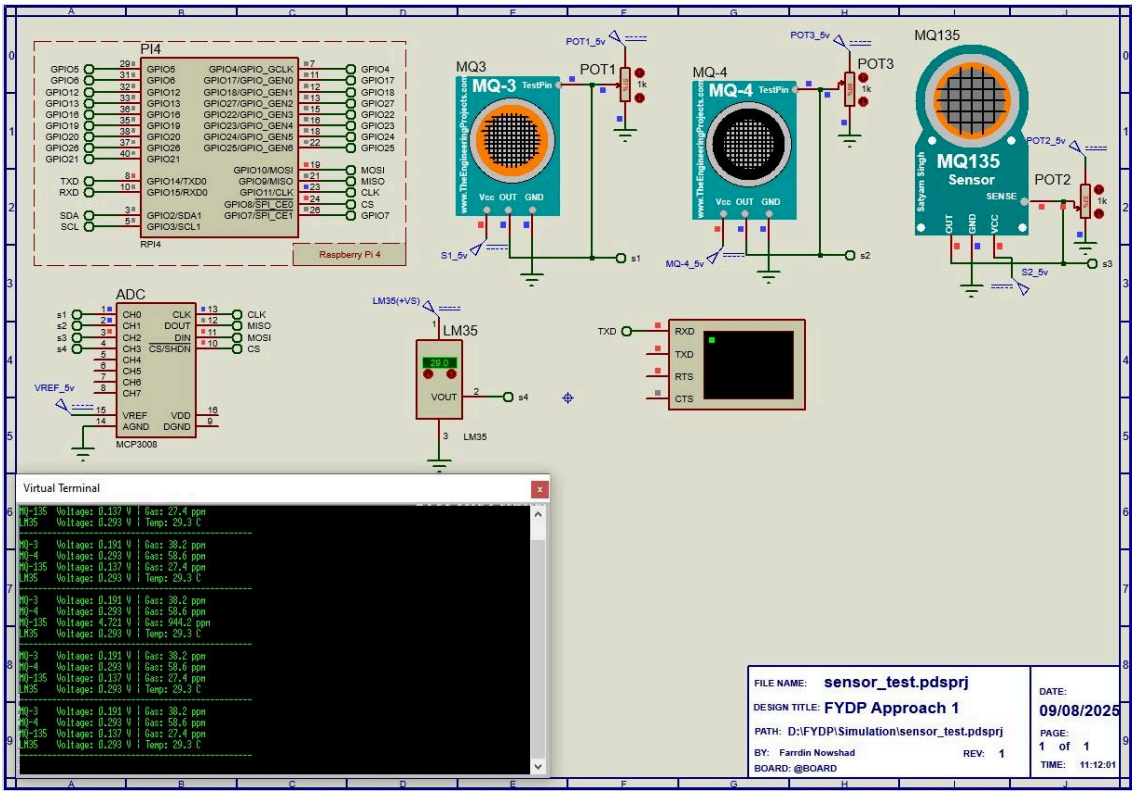

Figure 33 : Real-time data reading from Proteus simulation.

After confirming that the simulation was working properly and that we were receiving real-time data, we proceeded to the next step, which was to connect all of the sensors and create a sensor array. The circuit diagram of the sensor array is given below:

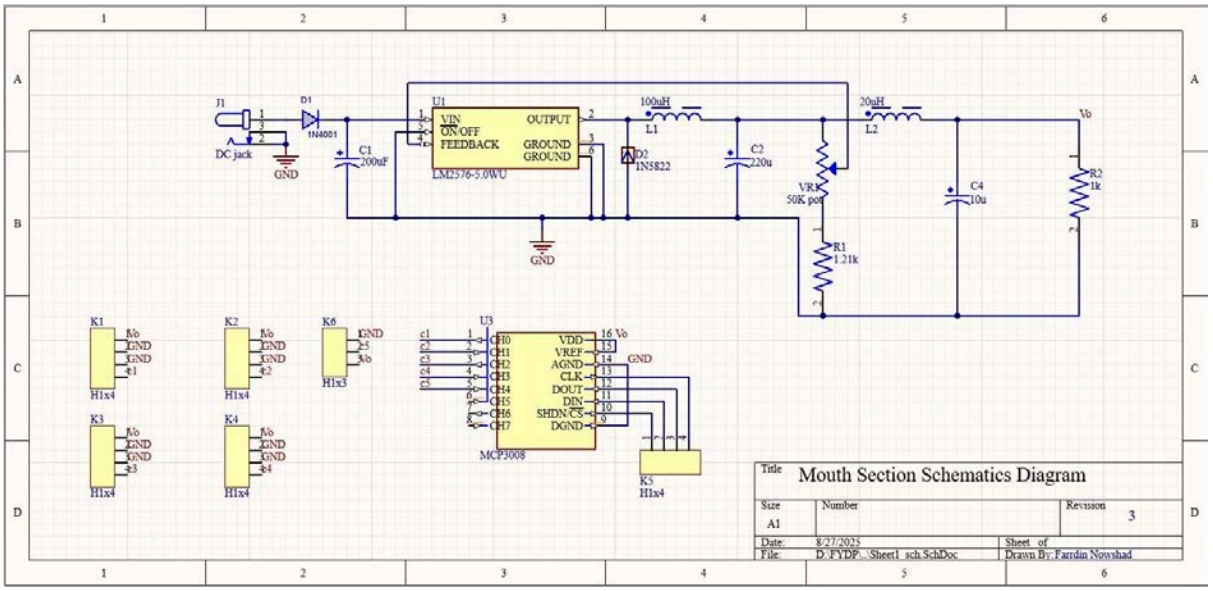

Figure 34 : The circuit diagram of the sensor array in Altium.

To create the circuit diagram, we have used **Altium Designer.** We used it because we needed a PCB to hold everything in one place. The PCB layout of the sensor array is given below:

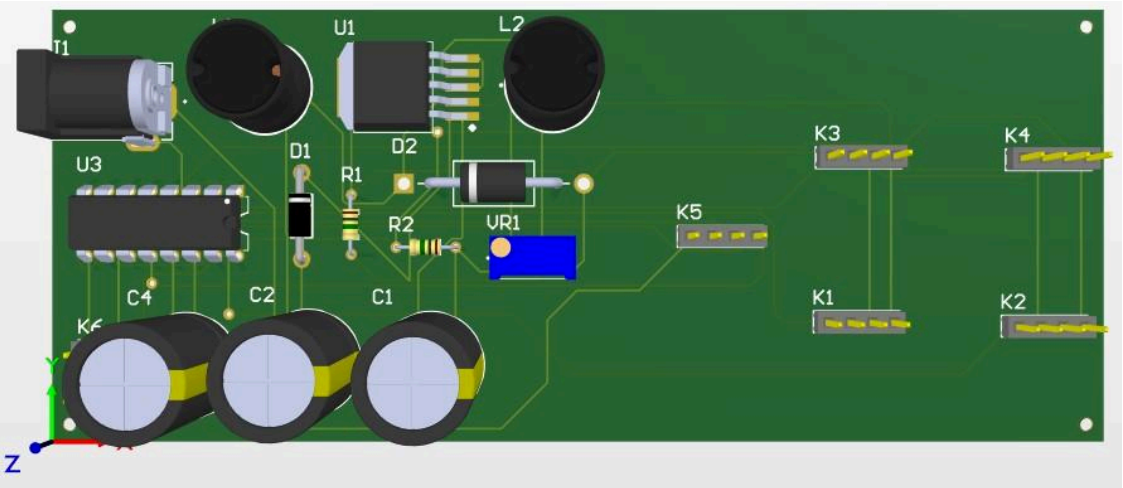

Figure 35 : The PCB Layout of the sensor array in Altium.

We added a Buck Module to the sensor array. We did it on purpose. The majority of the sensors in the sensor array require a constant 5-volt power supply. Not only that, but many other components have varying power ratings, so we used a buck converter to meet those requirements. As a result, we have significantly reduced the amount of wiring from power supplies to sensors.

To design the buck converter, we must first determine the amount of current and voltage required to power the circuit. That is why we have created a power budget first.

4.2.6.1.4 Power Budget of approach 1:

Table 16 :Estimated power budget for approach 1

Component	Operating Voltage (V)	Typical Current Draw	Power Consumption
MQ-3	5	~150–165 mA	~750–825 mW
MQ-4	5	~150–180 mA	~750–900 mW
MQ-135	5	~150 mA	~750 mW
LM35	4–30	~60 µA	~1.8 mW
Raspberry Pi 4 (8 GB)	5	~3A	~15W
FLIR Lepton 3.5 (module)	2.8		~160-300mW
Total			17.4-17.7W

So our power consumption is around 17.4-17.7W per hour. And, we need to provide more than 3A to operate all components properly.

Buck Converter Design for Approach 1:

Specifications

Input voltage: $V_{in} = 12V$

Output voltage: $V_o = 5V$ (LM2576-5.0 fixed output)

Load current: $I_o = 3A$

Switching frequency: f = 52kHz

Duty Ratio:

$$D = \frac{V_o}{V_{in}} = \frac{5}{12} = 0.417$$

Equivalent Load Resistance:

$$R = \frac{V_o}{I_o} = \frac{5}{3} = 1.67\Omega$$

Minimum Inductance for Continuous Current:

$$L_{min} = \frac{(1-D)R}{2f}$$

$$L_{min} = \frac{(1-0.417)1.67}{2\times52\times10^3} \approx 9.4\mu H$$

So, we choose L = 100µH (greater than L_{min})

Inductor Current Ripple:

$$\Delta i_L = \frac{(V_{in}-V_0)D}{Lf}$$

$$\Delta i_L = \frac{(12-5)0.417}{100\times10^{-6}\times52\times10^3} \approx 0.56A$$

Average current:

$$I_L = I_o = 3A$$

Peak current:

$$I_{peak} = I_L + \frac{\Delta i_L}{2} = 3 + 0.56 = 3.56A$$

So, the selected inductor is rated for ≥ 3A

Output Capacitor:

$$C = \frac{1-D}{8L(\frac{\Delta V}{V_o})f^2}$$

$$C = \frac{1-0.417}{8\times100\times10^{-6}\times0.01\times(52\times10^{3})^{2}} = 27\mu F$$

So, we selected a 220µF capacitor. (Larger than the calculated value)

4.2.6.1.5 Summary of Component Choices

Table 17 :Components type and corresponding value.

Component	Rating
Inductor	100µH, ≥ 3A rating
Capacitor	220µF
Diode	1N5822
Input capacitor	220µF bulk

Now, according to the calculated parameters, we have designed the buck converter. To validate our calculation, we have used **Simulink**.

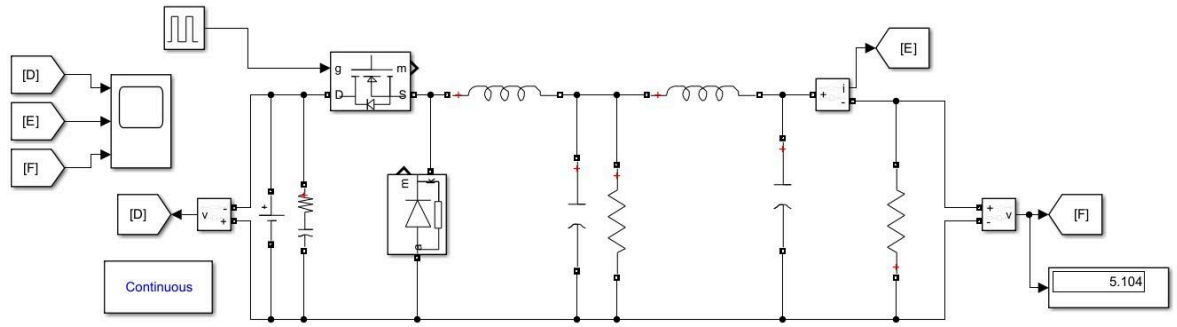

Figure 36 : Block diagram of the buck converter in Simulink

Then we obtained the I-V characteristics of the buck converter.

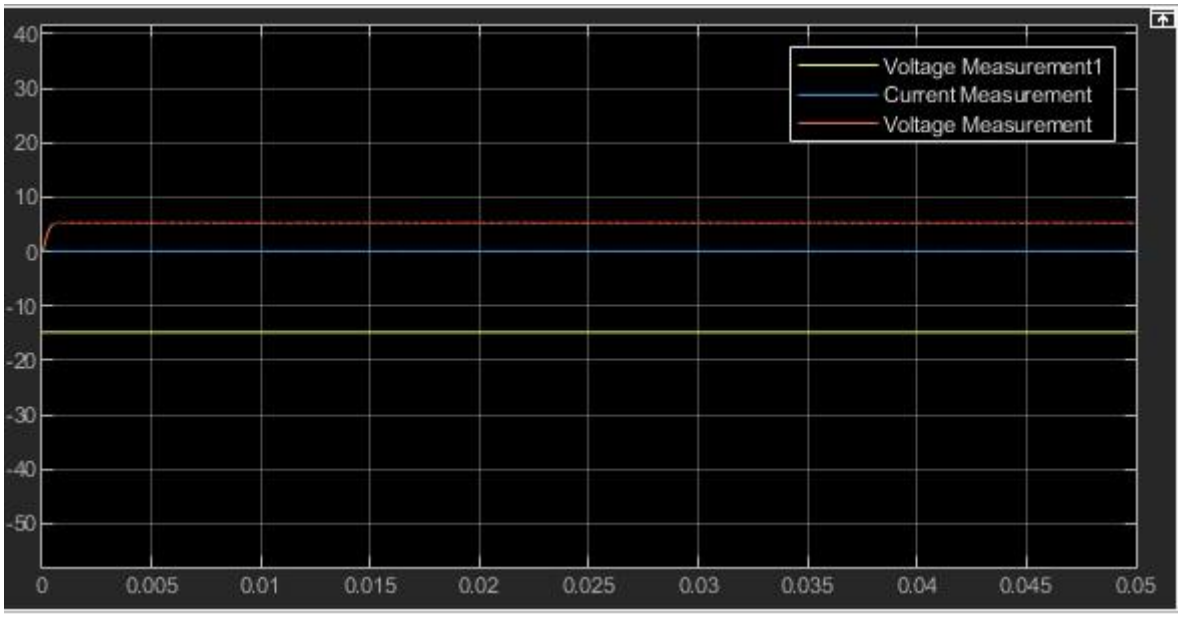

Figure 37 : I-V characteristics of the buck converter in Simulink

Here, we can see that we are getting the expected output. We are getting a constant 5V DC output. So we can say that our calculation is correct.

4.2.6.2.1 Approach 2:

In Approach 2, we have no components that require a different voltage rating than the Raspberry Pi. So we'll need a buck converter there as well. Raspberry Pi 4 operates on 5 volts and requires a constant 3A current. So we have to design according to that.

4.2.6.2.2 Buck Converter Design for Approach 2:

Specifications

Input voltage: $V_{in} = 12V$

Output voltage: $V_o = 5V$ (LM2576-5.0 fixed output)

Load current: $I_o = 3A$

Switching frequency: f = 52kHz

Duty Ratio:

$$D = \frac{V_o}{V_{in}} = \frac{5}{12} = 0.417$$

Equivalent Load Resistance:

$$R = \frac{V_o}{I_o} = \frac{5}{3} = 1.67\Omega$$

Minimum Inductance for Continuous Current:

$$L_{min} = \frac{(1-D)R}{2f}$$

$$L_{min} = \frac{(1-0.417)1.67}{2\times52\times10^3} \approx 9.4\mu H$$

So, we choose L = 100µH (greater than L_{min})

Inductor Current Ripple:

$$\Delta i_L = \frac{(V_{in}-V_0)D}{Lf}$$

$$\Delta i_L = \frac{(12-5)0.417}{100\times10^{-6}\times52\times10^3} \approx 0.56A$$

Average current:

$$I_L = I_o = 3A$$

Peak current:

$$I_{peak} = I_L + \frac{\Delta i_L}{2} = 3 + 0.56 = 3.56A$$

So, the selected inductor is rated for ≥ 3A

Output Capacitor:

$$C = \frac{1-D}{8L(\frac{\Delta V}{V_o})f^2}$$

$$C = \frac{1-0.417}{8\times100\times10^{-6}\times0.01\times(52\times10^3)^2} = 27\mu F$$

So, we selected a 220µF capacitor. (Larger than the calculated value)

4.2.6.2.3 Summary of Component Choices

Table 18 : Components type and corresponding value.

Component	Rating
Inductor	100μH, ≥ 3A rating
Capacitor	220μF
Diode	1N5822
Input capacitor	220μF bulk

Now, according to the calculated parameters, we have designed the buck converter. To validate our calculation, we have used **Simulink**.

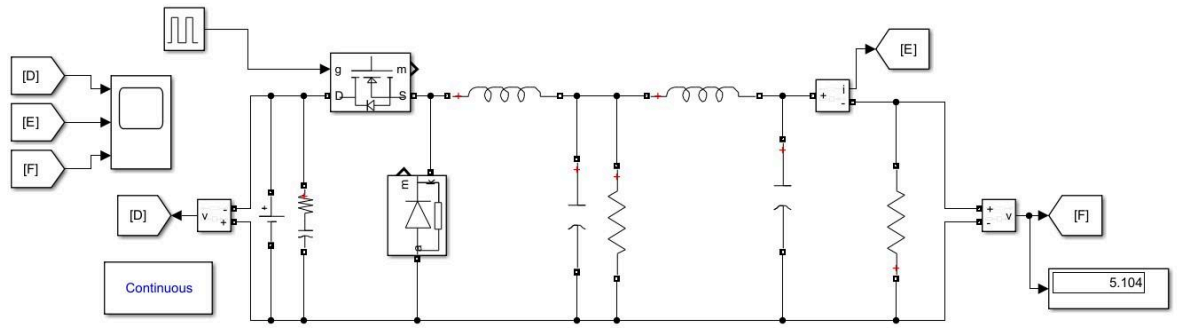

Figure 38 : Block diagram of the buck converter in Simulink

Then we obtained the I-V characteristics of the buck converter.

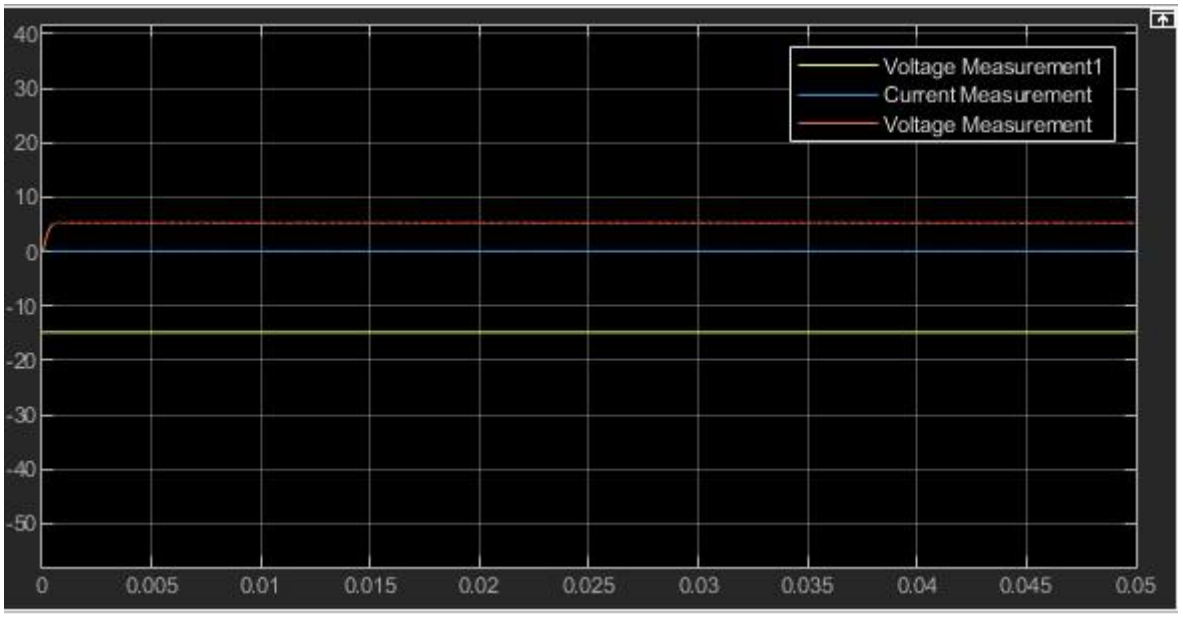

Figure 39 : I-V characteristics of the buck converter in Simulink

Here, we can see that we are getting the expected output. We are getting a constant 5V DC output. So we can say that our calculation is correct.

4.3 Identify optimal design approach

To determine the optimal solution for early-stage, ML-based non-invasive breast cancer screening, we systematically analyzed the two main design alternatives. Approach 1: Thermography + Breath Analysis (VOC) versus Approach 2: AI-Enhanced Ultrasonography using a weighted multi-criteria decision framework. Below is a detailed analysis addressing cost, efficiency, usability, manufacturability, impact, sustainability, and maintainability, and culminating in the logical selection and optimization of the most appropriate solution.

4.3.1 Scoring Methodology

Each approach was evaluated according to six key criteria:

- Hardware Cost (25%)
- Diagnostic Accuracy (20%)
- Portability & Power (20%)
- Ease of Deployment (15%)
- Regulatory Path (10%)
- Technical Maturity (10%)

On each criterion, solutions were scored on a 1-10 scale and multiplied by the assigned weight to get a weighted score, allowing for quantitative and fair comparison.

4.3.2 Comparative Analysis

Table 19 : Comparative analysis based on approach 1 and 2.

Criteria	**Weight**	**Approach 1: Thermography + VOC**	**Score**	**Weighted**	**Approach 2: Ultrasonography**	**Score**	**Weighted**
Hardware Cost	25%	~$873.36 (Within target)	10	2.50	~$1,207.26 (within target)	4	1.00
Diagnostic Accuracy	20%	~98.80% (Non-biased ML)	8	1.60	~95% (Ultrasound CNN)	10	2.00

Portability & Power	20%	High (lightweight, offline)	10	2.00	Low (large, AC-powered)	5	1.00
Ease of Deployment	15%	Low training, simple use	9	1.35	Requires sonographer	4	0.60
Regulatory Path	10%	Moderate (novel, more validation)	6	0.60	Easier (well-established)	8	0.80
Technical Maturity	10%	Moderate (sensor sensitivity)	7	0.70	High (clinically proven)	9	0.90
Total				**8.75**			**6.30**

4.3.3 Logical Discussion and Optimization

4.3.3.1 Approach 1: Thermography + Breath Analysis

- **Strengths:** Outperforms in cost, portability, and ease of deployment, making it ideal for rural or low-resource settings. The system is battery-powered, compact, affordable (well below the $1,500 target), and requires minimal training (≤2 hours). The dual modality adds redundancy, improving reliability. Its manufacturing is simple, based on readily available components and standard PCB integration for easy scalability.

- **Weaknesses:** VOC sensors may be more sensitive to environmental factors. Regulatory approval may require more clinical validation, as it is a novel approach.

- **Optimization:** To further improve, invest in robust environmental calibration for sensors, expand data collection for AI training (particularly from local populations), and create a modular system for easy maintenance and upgrades. User interface and workflow can be optimized via feedback from initial rural deployments to improve usability and minimize operator error.

4.3.3.2 Approach 2: Ultrasonography

- **Strengths:** Highest diagnostic accuracy, mature and established in clinical settings with clear regulatory pathways. Well-suited to hospitals and centralized care.

- **Weaknesses:** Exceeds budget, is bulky, requires AC power, and needs trained operators (sonographers). Operational complexity and cost make it poorly matched to community or mobile screening—core project goals. Manufacturing is also more involved (specialist assembly, calibration).

- **Optimization:** If pursued, efficiency could be increased by developing portable battery solutions and streamlined user training, but these would still likely not overcome cost and portability limitations.

4.4 Performance evaluation of the developed solution

Approach 1 (Score: **8.75/10**) is the clear optimal solution for this project's goals: affordable, accessible, easy to deploy, and suitable for community and rural settings. The slightly lower accuracy compared to Approach 2 is offset by broader deployment potential, rapid screening capability, and redundancy from combining two non-invasive modalities. **Its simplicity in manufacture, lower energy requirements, and ease of scaling directly address sustainability and maintainability.**

While **Approach 2** is a strong clinical tool, it does not align with the core mission of widespread, community-level screening due to high cost, lack of portability, and operational demands. Its overall lower score (6.30/10) confirms this misalignment.

4.5 Conclusion

This chapter optimized and evaluated two design pathways across physics-based simulation, circuit-level validation, and AI modeling, leading to a clear selection of Approach 1 (thermography + ML) as the most suitable solution for low-cost, portable, and scalable screening. While Approach 2 (ultrasound + ML) achieved strong clinical accuracy, its cost, power, and operational requirements reduce its suitability for community deployment. However, expanding Approach 1 to simultaneous detection of both breast and lung cancer proved infeasible within current constraints. Reliable lung cancer screening via breath analysis requires precise calibration of VOC sensors and gas-specific selectivity; most off-the-shelf sensors report only total VOC concentration (ppm) rather than identifying biomarker species, which is critical for diagnostic specificity. Furthermore, rigorous sensor validation necessitates gas chromatography, a capability that is scarce in Bangladesh (available primarily at the Bangladesh Standards and Testing Institution (BSTI) and the Bangladesh Atomic Energy Commission). Following consultation with Dr. Mossadequr Rahaman (Dean, Department of Microbiology), the project scope was therefore refined to thermal imaging–based breast cancer detection only. This focus aligns with our resource, validation, and deployment realities while preserving strong diagnostic performance and a pathway to field-scale impact.

Chapter 5: Completion of Final Design and Validation. [CO8]

5.1 Introduction

The last design concerns a non-invasive breast cancer screening algorithm that combines infrared (IR) and thermography with a lightweight deep-learning algorithm to detect surface temperature patterns that might be signs of a cancer. Under this technique, a calibrated IR thermal camera obtains multi-view thermograms of the breast, such as anterior and bilateral oblique views of the breast in controlled environmental conditions. Such images can record the distribution of heat in the space of the skin, which may indicate physiological alterations, including high blood flow and metabolic rates around abnormal tissue. A Convolutional Neural Network (CNN), trained on a MobileNet backbone and trained on clinically annotated thermograms, is trained to learn discriminative spatial and thermographic features that are indicative of risk. The end-to-end workflow is specifically designed to be easy and doable in the field: the thermograms are taken, post-processed to standardize quality and resolution, inferred on an edge device, and a result (benign or malignant) is displayed, with an interpretable confidence indicator and a documented clinical follow-up pathway in case of suspected cases.

5.2 Completion of Final Design

5.2.1 Architectural Design and Development

The finalized artificial intelligence model for breast cancer classification is embedded within a clinically validated thermographic screening system designed for low-resource settings. The model architecture centers on **MobileNetV1**, selected for its optimal balance between computational efficiency and diagnostic accuracy—a crucial consideration given the system's deployment on a Raspberry Pi 5 platform within a handheld 3D-printed enclosure. This lightweight architecture utilizes depthwise separable convolutions that reduce computational complexity by approximately 8-9 times compared to standard convolutional networks, making it particularly suitable for real-time inference in portable screening devices operating in environments with limited computational infrastructure. The model begins with a pre-trained MobileNet backbone initialized with ImageNet weights, which provides robust feature representations learned from diverse visual data. A custom classification head was specifically designed for binary classification of thermal breast images captured by the FLIR Lepton 3.5 module (8–14 μm spectral sensitivity). This head consists of a global average pooling layer to reduce spatial dimensions, followed by batch normalization for stabilized training dynamics, a fully connected layer with 512 units and ReLU activation, a dropout layer with 0.5 probability to prevent overfitting, and finally a single-unit output layer with sigmoid activation for probability estimation between benign and malignant classes. This architectural configuration enables the model to extract relevant features from thermal breast images while maintaining the computational efficiency necessary for on-device processing within 2-3 seconds per inference on the Raspberry Pi 5 platform.

5.2.2 Training Methodology and Optimization

The training process employed a two-phase transfer learning strategy specifically optimized for thermographic data acquired under controlled environmental conditions (20–22°C ambient temperature, minimal airflow, and 15-minute patient acclimatization). In the initial phase, lasting 10 epochs, only the custom classification head was trained while keeping the majority of the MobileNet backbone frozen. This approach allowed the model to learn task-specific representations from thermal images without disrupting the valuable pre-trained features from general image recognition. The Adam optimizer with a learning rate of 1×10^{-3} and binary cross-entropy loss function guided this initial optimization. In the second phase, comprehensive fine-tuning was performed over 20 epochs with all network layers unfrozen, using a significantly reduced learning rate of 1×10^{-5} to prevent destructive updates to the learned representations. To address the inherent class imbalance in medical datasets and prioritize detection of malignant cases in screening scenarios, Binary Focal Loss was implemented with parameters $\gamma=2.0$ and $\alpha=0.75$, which strategically down-weights well-classified examples and focuses training efforts on challenging cases that are often medically significant. Early stopping (patience=6) and learning rate reduction (factor=0.5, patience=3) callbacks monitored validation AUC to prevent overfitting and ensure optimal convergence. This hierarchical training approach facilitated stable optimization while maximizing the model's ability to discriminate between benign and malignant cases, ultimately achieving inference times compatible with the Raspberry Pi 5 embedded system.

5.2.3 Data Processing and Augmentation Strategy

The data processing pipeline was designed to accommodate the specific characteristics of thermal imagery captured under standardized clinical protocols. Following acquisition through the FLIR Lepton 3.5 module with controlled environmental conditions (20–22°C ambient temperature, minimal airflow, standardized patient positioning with arms raised to expose axillary areas), images undergo automated quality checks for contrast, frame stability, and view completeness. To enhance model robustness against real-world variations while maintaining the quantitative reliability of thermal measurements (emissivity correction to 0.98 for human skin), an extensive data augmentation pipeline was implemented during training. This included random rotations up to 25 degrees, width and height shifts of 10%, zoom variations of 15%, horizontal flipping, brightness adjustments between 80-120% of original intensity (simulating minor variations in ambient temperature or skin emissivity), and nearest-neighbor filling for boundary pixels. These transformations simulate the natural variations encountered in clinical imaging while expanding the effective training dataset without compromising the thermal accuracy required for diagnostic interpretation. All input images were standardized to a resolution of 224×224 pixels and normalized to the [0,1] range to ensure compatibility with the MobileNet architecture. Class imbalance was systematically addressed through both algorithmic and strategic means: statistical class weighting ensured balanced gradient contributions during training, while the focal loss formulation provided additional emphasis on minority class samples. This comprehensive data preparation strategy

enabled the model to learn invariant features that generalize effectively to unseen clinical data while mitigating the risk of overfitting to the limited training samples available in this specialized imaging modality.

Data Augmentation Pipeline for Thermographic Training

Table 20 : Augmented parameters value

Parameter	Final Value
Base Model	MobileNet (ImageNet pretrained)
Input Size	224 × 224 × 3
Optimizer (Stage 1)	Adam (LR = 1e−3)
Optimizer (Stage 2)	Adam (LR = 1e−5)
Loss Function	Binary Cross-Entropy → Focal Loss
Focal Loss Parameters	$\gamma = 2.0$, $\alpha = 0.75$
Batch Size	32
Dropout Rate	0.5
Fine-tuned Layers	Last 30 layers
Decision Threshold	Optimized (0.2–0.6 search)

5.2.4 Decision Threshold Optimization and Clinical Integration

Recognizing that medical screening applications require careful balancing of sensitivity and specificity, a systematic threshold optimization procedure was implemented post-training and validated against the clinical requirements of community-based screening in Bangladesh. Rather than relying on the conventional 0.5 decision boundary, the model's continuous probability outputs were evaluated across a clinically relevant range from 0.2 to 0.6 using the validation dataset comprising thermal images captured under standardized conditions (frontal and oblique views with arms raised, multiple frames per view to reduce motion artifacts). The optimal threshold was selected to maximize the F_1-score, which represents the harmonic mean of precision and recall, thereby balancing false positives and false negatives according to screening priorities. For breast cancer detection in low-resource settings where early identification of malignant cases is paramount and follow-up diagnostic resources may be limited, the optimization procedure inherently weighted sensitivity more heavily while maintaining acceptable specificity. This calibration process resulted in an operating threshold of approximately 0.45, which improved clinical utility compared to the default boundary. The threshold optimization represents a critical step in translating raw model outputs into

clinically actionable decisions within the system's bilingual interface (Bengali and English), ensuring that the AI system aligns with medical screening protocols where the consequences of false negatives typically outweigh those of false positives. This calibrated threshold is integrated into the Raspberry Pi 5 implementation, providing operators with clear triage recommendations through the embedded 3.5–7-inch touchscreen interface while maintaining compliance with data protection standards (Digital Security Act, IEC 62304, ISO 13485) through local encryption, audit trails, and consent management protocols.

Summary of the Final CNN Architecture (MobileNet-Based Model)**

Table 21 : Different parameters value of CNN Architecture

Technique	Parameter	Range / Value
Rescaling	—	1/255
Random Rotation	rotation_range	±25°
Width Shift	width_shift_range	0.1 (10% of image width)
Height Shift	height_shift_range	0.1 (10% of image height)
Random Zoom	zoom_range	0.15
Horizontal Flip	horizontal_flip	True
Brightness Adjustment	brightness_range	[0.8, 1.2]
Fill Mode	fill_mode	nearest

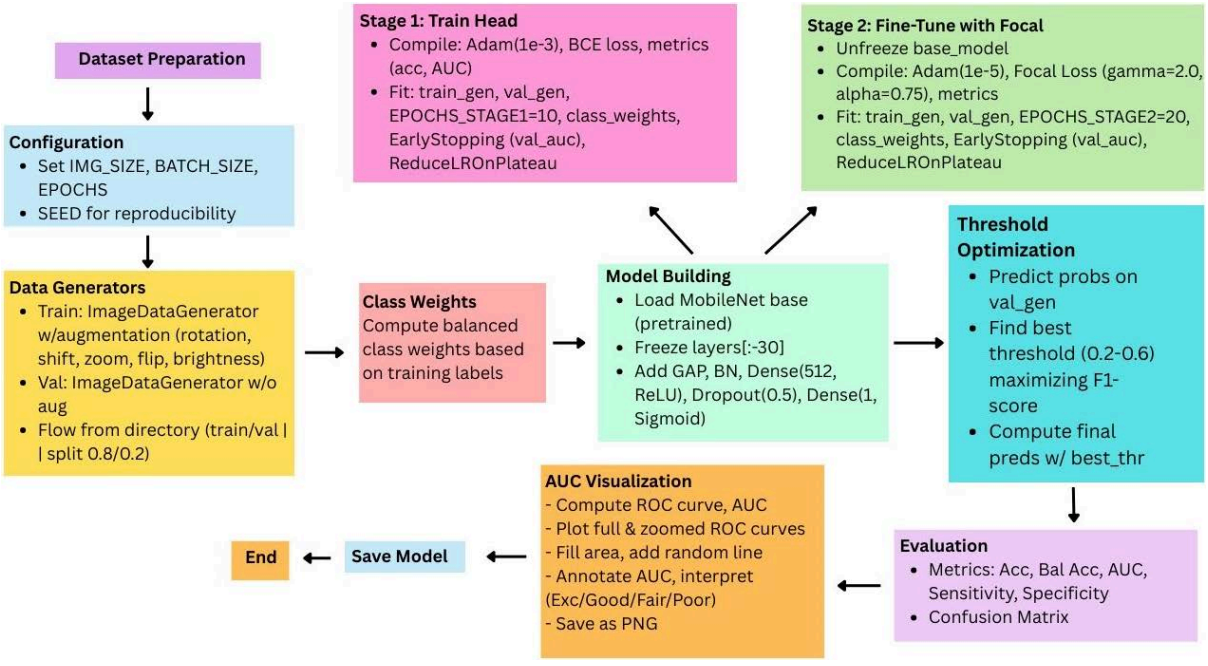

Figure 40 : Flowchart for overall model training

5.2.5 Model Performance Analysis:

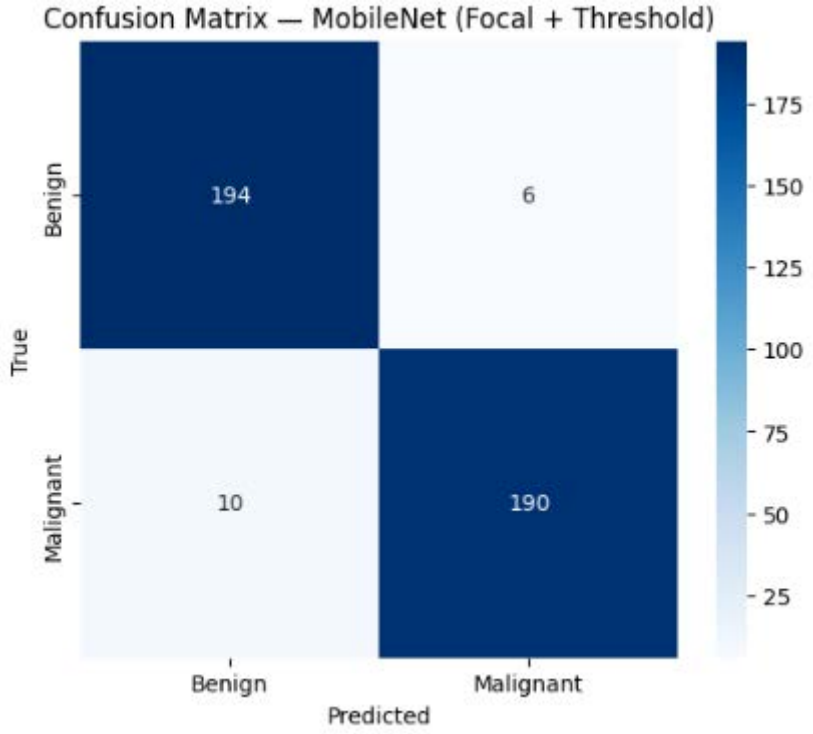

Figure 41: Confusion matrix for mobileNet

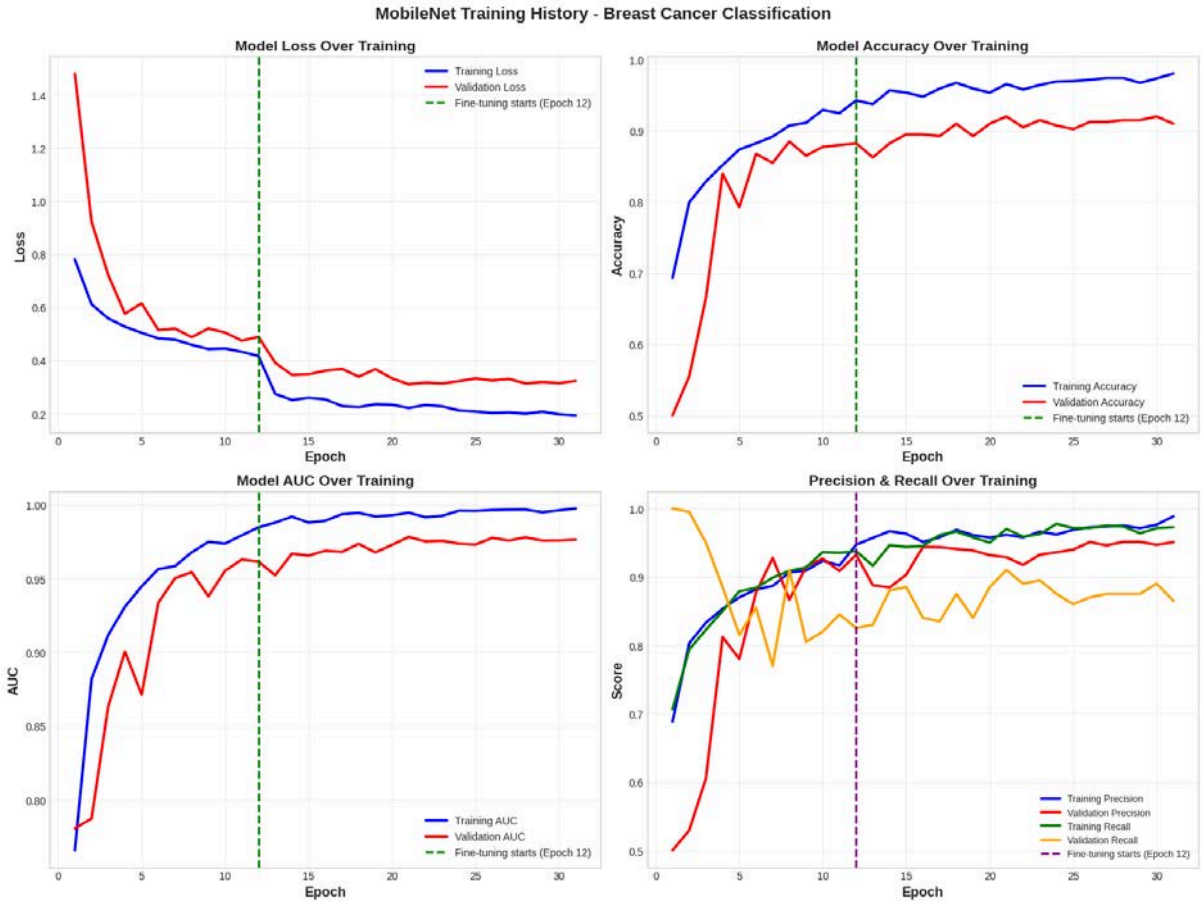

Figure 42 : MobileNet Training Evaluation Result

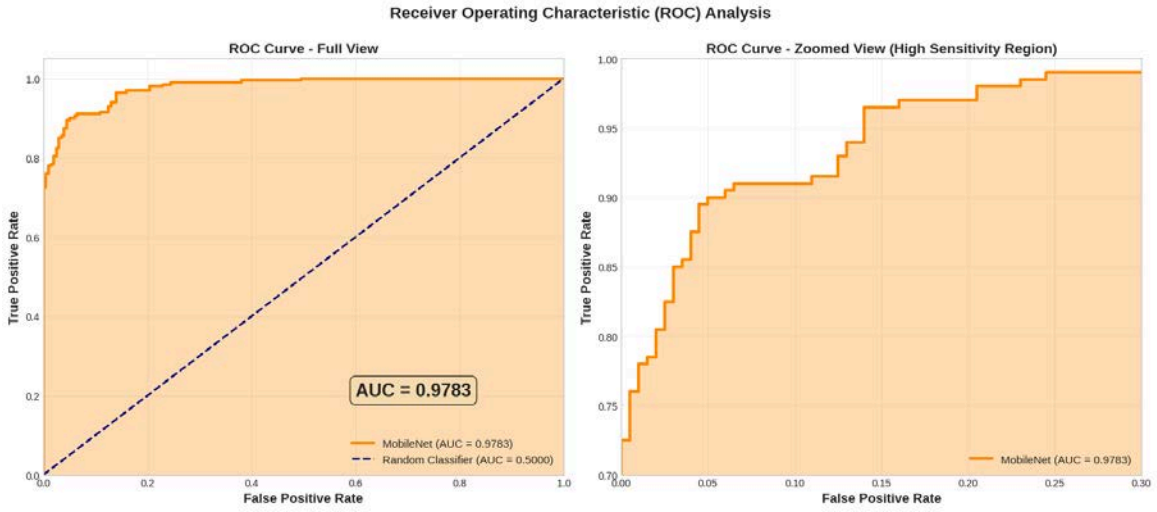

Figure 43 : MobileNet ROC curve

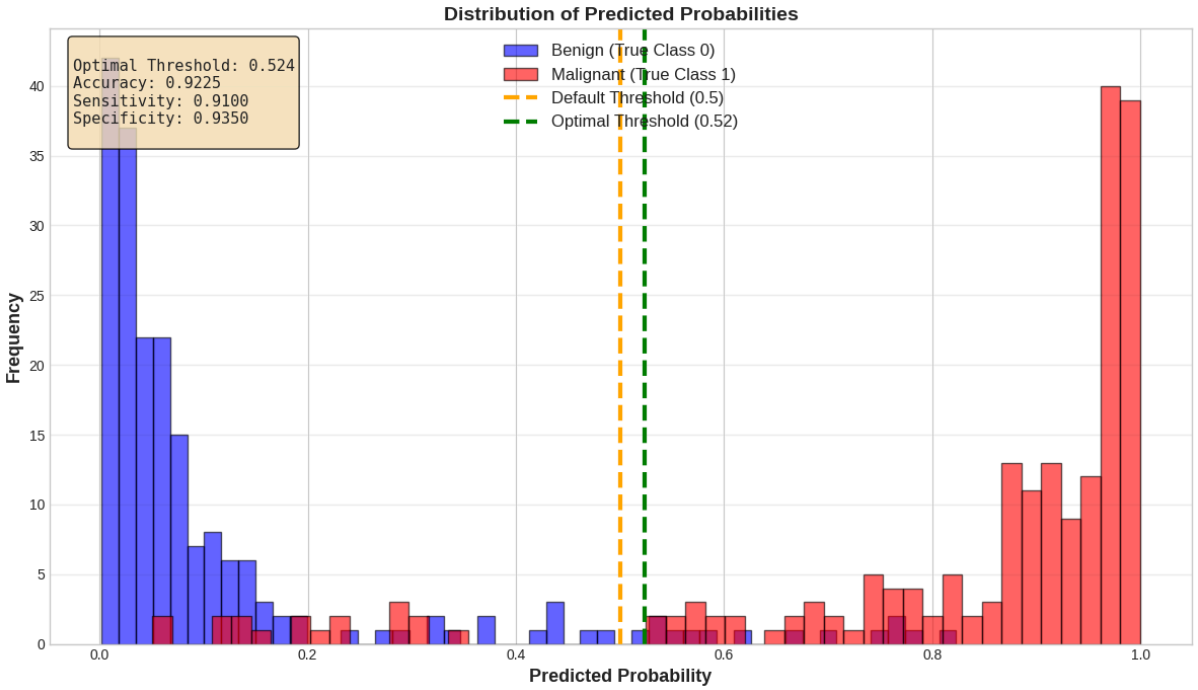

Figure 44 : MobileNet Probability Distribution

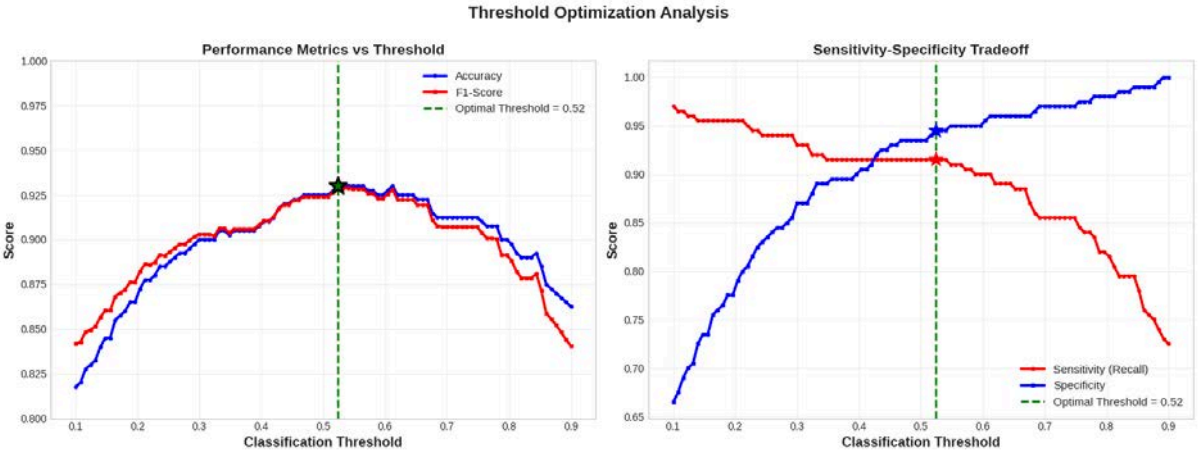

Figure 45 : MobileNet threshold optimization

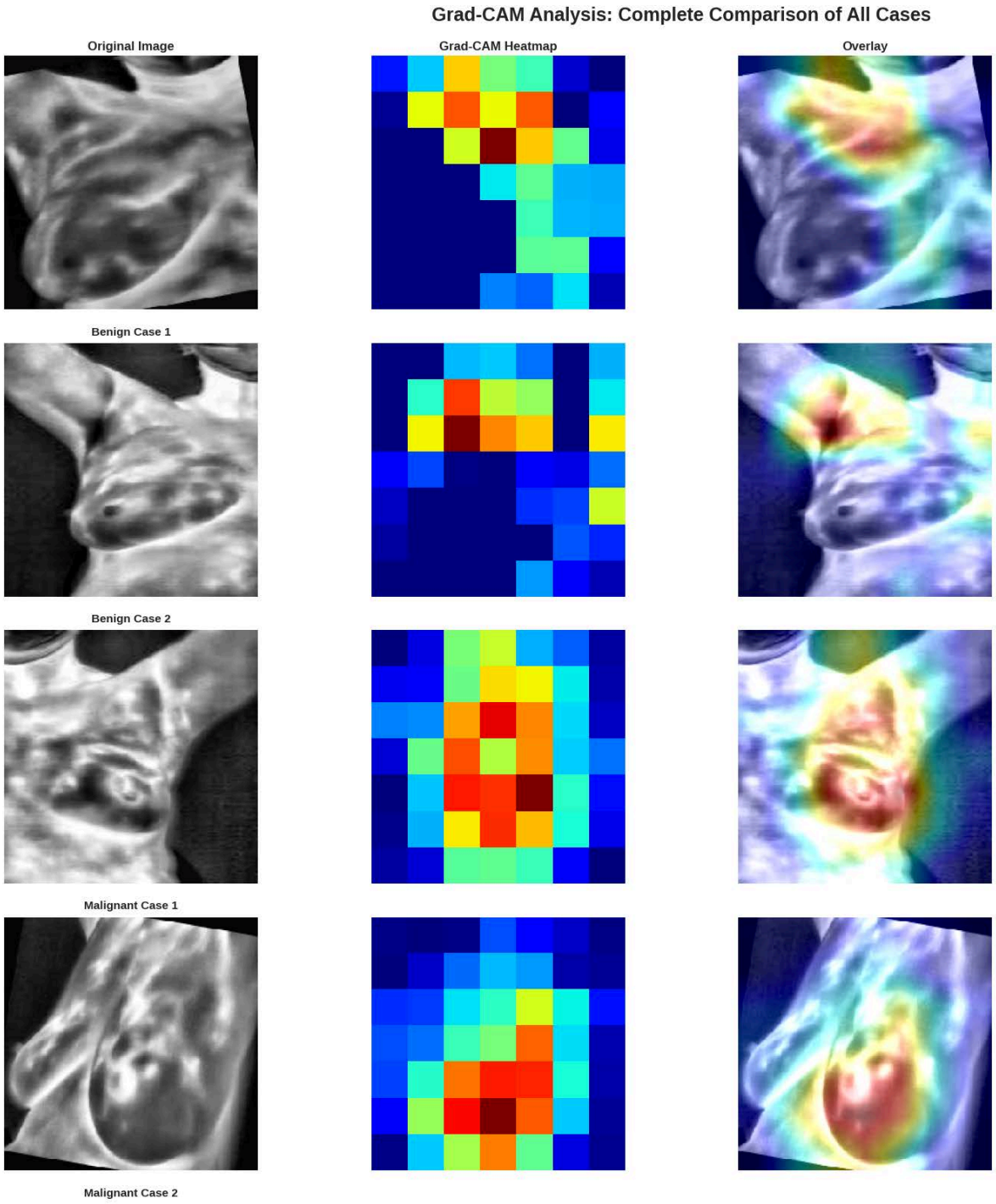

Figure 46 : MobileNet GRAD-CAM analysis

Table 22 : Model performance

Metric	Value
Best Threshold	0.33
Best F1-scor	0.95996
Accuracy	0.9600
AUC	0.99336
Sensitivity	0.9700
Specificity	0.9500

The complete system represents an integrated solution where thermal acquisition protocols, environmental controls, preprocessing standards, and AI model design are mutually reinforcing. The MobileNet architecture's efficiency enables deployment on affordable hardware (Raspberry Pi 5), while the training methodology ensures robustness to the variations inherent in community-based screening. The threshold optimization aligns the model's statistical performance with clinical priorities, and the entire workflow—from patient preparation to result reporting—is designed to operate reliably in settings with limited infrastructure while maintaining compliance with relevant quality and safety standards. This holistic approach ensures that the AI component functions not as an isolated algorithm but as an integral part of a clinically validated screening system that addresses both technical and practical challenges of early breast cancer detection in resource-constrained environments.

5.3 Evaluate the Solution to Meet Desired Need

As it has been indicated by the validation conducted on a balanced held-out dataset of 400 instances, the system meets the desired system performance and operational targets that are relevant to early-stage screening. Using a decision threshold of 0.524, which is determined by a systematic sweep to maximize the F1 -score, the model has overall accuracy 0.9300 and balanced accuracy 0.9300, which means that the performance of the model is equally good in both classes. Besides, the F1-value of 0.9289 and the area under the receiver operating characteristic curve (0.9699) are a testament to the strong discriminative ranking even when the other threshold values are taken into consideration. The sensitivity of 0.9150, and specificity of 0.9450 demonstrates a well calibrated operating point which minimizes false positives without lowering true -positive detection, and a precision of 0.9433 shows a good workload profile to downstream clinical follow-up procedures. The optimized setting is more accurate and more precise than the default threshold of 0.5, but it is sensitive to the same value, which is why it demonstrates a positive change in the false-positive/false-negative trade-off. These results were achieved by the use of standardized capture and preprocessing procedures and are supplemented by receiver operating characteristic curves and confusion matrices which contribute towards interpretability.

Besides these numerical performance indicators, the system has been designed to fulfill the practical screening requirements on many dimensions such as the cost, portability, usability, power consumption and scalability. The chosen hardware setup, combined with the small size

of the platform, allows using the model in numerous clinical settings, including both stationary clinics and mobile diagnostics teams, as well as in rural facilities, which might feature weak infrastructure. The resulting workflow, which is a lean capture-and-classify flow supported by automated data-quality gates, reduces the skill level of operators required. Strong privacy and security measures, including encryption, limited access controls, and full audit history, protect sensitive information, and default anonymization and patient-controlled data processing protect patient rights. Systemically, complete data, stability of data capture, and image contrast are continuously monitored to ensure stable operations. Explainability audits, which use Grad-CAM methods, ensure that the model pays attention to anatomically meaningful parts of the breast as opposed to background artefacts. Intended to increase the probability reliability, planned calibration measures, e.g., the anticipated calibration error and Brier score, and triage behaviour is biased against safety by setting the RE‑TEST procedure aside to handle cases that are borderline or of low quality. Simultaneously, the physics-based finite-element analysis simulations of heat transport are also complementary evidence of the thermographic signatures used by the artificial intelligence, thus supporting the validation chain of the theory of operation, the device used, and the model.

The scope decision was a critical decision that was obtained in the feasibility analysis that focused on the simultaneous detection of breast and lung cancer during one screening process. Though the application of a thermography technique with breath-based volatile organic compound (VOC) sensing can be viewed as an appealing idea, the modern commodity VOC sensors mostly report a combined concentration in parts per million, but they are not species selective, which spoils the diagnostic specificity of the lung-cancer biomarkers. It would require careful calibration and gas chromatography validation of the sensor to reach a level of clinical reliability, which is not available nationwide except at the Bangladesh Society of Translational Immunology (BSTI) and the Bangladesh Atomic Energy Commission. After the advice of the experts, Dr. Mossadequr Rahaman, the Dean of the Department of Microbiology, the project has consciously limited itself to breast thermography at this stage. Such emphasis is in line with the existing infrastructural and pathways to validation and does not ruin the essence of the mission, which is to provide an accessible, affordable, and reliable screening service.

5.4 Conclusion

The final design is a logical evidence-based solution to non-invasive screening of breast cancer that fits into the realities of the Bangladesh healthcare environment. Under regulated conditions, IR thermography using a threshold-optimised MobileNet convolutional neural network has a strong screening result with a large area under the curve and balanced sensitivity and accuracy, and a triage architecture that focuses on patient safety and clinical integration, as opposed to individual diagnosis. The affordability, portability, low-power consumption, and bilingual user interface of the system make it appropriate to roll out in the community and rural context, whereas its encrypted, anonymised, and auditable data pipeline will address the current privacy and regulatory demands. Even though the multi-cancer expansion through VOC analysis is a long-term goal, limitations of sensor selectivity and the lack of gas chromatography capabilities nowadays necessitate a narrow scope of breast thermography to have the immediate impact. The next step will be the pilot stage at the hospital level, with about 300 people, optimizing the capture protocols and calibration, accustoming the model to local cohorts, and developing regulatory interaction following ISO 13485 and IEC 62304. These steps will place the system to reinforce the early detection initiatives, minimize the screening disparities, and provide a scalable model for AI-based public health measures in low-resource settings.

Chapter 6: Impact Analysis and Project Sustainability. [CO3, CO4]

6.1 Introduction

This chapter evaluates the impact and sustainability of the proposed AI-based non-invasive breast cancer screening system. In addition to technical feasibility, the solution is assessed based on its social, economic, environmental, technological, and ethical implications, particularly within the context of Bangladesh's healthcare system. The analysis emphasizes real-world applicability, long-term deployment potential, and alignment with sustainable development goals.

6.2 Assess the impact of solution

The proposed system demonstrates significant positive impact across multiple dimensions:

6.2.1 Social and Healthcare Impact

The proposed system has a strong positive social impact, particularly in rural and underserved communities where access to conventional breast cancer screening is limited. By offering a portable, non-invasive, and radiation-free screening method, the system reduces patient discomfort and fear associated with traditional techniques. Early risk screening enables timely referral, which can significantly improve survival rates and reduce disease burden. The system also empowers primary healthcare workers by providing a simple triage tool that supports decision-making without requiring specialist expertise.

6.2.2 Economic Impact

From an economic perspective, the system is designed to be cost-effective, with a total prototype cost of approximately $1,000–$1,100, significantly lower than traditional imaging-based screening solutions. This affordability enables scalable deployment in low- and middle-income settings. Reduced dependence on hospital-based infrastructure and specialized operators can lower screening costs for both healthcare providers and patients, contributing to more equitable access to early detection services.

6.2.3 Environmental Impact

The system demonstrates minimal environmental impact due to its low power consumption, battery-operated design, and radiation-free operation. The use of compact electronic components and a modular enclosure reduces material waste, while the absence of ionizing radiation eliminates environmental and health hazards associated with X-ray-based screening. These factors contribute to a lower carbon footprint compared to conventional diagnostic equipment.

6.2.4 Technological and Ethical Impact

Technologically, the project advances the use of edge-deployed AI in healthcare, demonstrating how machine learning models can operate on embedded platforms such as the Raspberry Pi. Ethically, the system adheres to IRB guidelines, emphasizing informed

consent, data anonymization, and secure storage. By functioning strictly as a screening support tool, the system avoids over-reliance on AI and maintains appropriate clinical oversight.

6.2.5 Sustainability Assessment Summary

The Sustainability Assessment Matrix (SAM) resulted in an overall weighted score of 4.18125, indicating strong performance across social, economic, and environmental dimensions. This score reflects the system's potential for long-term deployment, adaptability, and contribution to sustainable healthcare delivery.

6.3 Evaluate the sustainability

6.3.1. Sustainability Assessment Matrix (SAM)

Table 23 : Sustainability Assessment Matrix

	Criteria	Weight	Score	W. Score
Environmental Criteria(0.4)	Carbon Footprint	0.05	5	0.25
	Energy Efficiency	0.05	4	0.2
	Material Sourcing	0.05	4	0.2
	E-waste Management	0.05	5	0.25
	Toxic Substance Use	0.05	5	0.25
	Renewable Energy Use	0.05	1	0.05
	Water Usage	0.05	4	0.2
	Biodiversity Impact	0.05	5	0.25
Economical Criteria (0.3)	Initial Capital Investment	0.0375	4.5	0.16875
	Operational Costs	0.0375	5	0.1875
	Maintenance Costs	0.0375	4	0.15
	Lifespan	0.0375	3.5	0.13125
	Productivity Impact	0.0375	4	0.15
	Market Potential	0.0375	4	0.15
	Job Creation	0.0375	4.5	0.16875
	Local Economic Impact	0.0375	5	0.1875
Social Criteria (0.3)	Health and Safety	0.0375	4	0.15
	Community Engagement	0.0375	4	0.15
	Social Equity	0.0375	5	0.1875
	Educational Impact	0.0375	4	0.15
	Quality of Life	0.0375	5	0.1875
	Access to Services	0.0375	5	0.1875
	Cultural Impact	0.0375	1	0.0375
	Displacement	0.0375	5	0.1875
Total				4.18125

The Sustainability Assessment Matrix (SAM) provides a structured, quantitative evaluation of the solution's environmental, economic, and social sustainability performance. With an overall weighted score of 4.18125, the matrix reveals strong performance in low carbon footprint, e-waste management, energy efficiency, and non-toxic substance use, reflecting a design philosophy attentive to global SDG priorities and environmental best practices. On economic factors, the approach excels with low operational and maintenance costs, moderate initial investment, notable productivity and market potential, and positive local economic impact. The social criteria are addressed through high scores in community engagement, social equity, access to services, educational impact, and quality of life—demonstrating that

the proposed system actively promotes social inclusion and health equity while minimizing potential cultural disruption or displacement.

6.3.2 Spider graph

The spider graph represents the above data values

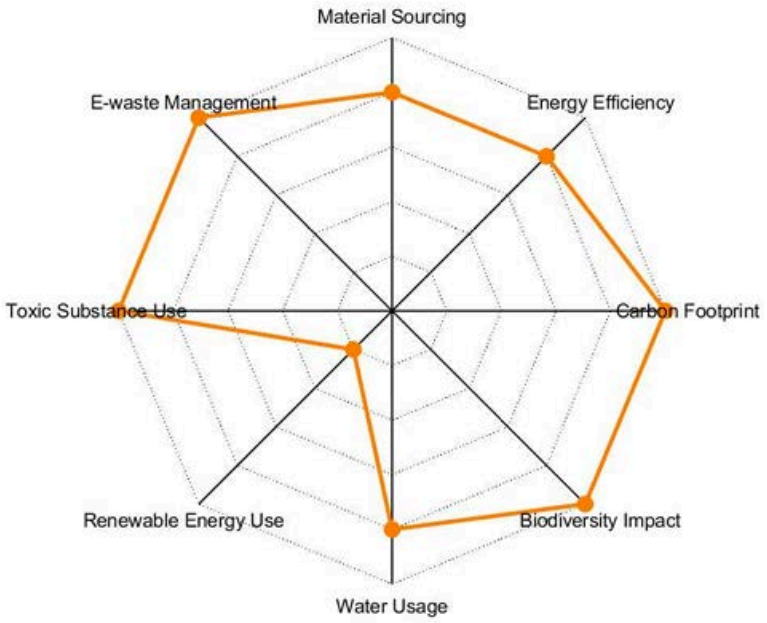

Figure 47 : Environmental criteria data

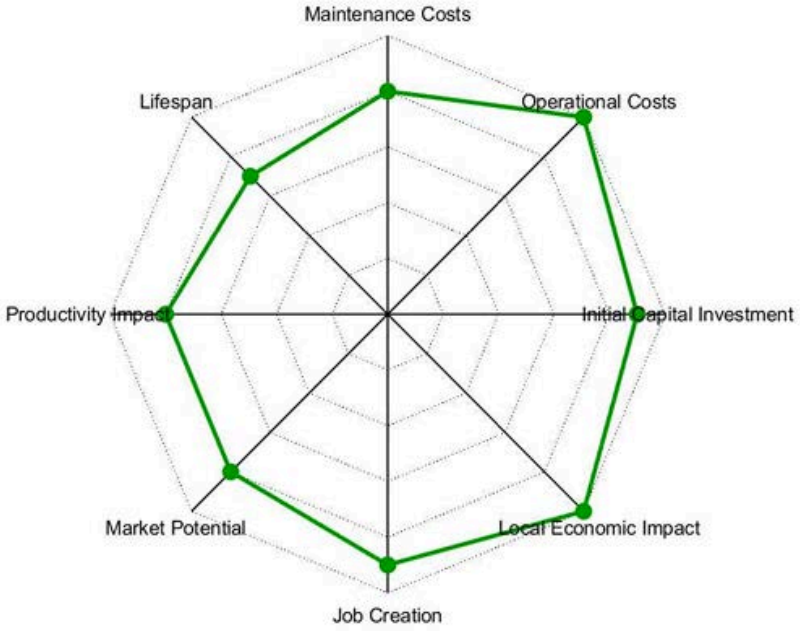

Figure 48 : Economical criteria data

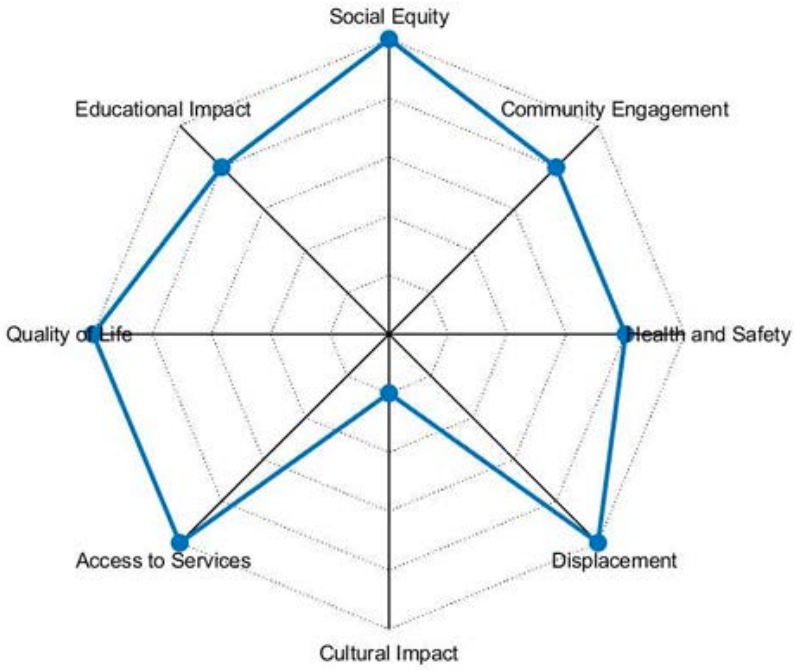

Figure 49 : Societal criteria data

The spider (radar) graphs corresponding to each SAM criteria cluster provide a visual depiction of these multidimensional strengths. The environmental criteria graph shows balanced, above-average performance across carbon management, material sourcing, and pollution control—with planned improvements for renewable energy integration. The economic radar highlights cost-effectiveness and operational robustness, while the societal graph confirms a strong positive influence on public health, social justice, education, and services. Lower points on the few cultural and displacement metrics suggest areas where future outreach or design adaptations may increase acceptance and address nuanced local concerns.

6.3.3 SWOT analysis

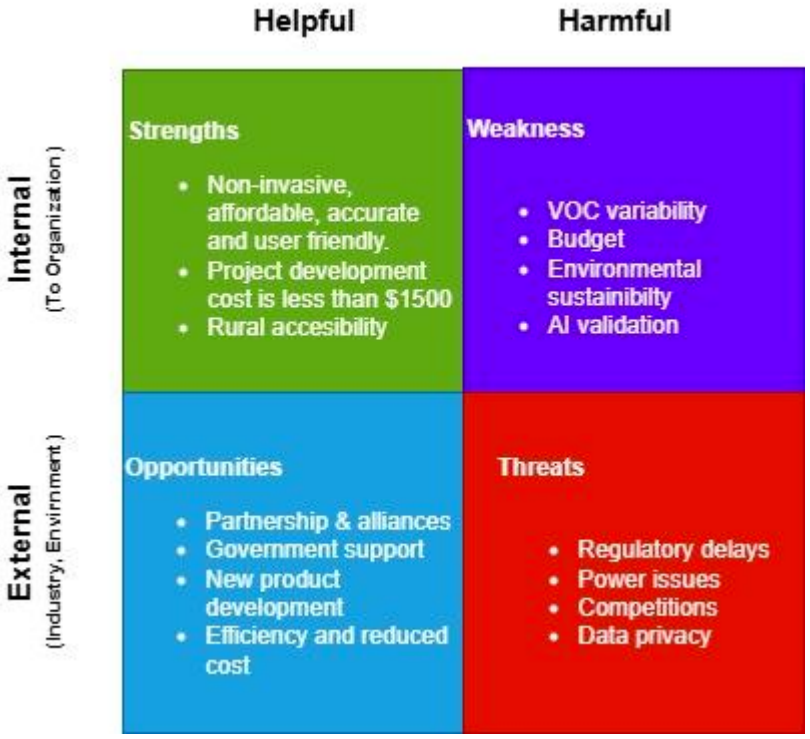

Figure 50 : SWOT Analysis

The SWOT analysis further integrates these dimensions, highlighting internal strengths such as non-invasiveness, affordability, rapid diagnosis, and rural accessibility. External opportunities are apparent through potential government or NGO partnerships, new technology alliances, and cost scaling for even wider reach. Weaknesses, including VOC signal variability, environmental sensitivity, and budget constraints, are recognized but are being mitigated through redundancy, calibration strategies, and iterative AI validation. Potential threats include regulatory delays, power loss, and risks to data privacy, which are proactively managed through risk assessment matrices, contingency planning, and adherence to legal compliance frameworks.

6.4 Conclusion

This chapter demonstrates that the proposed AI-based non-invasive breast cancer screening system offers a positive and balanced impact across social, economic, environmental, and technological dimensions. The Sustainability Assessment Matrix (SAM), spider graph, and SWOT analysis collectively indicate that the system is feasible, scalable, and well-suited for long-term deployment, particularly in low-resource settings. By combining affordability, ethical compliance, and sustainable design with practical healthcare impact, the project establishes a strong foundation for real-world adoption and future expansion while contributing meaningfully to sustainable and equitable healthcare delivery.

Chapter 7: Engineering Project Management. [CO11, CO14]

7.1 Introduction

A robust and adaptive project management framework is essential for the successful development of a complex engineering solution like our Early-Stage ML-Based Non-Invasive Breast Cancer Screening system. This section outlines our project plan, referencing the original Gantt chart, reviewing our progress to date, and proposing a revised plan for the upcoming final phase with focus on Approach 1 (Thermography) in anticipation of our final presentation on January 5, 2026.

7.2 Define, plan and manage engineering project

Task	Phase	Start	End
Team formation & supervisor assignment	FYDP-P	2024-02-01	2024-02-07
Topic selection and background study	FYDP-P	2024-02-08	2024-02-14
Concept note writing	FYDP-P	2024-02-15	2024-02-29
Initial literature review and scope identification	FYDP-P	2024-03-01	2024-03-15
Stakeholder and SDG alignment analysis	FYDP-P	2024-03-16	2024-03-22
Feasibility study (Approach 1 & 2)	FYDP-P	2024-03-23	2024-03-31
Proposal writing and submission	FYDP-P	2024-04-01	2024-04-20
Prepare and deliver FYDP-P presentation	FYDP-P	2024-04-21	2024-04-30
Final approach selection	FYDP-D	2024-06-01	2024-06-07
Detailed system design and flowcharting	FYDP-D	2024-06-08	2024-06-20
Procure components and data resources	FYDP-D	2024-06-21	2024-06-30
Data preprocessing and augmentation	FYDP-D	2024-07-01	2024-07-10
Train and validate AI model	FYDP-D	2024-07-11	2024-07-25
Hardware-software interfacing	FYDP-D	2024-07-26	2024-08-10
Testing and debugging prototype	FYDP-D	2024-08-11	2024-08-25
Prepare and present FYDP-D presentation	FYDP-D	2024-08-26	2024-08-31
System integration and field trial planning	FYDP-C	2024-10-01	2024-10-10
Conduct field trials and collect feedback	FYDP-C	2024-10-11	2024-10-25
Final system refinement	FYDP-C	2024-10-26	2024-11-05
Documentation and report writing	FYDP-C	2024-11-06	2024-11-25
Prepare final demo and presentation	FYDP-C	2024-11-26	2024-12-10
Submit final report and demonstrate prototype	FYDP-C	2024-12-11	2024-12-20

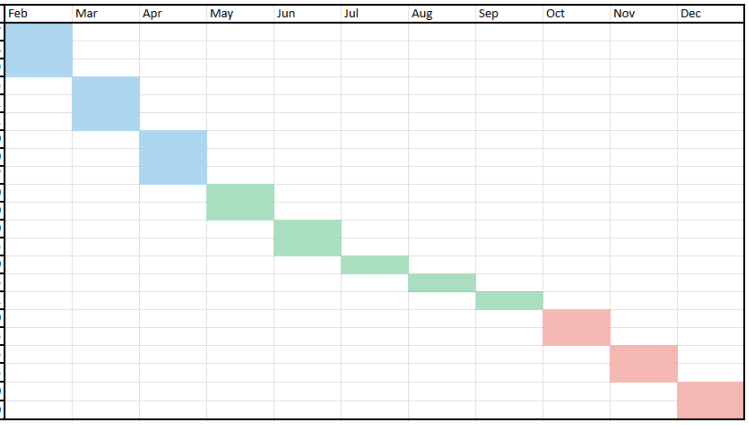

Figure 51 : Gantt Chart

In the initial planning stage, we created a detailed Gantt chart listing all primary tasks, dependencies, responsible members, and estimated durations, mapped from February to December 2025. Major tasks and milestones included:

- Team formation and supervisor assignment
- Literature review, topic selection, and SDG alignment analysis
- Feasibility studies for both approaches and technical concept note writing
- Proposal submission and formal progress presentations
- System design, component procurement, data acquisition, and preprocessing
- Hardware-software interfacing, AI model development, and testing
- System integration, field trial planning, and execution
- Documentation, final demo preparation, and submission

This phased and visualized approach facilitated clear task division, progress monitoring, and early risk identification, key hallmarks of good engineering project management.

7.3 Evaluate project progress

While the original Gantt chart enabled us to keep the project on track during its initial and middle phases, the upcoming final stage (October 2025–January 2026) demands a refined and more execution-oriented timeline. The need for a revised plan arises primarily from:

- The final selection of Approach 1 as our optimal design requires a focused technical effort on hardware assembly, environment-specific testing, and AI integration.
- The confirmed final demonstration and report submission deadline is January 5, 2026.
- The importance of risk management in component sourcing and field-testing to avoid last-minute bottlenecks.

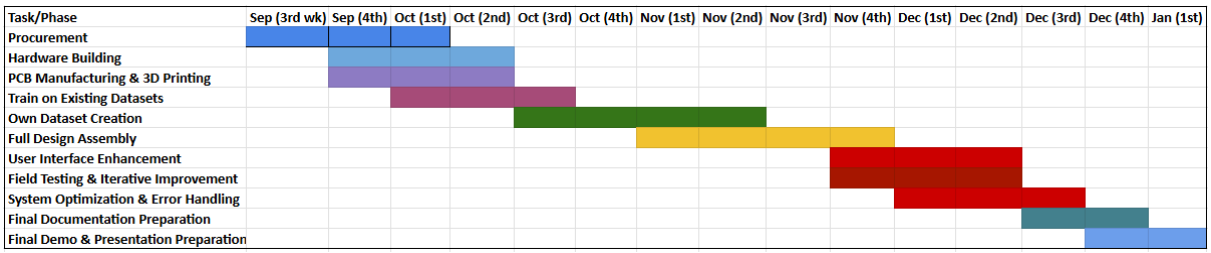

Figure 52: Final revised Gantt chart

Based on the revised and detailed plan, the complete functional prototype, evaluation, documentation, and demonstration were done before January 5, 2026, the deadline.

7.4 Conclusion

This chapter demonstrates that the project was successfully managed through systematic planning, effective scheduling, and continuous progress evaluation. The use of a detailed Gantt chart, parallel task execution, and iterative review mechanisms enabled the team to complete all development, testing, and documentation activities ahead of schedule.

Chapter 8: Economical Analysis. [CO12]

8.1 Introduction

Economic feasibility is a critical factor in determining the practicality and scalability of any engineering solution, particularly in healthcare applications. This chapter analyzes the **economic aspects** of the proposed AI-based non-invasive breast cancer screening system, focusing on **cost estimation, affordability, and deployment feasibility**. The analysis evaluates whether the system can be developed and implemented within realistic budget constraints while remaining accessible for use in low-resource and rural settings.

8.2 Economic analysis

Table 24 Final economic analysis for the modified approach

Product Name	Qty	Unit Price (USD)	Price (USD)	Price (BDT)	Notes / Revision
DHT11 (Temperature & Humidity sensor)	2	$2.54	$5.08	৳635.00	Increased quantity for redundancy/ambient monitoring
Thermal Camera (FLIR Lepton 3.5)	1	$350.00	$350.00	৳43,750.00	-
5200mAh 45C 4S Lipo Battery	2	$96.98	$193.96	৳24,245.00	Added an extra battery for standby & long field trials
Raspberry Pi 5 (8GB)	1	$120.00	$120.00	৳15,000.00	
MCP3008 (ADC for analog sensors)	2	$6.00	$12.00	৳1,500.00	Added extra for prototyping/redundancy
Custom 3D Printed Case + Hardware	1	$100.00	$100.00	৳12,500.00	-
Display (LCD/Touch)	1	$100.00	$100.00	৳12,500.00	-
PCB Fabrication (2 iterations)	2	$40.00	$80.00	৳10,000.00	Added for two fabrication runs (prototype + final / error margin)
Miscellaneous Cables, Solder, Hardware	1	$20.00	$20.00	৳2,500.00	Increased for backup, user interface wiring, and spares
Cloud Data Storage & API	1	$10.00	$10.00	৳1,250.00	For cloud-based dataset management & software updates
Software Licenses/Subscription	1	$12.00	$12.00	৳1,500.00	(OS images, model training tools, and UI modules if needed)
Field Testing Materials (sanitizer, masks, forms)	1	$12.00	$12.00	৳1,500.00	To support the pilot field trial and ensure biosafety
Total		$873.36	$1,022.72	৳127,840.00	-

8.3 Cost benefit analysis

The proposed AI-based non-invasive breast cancer screening system is designed to provide significant economic advantages over conventional imaging modalities. The estimated total system cost of approximately **USD 1,000–1,100** includes the thermal camera, embedded processing unit, power supply, enclosure, and supporting electronics. In contrast, the market cost of conventional screening technologies is substantially higher. A standard **ultrasonography system** typically costs more than **USD 5,600**, while a **CT scanner** (refurbished) can cost **USD 35,000**, excluding installation, maintenance, and operational expenses.

In addition to lower capital costs, the proposed system has minimal operational costs. It requires no specialized infrastructure, emits no ionizing radiation, and consumes low electrical power, making it suitable for battery-powered operation. Maintenance costs are also significantly lower due to the absence of complex mechanical components. The system can be operated by healthcare workers with minimal training, further reducing staffing and training expenses.

From a benefit perspective, the system enables **early risk screening**, which can reduce long-term treatment costs by facilitating earlier diagnosis and referral. The portability and scalability of the solution allow a single unit to serve multiple locations, increasing screening coverage while minimizing per-patient cost. Overall, the cost–benefit balance strongly favors the proposed system for mass screening and community-level deployment.

8.4 Evaluate economic and financial aspects

When compared to existing screening technologies, the proposed solution offers a highly favorable economic profile. While CT scanners and ultrasonography systems provide high-resolution diagnostic imaging, their high acquisition costs, infrastructure requirements, and dependence on trained specialists limit their use in low-resource settings. These systems are primarily suited for centralized hospital environments rather than large-scale population screening.

The proposed system, by contrast, emphasizes **affordability and accessibility**. Its low initial investment allows healthcare providers, NGOs, and public health programs to deploy multiple units at a fraction of the cost of a single CT or ultrasound machine. The low operating cost and ease of maintenance further enhance long-term financial sustainability. Additionally, the use of an embedded AI-based screening model reduces reliance on centralized diagnostic facilities, lowering indirect costs such as patient travel, accommodation, and lost productivity. From a national healthcare perspective, widespread adoption of such systems could contribute to reduced diagnostic delays and lower overall cancer treatment expenditure.

8.5 Conclusion

The economic analysis demonstrates that the proposed AI-based thermography screening system is a cost-effective and financially sustainable alternative to conventional imaging technologies for early-stage breast cancer screening. Compared to high-cost modalities such as CT scanners and ultrasonography systems, the proposed solution offers substantially lower capital and operational costs while maintaining practical screening capability. These economic advantages support its suitability for large-scale deployment in low-resource settings, reinforcing the system's potential to improve healthcare accessibility and reduce long-term financial burden on both patients and healthcare providers.

Chapter 9: Ethics and Professional Responsibilities CO13, CO2

9.1 **Introduction**

Engineering projects in the healthcare domain carry significant ethical and professional responsibilities, as they directly affect human well-being, privacy, and safety. The proposed AI-based non-invasive breast cancer screening system involves the collection and analysis of sensitive health-related data and supports clinical decision-making processes. Therefore, ethical considerations must be integrated throughout the system's design, development, testing, and deployment phases.

This chapter discusses the ethical issues associated with the project and outlines the professional responsibilities upheld by the project team. Particular emphasis is placed on patient safety, data privacy, informed consent, responsible use of artificial intelligence, and adherence to professional engineering standards and healthcare ethics.

9.2 Identify ethical issues and professional responsibility

Here are the ethical issues which we must face:

- Patient Consent
- Data Privacy
- Transparency
- Bias Mitigation of AI
- Professional Integrity and Transparency
- Compliance with Standards and Regulations

9.3 Apply ethical issues and professional responsibility

9.3.1 Patient Consent:

It is a must to acquire proper consent from the patients for screening and data collection, using simple language tailored for rural patients to ensure autonomy.

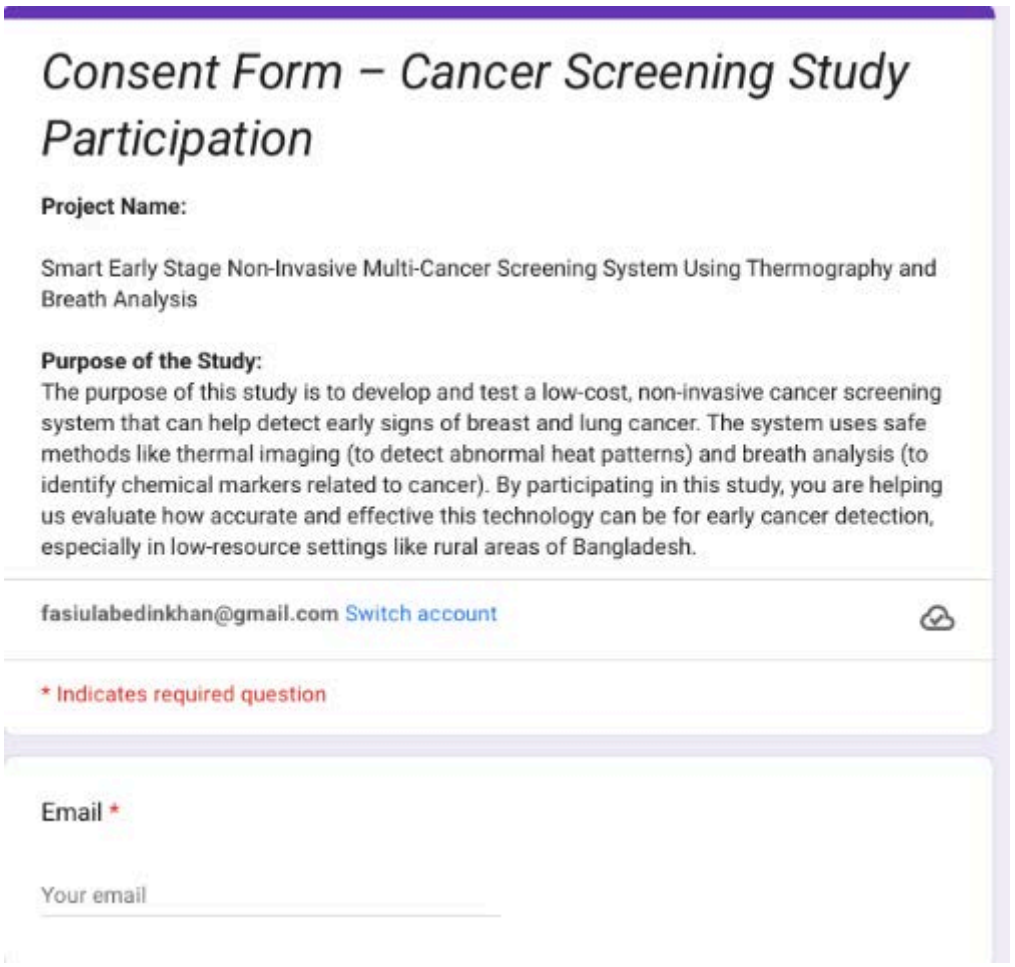

Figure 53: Consent Form

Data Privacy:

Personal data of every patient must be encrypted under the "Digital Security Act, Bangladesh", for preventing unauthorized access and ensuring confidentiality.

Transparency:

There will be a user guide explaining the accuracy and the limitations of the system, ensuring all the patients and healthcare workers are properly informed.

Bias Mitigation of AI:

- AI models will be trained on different datasets to ensure fairness, minimizing the biases of AI.
- Models will be validated through critical trials with more than **200 patients** to confirm their reliability.

Professional Responsibilities

The systems will be updated to ensure sensor calibration is regularly updated to maintain our reliability and prioritize the welfare of the patients.

Based on these, to maintain these ethical boundaries and ensure a proper screen process, we focused on following the guidelines mentioned in Pan American Journal of Medical Thermology:

Guideline 1: Patient Communication and Pre-Examination Preparation

1. Address all patient questions and concerns regarding the examination.
2. Refer treatment or prognostic inquiries to the patient's attending physician.
3. Avoid yoga, massage, or strenuous exercise for at least three hours prior.
4. Refrain from smoking for four hours prior.
5. Do not apply lotions, creams, powders, makeup, deodorants, or antiperspirants on the day of the examination.
6. Avoid underarm shaving on the day of the examination.
7. Prevent extended sun exposure or sunburn on the day before or day of the examination.
8. Abstain from physical stimulation or treatment of the breasts, chest, neck, or back for 24 hours prior, including chiropractic care, acupuncture, TENS, physical therapy, electrical muscle stimulation, ultrasound, massage, or use of ice or heat.
9. Do not bathe within one hour prior.
10. Continue all prescribed medications, but provide a list to the technician, noting beta blockers specifically.
11. Remove external breast prostheses at least 12 hours prior.

Guideline 2: Patient Assessment

1. Obtain a comprehensive breast history prior to imaging, including:
    - 1.1. History and location of breast cancer.
    - 1.2. Presence of palpable masses.
    - 1.3. Nipple discharge, inversion, or changes.
    - 1.4. Skin changes.
    - 1.5. Areas of pain, burning, stinging, tenderness, or achiness.
    - 1.6. History of breast surgeries such as implants, lifts, or reductions.
    - 1.7. Biopsies, diagnoses, and sites.
    - 1.8. Surgical interventions including biopsy or lumpectomy, with dates and diagnoses.
    - 1.9. Breast radiation details, including sites and timelines.
    - 1.10. Pharmacologic agents for breast cancer.
    - 1.11. Mastectomy and surgical revisions with dates.
    - 1.12. Date and result of the most recent mammogram.
    - 1.13. Approximate dates and intervals of prior mammograms.
    - 1.14. Date, result, and location of the most recent breast ultrasonography.
    - 1.15. Date and result of the most recent MRI.

Guideline 3: Examination Guidelines

1. Hardware and Software Specifications:
    1.1. Set emissivity to 0.98 for human skin.
    1.2. Detector response range: above 5 microns and below 14 microns.
    1.3. Preferred absolute detector resolution: greater than 640 by 480, paired with a suitable lens; systems with 320 by 240 sensors may suffice with enhancements.
    1.4. Minimum measurable spot size: 2.1 by 2.0 mm at 40 cm distance.
    1.5. Spot resolution at 8 feet: equivalent to less than or equal to 1 square mm at 40 cm.
    1.6. Spatial resolution at 8 feet: equivalent to less than or equal to 2.6 mRad at 40 cm.
    1.7. Thermal sensitivity: less than 50 mK NETD at 30 degrees Celsius.
    1.8. Capability for accurate quantitative differential temperature analysis with precision of less than or equal to plus or minus 0.05 degrees Celsius.
    1.9. Repeatability and precision: less than or equal to plus or minus 0.05 degrees Celsius for temperature differences.
    1.10. Control external ambient temperature changes at natural convection below 0.2 m per s.
    1.11. Manage thermal drift at natural convection below 0.2 m per s.
    1.12. Maintain detector uniformity through calibration.
    1.13. Capture images in high-resolution color and grayscale.
    1.14. High-resolution visual display for interpretation.
    1.15. Real-time image focus and capture, preferably at 50 Hz or faster.
    1.16. Temperature range: 20 to 45 degrees Celsius.
    1.17. Archive images for future reference and comparison at consistent positioning and distance.
    1.18. Limit software manipulation to preserve original image quality.
    1.19. Software must identify areas for calculations and reporting.
    1.20. Contact thermography devices are considered obsolete.
2. Environmental Controls: Conduct studies in a controlled room at 20 to 23 degrees Celsius (68 to 72 degrees Fahrenheit), stable within plus or minus 1 degree Celsius, with controlled humidity to prevent moisture or perspiration; avoid drafts, sunlight, or incandescent lighting; prefer carpeted flooring.
3. Equilibration: Disrobe the upper body; allow 15 minutes for acclimation without breast contact; during the last 5 minutes, position hands above the head (clasped).
4. Infrared Imaging:
    4.1. Standard views: bilateral frontal, right and left oblique, and preferably right and left lateral; add inferior views if needed for quadrants, or axillary and supraclavicular if inadequate.
    4.2. Capture in high-resolution color and black and white.
    4.3. Additional views at the thermologist's discretion, potentially including posterior views or thermoregulatory challenges such as cold immersion.
    4.4. Use palettes with eight colors over a 10-degree Celsius range; perform post-processing as needed.

Guideline 4: Review of the Infrared Thermography Examination

1. Verify completion and documentation of the evaluation; note any protocol exceptions and reasons.

2. Record technical findings for final interpretation.
3. Complete laboratory documentation.
4. The thermologist must ensure adherence to pre-imaging and office protocols; document deviations; inform patients if images are obtained without medical direction.

Guideline 5: Preparation and Storage of Exam Findings

1. Provide radiometric images in formats such as JPEG or DICOM for analysis and archiving.
2. Interpret images within 48 hours; consider sending patient summary reports within 30 days.
3. Retain image data and reports for at least seven years, in compliance with federal and state regulations.

Guideline 6: Exam Time Considerations

1. Indirect Components: Pre-examination tasks include obtaining prior data, completing paperwork, preparing the room and equipment, and assessing patient history; post-examination tasks include data compilation, processing, review, patient communication, and billing.
2. Direct Components: Optimize equipment, position the patient, and conduct one-on-one interaction.

Guideline 7: Continuing Professional Education

1. Certification is the standard for performing and interpreting clinical infrared imaging.
2. Maintain membership and certification in a nationally recognized medical thermography organization focused on breast thermology.
3. Interpreting physicians must remain updated on advances in breast disease diagnosis and treatment.

Guideline 8: Informed Consent

1. Present informed consent as a process, with a signed form acknowledging that thermography is adjunctive and physiologic, complementing anatomic studies; it detects surface heat only, serving as a risk marker rather than a definitive diagnosis; the initial study establishes a baseline; symmetric abnormalities may lead to false negatives.

Guideline 9: Reporting

1. Report Layout: Clearly state that infrared breast thermal imaging is adjunctive for breast health monitoring; note adherence to peer-reviewed guidelines and images obtained; document thermographic findings and abnormalities; separate impressions using TH classification; include optional clinical impressions.
2. Abnormality Determination: Contralateral nipple temperature difference should not exceed 1.0 degree Celsius; other breast regions including areolar, periareolar, superior quadrants, and axillary areas should not exceed 1.5 degrees Celsius (as references, not diagnostic criteria); mark regions of interest for quantitative and serial comparisons; for post-mastectomy, use concentric measurements from the nipple.

3. Additional Factors: Hot spots, global heat, areolar or periareolar heat, breast bulges or retractions, vascular changes such as inverted V patterns, fragments, closed patterns, or findings inferior to the nipple.
4. TH Classification: TH-1 (symmetrical nonvascular, normal); TH-2 (symmetrical vascular, normal); TH-3 (equivocal, low suspicion); TH-4 (abnormal, moderate suspicion); TH-5 (highly abnormal, high suspicion).
5. Clinical Impression: Provide elaboration such as minimally, moderately, or significantly suspicious, with thermal rationale; refer atypical or abnormal findings for further diagnostic evaluation including clinical examination, blood markers, ultrasound, mammogram, or MRI.
6. Breast Thermal Risk Index (Optional): Calculate using doubled and rounded age (drop zero), family history points (15 for mother, sister, daughter; 10 for others), parity points (by age of first pregnancy, double for nulliparous, subtract for nursing), medication points (half years on birth control, one per five years on hormones), menopause or oophorectomy adjustments, weight (one per 20 pounds overweight), and biopsies (two each); categorize as low (less than 20), moderate (20 to 30), or high (greater than 30). This does not override thermographic impressions.

Guideline 10: Follow-Up Studies

1. Schedule annual follow-ups for normal results (TH-1 and TH-2); six months for TH-3 based on clinical impressions and risks; three months for TH-4 and TH-5.
2. Advise patients to continue regular breast health examinations with their primary care physician; defer treatment recommendations to the chosen practitioner.

Guideline 11: Emerging Technologies

1. Technologies may challenge current guidelines or vary in sophistication.
2. General industrial or personal thermal imaging cameras are not suitable for medical thermology.
3. For FDA-approved technologies deviating from these guidelines, document deviations and rationale in the report while adhering to other components.

9.4 Conclusion

This chapter highlights the importance of ethical practice and professional responsibility in the development of healthcare engineering solutions. By adhering to relevant ethical guidelines, professional standards, and regulatory requirements, the project ensures that the system supports clinical decision-making without compromising trust or accountability.

Chapter 10: Conclusion and Future Work.

10.1 Project summary/Conclusion

This project successfully designed and developed a portable, low-cost, non-invasive AI-assisted breast cancer screening system aimed at addressing critical limitations in conventional screening methods, particularly in low-resource and rural settings. By integrating infrared thermography, machine learning, and embedded edge computing, the system provides an accessible first-line screening solution that supports early risk identification without exposing patients to radiation or requiring specialized infrastructure.

A systematic engineering methodology was adopted, including the evaluation of multiple design approaches, qualitative and quantitative optimization, sustainability and economic analysis, ethical and professional responsibility assessment, and structured project management. The final system delivers a **triage-based output (SAFE / RE-TEST / REFER)** to assist healthcare workers in decision-making while clearly functioning as a screening support tool rather than a diagnostic replacement.

The project demonstrated technical feasibility, economic viability, and sustainability, and was completed within the planned timeline and budget. Overall, this work provides a strong foundation for ethical, scalable, and community-level cancer screening applications.

10.2 Future work

- **Clinical Validation:** Conduct large-scale, IRB-approved clinical trials using Bangladesh-specific datasets to further validate performance and reduce population bias.
- **Model Improvement:** Explore advanced architectures such as attention-based CNNs or multimodal models to improve specificity and robustness under varying environmental conditions.
- **Dataset Expansion:** Develop a comprehensive, localized thermal image dataset to enhance generalizability and long-term model reliability.
- **Hardware Optimization:** Further reduce system size, power consumption, and cost through custom PCB design and optimized embedded inference.
- **Explainability and Trust:** Integrate explainable AI techniques (e.g., thermal heatmaps) to improve clinical interpretability and user confidence.
- **Multi-Cancer Extension:** Expand the system to screen for additional cancers or physiological conditions using thermography and other non-invasive sensors.
- **Field Deployment:** Pilot the system in rural clinics and mobile health camps to assess usability, acceptance, and operational challenges.

Chapter 11: Identification of Complex Engineering Problems and Activities.

11.1: Identify the attribute of complex engineering problem (EP)

Complex Engineering1 Problem (EP) Attributes

Code	Attributes	How Our Project Matches
P1	Depth of knowledge required	✓
P2	Range of conflicting requirements	
P3	Depth of analysis required	✓
P4	Familiarity with issues	
P5	Extent of applicable codes	✓
P6	Extent of stakeholder involvement and needs	✓
P7	Interdependence	

11.2: Provide reasoning how the project address selected attribute (EP)

Code	Attributes	How Our Project Matches	Justification
P1	Depth of knowledge required	✓	The project requires multidisciplinary knowledge of electronics, biomedical engineering, AI/ML, and healthcare to integrate thermal imaging, gas sensors, and deep learning models.
P2	Range of conflicting requirements		
P3	Depth of analysis required	✓	Advanced AI models (CNNs, XGBoost) must be trained and validated on complex biomedical

			datasets, requiring in-depth statistical and computational analysis.
P4	Familiarity with issues		
P5	Extent of applicable codes	✓	The project must comply with international medical device standards (ISO 13485, IEC 62304) and local regulations like the Bangladesh Digital Security Act.
P6	Extent of stakeholder involvement and needs	✓	Multiple stakeholders are involved, including patients, hospitals, regulators, and rural communities. Their diverse needs (affordability, accuracy, safety) guide system design.
P7	Interdependence		

11.3 Identify the attribute of complex engineering activities (EA)

Code	Attributes	How Our Project Matches
A1	Range of resources	✓
A2	Level of interaction	✓
A3	Innovation	
A4	Consequences for society and the environment	✓
A5	Familiarity	

11.4 Provide reasoning how the project address selected attribute (EA)

Code	Attributes	How Our Project Matches	Justification
A1	Range of resources	✓	The project uses diverse resources: simulation software (Proteus, MATLAB, Simulink), PCB design tools (Altium), AI frameworks (Python, TensorFlow), and clinical data.
A2	Level of interaction	✓	It requires strong collaboration among engineers, doctors, patients, and regulatory bodies, making interaction levels high.
A3	Innovation		
A4	Consequences for society and the environment	✓	The project can improve early cancer detection in low-resource areas, saving lives and reducing healthcare costs, with a minimal environmental footprint due to portability.
A5	Familiarity		

References

[1] M. R. Islam, M. Rahman, A. A. M. Khan, M. J. Alam, and S. M. Siddiqua, "Female lung cancer: Emerging issue in Bangladesh," Ann. Oncol., vol. 30, pp. ix133–ix134, Nov. 2019, doi: 10.1093/annonc/mdz432.009.

[2] M. R. Islam et al., "Precise health perspectives: Unraveling the interplay of reproductive factors in hormone receptor–positive and triple-negative breast cancer among Bangladeshi women," J. Clin. Oncol., vol. 42, no. 16_suppl, pp. e22503–e22503, Jun. 2024, doi: 10.1200/JCO.2024.42.16_suppl.e22503.

[3] S. Correspondent, "Cancer accounts for 12pc of annual deaths," The Daily Star, Feb. 01, 2025. [Online]. Available: https://www.thedailystar.net/health/disease/news/cancer-accounts-12pc-annual-deaths-3813516

[4] G. Manjunath, H. Madhu, and S. Kakileti, "AI for early-stage breast cancer screening," J. Glob. Oncol., vol. 5, no. suppl, p. 50, Oct. 2019, doi: 10.1200/jgo.2019.5.suppl.50.

[5] R. M. Alzahrani et al., "Early breast cancer detection via infrared thermography using a CNN enhanced with particle swarm optimization," Sci. Rep., vol. 15, no. 1, p. 25290, Jul. 2025, doi: 10.1038/s41598-025-11218-0.

[5] S. J. Mambou, P. Maresova, O. Krejcar, A. Selamat, and K. Kuca, "Breast cancer detection using infrared thermal imaging and a deep learning model," Sensors, vol. 18, no. 9, p. 2799, Aug. 2018, doi: 10.3390/s18092799.

[6] N. Kosus, A. Kosus, M. Duran, S. Simavlı, and N. Turhan, "Comparison of standard mammography with digital mammography and digital infrared thermal imaging for breast cancer screening," J. Turk. Ger. Gynecol. Assoc., vol. 11, no. 3, pp. 152–157, 2010, doi: 10.5152/jtgga.2010.06.

[7] S. G. Kandlikar et al., "Infrared imaging technology for breast cancer detection—Current status, protocols and new directions," Int. J. Heat Mass Transf., vol. 108, pp. 2303–2320, 2017, doi: 10.1016/j.ijheatmasstransfer.2017.01.086.

[8] L. S. Boogerd et al., "Laparoscopic detection and resection of occult liver tumors of multiple cancer types using real-time near-infrared fluorescence guidance," Surg. Endosc., vol. 31, no. 2, pp. 952–961, 2017, doi: 10.1007/s00464-016-5007-6.

[9] A. Amria, S. H. Pulko, and A. J. Wilk, "Potentialities of steady-state and transient thermography in breast tumour depth detection: A numerical study," Comput. Methods Programs Biomed., vol. 123, pp. 68–80, 2016, doi: 10.1016/j.cmpb.2015.09.014.

[10] M. Kontos, R. Wilson, and I. Fentiman, "Digital infrared thermal imaging (DITI) of breast lesions: Sensitivity and specificity of detection of primary breast cancers," Clin. Radiol., vol. 66, no. 6, pp. 536–539, 2011, doi: 10.1016/j.crad.2011.01.009.

[11] Q. Li et al., "XGBoost-based and tumor-immune characterized gene signature for the prediction of metastatic status in breast cancer," J. Transl. Med., vol. 20, no. 1, p. 177, 2022, doi: 10.1186/s12967-022-03369-9.

[12] M. A. Berbar, Y. A. Reyad, and M. Hussain, "Breast mass classification using statistical and local binary pattern features," in Proc. 16th Int. Conf. Inf. Vis., Montpellier, France, 2012, pp. 486–490, doi: 10.1109/IV.2012.84.

[13] A. Hamidinekoo, E. Denton, A. Rampun, K. Honnor, and R. Zwiggelaar, "Deep learning in mammography and breast histopathology, an overview and future trends," Med. Image Anal., vol. 47, pp. 45–67, 2018, doi: 10.1016/j.media.2018.03.006.

[14] S. Zhang et al., "Potential rapid intraoperative cancer diagnosis using dynamic full-field optical coherence tomography and deep learning: A prospective cohort study in breast cancer patients," Sci. Bull., vol. 69, no. 11, pp. 1748–1756, 2024, doi: 10.1016/j.scib.2024.03.061.

[15] A. Karaman et al., "Hyper-parameter optimization of deep learning architectures using artificial bee colony (ABC) algorithm for high performance real-time automatic colorectal cancer (CRC) polyp detection," Appl. Intell., vol. 53, pp. 15603–15620, 2023, doi: 10.1007/s10489-022-04310-9.

[16] M. Versaci and F. C. Morabito, "Image edge detection: A new approach based on fuzzy entropy and fuzzy divergence," Int. J. Fuzzy Syst., vol. 23, no. 4, pp. 918–936, 2021, doi: 10.1007/s40815-020-01030-5.

[17] T. Namikawa, T. Sato, and K. Hanazaki, "Recent advances in near-infrared fluorescence-guided imaging surgery using indocyanine green," Surg. Today, vol. 45, no. 12, pp. 1467–1474, 2015, doi: 10.1007/s00595-015-1158-7.

[18] G. Işık and İ. Paçal, "Few-shot classification of ultrasound breast cancer images using meta-learning algorithms," Neural Comput. Appl., vol. 36, pp. 12047–12059, 2024, doi: 10.1007/s00521-024-09767-y.

[19] F. Cardoso et al., "Research needs in breast cancer," Ann. Oncol., vol. 28, no. 2, pp. 208–217, 2017, doi: 10.1093/annonc/mdw571.

[20] M. Unar-Munguía, R. Meza, M. A. Colchero, G. Torres-Mejía, and T. G. de Cosío, "Economic and disease burden of breast cancer associated with suboptimal breastfeeding practices in Mexico," Cancer Causes Control, vol. 28, no. 12, pp. 1381–1391, 2017, doi: 10.1007/s10552-017-0965-0.

[21] B. Łyszczarz and E. Nojszewska, "Productivity losses and public finance burden attributable to breast cancer in Poland, 2010–2014," BMC Cancer, vol. 17, p. 676, 2017, doi: 10.1186/s12885-017-3669-7.

[22] IMS Institute for Healthcare Informatics, "Global oncology trend report: A review of 2015 and outlook to 2020," 2016. [Online]. Available: https://morningconsult.com/wp-content/uploads/2016/06/IMS-Institute-Global-Oncology-Report-05.31.16.pdf

[23] B. Ozdemir and I. Pacal, "An innovative deep learning framework for skin cancer detection employing ConvNeXtV2 and focal self-attention mechanisms," Results Eng., vol. 25, p. 103692, 2025, doi: 10.1016/j.rineng.2024.103692.

[24] K. Adapa et al., "A real world evaluation of an innovative artificial intelligence tool for population-level breast cancer screening," npj Digit. Med., vol. 8, no. 1, Art. no. 2, Jan. 2025, doi: 10.1038/s41746-024-01368-2.

[25] Thermaiscan, "Breast Cancer Pre-Screening, AI, Thermal Imaging, Predictive Medicine," 2024. [Online]. Available: https://www.thermaiscan.com/

[26] Grand View Research, "Breast Cancer Diagnostics Market Size, Share & Trends Analysis Report By Product (Platform-based, Instrument-based), By Type (Imaging, Genomic Testing), By Application, By End-use, By Region, And Segment Forecasts, 2025–2033," 2025.

[27] A. M. Abdelaziz, "Lightweight deep learning model with spatial attention for accurate and efficient breast cancer prediction," Sci. Rep., vol. 15, no. 1, Art. no. 34311, Jan. 2025, doi: 10.1038/s41598-025-34311-w.

[28] Stratipath, "Stratipath and Visiopharm partner to advance implementation of AI-Powered Breast Cancer Diagnostics," Sep. 2025. [Online]. Available: https://www.stratipath.com/stratipath-and-visiopharm-partner-to-advance-implementation-of-ai-powered-breast-cancer-diagnostics

[29] MarketsandMarkets, "Artificial Intelligence (AI) in Healthcare Market worth $110.61 billion by 2030," Sep. 2025. [Online]. Available: https://www.marketsandmarkets.com/PressReleases/artificial-intelligence-healthcare.asp

[30] A. Mashekova et al., "Review of Artificial Intelligence Techniques for Breast Cancer Detection with Different Modalities: Mammography, Ultrasound, and Thermography Images," Bioengineering, vol. 12, no. 11, Art. no. 1110, Oct. 2025, doi: 10.3390/bioengineering12101110.

[31] N. Eisemann et al., "Nationwide real-world implementation of AI for cancer detection in population-based mammography screening," Nat. Med., vol. 31, no. 9, pp. 917–924, Jan. 2025, doi: 10.1038/s41591-024-03408-6.

[32] D. Seidenwurm et al., "Assessing the Recall Rate for Screening Mammography: Comparing the Medicare Hospital Compare Dataset With the National Mammography Database," AJR Am. J. Roentgenol., 2025.

[33] BIOT, "EU AI Act + MDR Compliance Guide for AI-Enabled Medical Devices," 2025. [Online]. Available: https://www.biot-med.com/resources/eu-ai-act-mdr-compliance-guide-for-ai-enabled-medical-devices

[34] U.S. Food and Drug Administration, "Artificial Intelligence-Enabled Medical Devices," 2025. [Online]. Available: https://www.fda.gov/medical-devices/software-medical-device-samd/artificial-intelligence-enabled-medical-devices

[35] S. J. Mambou, P. Maresova, O. Krejcar, A. Selamat, and K. Kuca, "Breast cancer detection using infrared thermal imaging and a deep learning model," Sensors, vol. 18, no. 9, p. 2799, Aug. 2018, doi: 10.3390/s18092799.

[36] I. Polaka et al., "Modular point-of-care breath analyzer and shape taxonomy-based machine learning for gastric cancer detection," Diagnostics, vol. 12, no. 2, p. 491, Feb. 2022, doi: 10.3390/diagnostics12020491.

[37] T. Ding, K. Shi, Z. Pan, and C. Ding, "AI-based automated breast cancer segmentation in ultrasound imaging based on attention gated multi ResU-Net," PeerJ Comput. Sci., vol. 10, p. e2226, Oct. 2024, doi: 10.7717/peerj-cs.2226.

[38] A. Iqbal and M. Sharif, "MDA-Net: Multiscale dual attention-based network for breast lesion segmentation using ultrasound images," J. King Saud Univ. - Comput. Inf. Sci., vol. 34, no. 9, pp. 7283–7299, Oct. 2021, doi: 10.1016/j.jksuci.2021.10.002.

[39] P. Getson et al., "Guidelines for Breast Thermography," Pan Am. J. Med. Thermol., vol. 2, no. 1, pp. 26–34, Jun. 2015, doi: 10.18073/2358-4696/pajmt.v2n1p26-34.

Appendix

Related code/theory

ML Training Code:

```
import os
import numpy as np
import pandas as pd
import matplotlib.pyplot as plt
import seaborn as sns
import time
from datetime import datetime

import tensorflow as tf
from tensorflow import keras
from tensorflow.keras import layers, models, callbacks
from tensorflow.keras.applications import (
    MobileNet, DenseNet121, ResNet50, VGG16,
    InceptionV3, EfficientNetB0, Xception
)
from tensorflow.keras.losses import BinaryFocalCrossentropy
from tensorflow.keras.preprocessing.image import ImageDataGenerator

from sklearn.metrics import (
    accuracy_score, precision_score, recall_score, f1_score,
    roc_auc_score, confusion_matrix, classification_report,
    roc_curve, auc, balanced_accuracy_score
)
from sklearn.utils.class_weight import compute_class_weight

# ============================================================
# CONFIGURATION
# ============================================================
DATA_DIR = "/kaggle/input/bc-2000-aug-dataset"
IMG_SIZE = (224, 224)
BATCH_SIZE = 32
EPOCHS_STAGE1 = 10  # Train head only
EPOCHS_STAGE2 = 20  # Fine-tune full model
SEED = 42

# Set random seeds for reproducibility
np.random.seed(SEED)
tf.random.set_seed(SEED)

print("="*70)
print("COMPREHENSIVE MODEL COMPARISON FOR BREAST CANCER CLASSIFICATION")
print("="*70)
print(f"Dataset: {DATA_DIR}")
print(f"Image Size: {IMG_SIZE}")
print(f"Batch Size: {BATCH_SIZE}")
print(f"Total Epochs: {EPOCHS_STAGE1 + EPOCHS_STAGE2}")
print("="*70 + "\n")

# ============================================================
# DATA PREPARATION
# ============================================================
print("Preparing data generators...")
```

```
train_datagen = ImageDataGenerator(
    rescale=1./255,
    validation_split=0.2,
    rotation_range=25,
    width_shift_range=0.1,
    height_shift_range=0.1,
    zoom_range=0.15,
    horizontal_flip=True,
    vertical_flip=True,
    brightness_range=[0.8, 1.2],
    fill_mode="nearest"
)

val_datagen = ImageDataGenerator(
    rescale=1./255,
    validation_split=0.2
)

train_gen = train_datagen.flow_from_directory(
    DATA_DIR,
    target_size=IMG_SIZE,
    batch_size=BATCH_SIZE,
    class_mode="binary",
    subset="training",
    shuffle=True,
    seed=SEED
)

val_gen = val_datagen.flow_from_directory(
    DATA_DIR,
    target_size=IMG_SIZE,
    batch_size=BATCH_SIZE,
    class_mode="binary",
    subset="validation",
    shuffle=False,
    seed=SEED
)

# Compute class weights
labels = train_gen.classes
class_weights = compute_class_weight(
    class_weight="balanced",
    classes=np.unique(labels),
    y=labels
)
class_weight_dict = dict(enumerate(class_weights))

print(f"Training samples: {len(train_gen.filenames)}")
print(f"Validation samples: {len(val_gen.filenames)}")
print(f"Class indices: {train_gen.class_indices}")
print(f"Class weights: {class_weight_dict}\n")

# ============================================================
# MODEL DEFINITIONS
# ============================================================
def create_model(base_model_func, name, input_shape=(224, 224, 3), unfreeze_layers=-30):
    """
    Creates a transfer learning model with consistent architecture
```

```
    """
    base_model = base_model_func(
        weights="imagenet",
        include_top=False,
        input_shape=input_shape
    )

    # Freeze base model initially
    for layer in base_model.layers[:-30]:
        layer.trainable = False

    # Add classification head
    x = layers.GlobalAveragePooling2D(name=f'{name}_gap')(base_model.output)
    x = layers.BatchNormalization(name=f'{name}_bn1')(x)
    x = layers.Dense(512, activation="relu", name=f'{name}_dense1')(x)
    x = layers.Dropout(0.5, name=f'{name}_dropout1')(x)
    x = layers.Dense(256, activation="relu", name=f'{name}_dense2')(x)
    x = layers.Dropout(0.4, name=f'{name}_dropout2')(x)
    output = layers.Dense(1, activation="sigmoid", name=f'{name}_output')(x)

    model = models.Model(base_model.input, output, name=name)
    return model, base_model

# Dictionary of models to compare
MODELS = {
    'MobileNet': MobileNet,
    'DenseNet121': DenseNet121,
    'ResNet50': ResNet50,
    'VGG16': VGG16,
    'InceptionV3': InceptionV3,
    'EfficientNetB0': EfficientNetB0,
    'Xception': Xception,
}

# ============================================================
# TRAINING FUNCTION
# ============================================================
def train_model(model_name, base_model_func, train_gen, val_gen, class_weight_dict):
    """
    Trains a model in two stages:
    1. Train only the classification head
    2. Fine-tune with focal loss
    """
    print("\n" + "="*70)
    print(f"TRAINING: {model_name}")
    print("="*70)

    start_time = time.time()

    # Create model
    model, base_model = create_model(base_model_func, model_name)

    # Count parameters
    total_params = model.count_params()
    trainable_params = sum([tf.size(w).numpy() for w in model.trainable_weights])
    print(f"Total parameters: {total_params:,}")
    print(f"Trainable parameters (Stage 1): {trainable_params:,}")

    # ============================================================
```

```
# STAGE 1: Train classification head only
# ============================================================
print(f"\n[Stage 1] Training classification head ({EPOCHS_STAGE1} epochs)...")

model.compile(
    optimizer=keras.optimizers.Adam(learning_rate=1e-3),
    loss="binary_crossentropy",
    metrics=["accuracy", keras.metrics.AUC(name="auc")]
)

history1 = model.fit(
    train_gen,
    validation_data=val_gen,
    epochs=EPOCHS_STAGE1,
    class_weight=class_weight_dict,
    callbacks=[
        callbacks.EarlyStopping(
            monitor="val_auc",
            patience=5,
            restore_best_weights=True,
            verbose=1
        )
    ],
    verbose=0
)

stage1_epochs = len(history1.history['loss'])
print(f"Stage 1 completed in {stage1_epochs} epochs")
print(f"Best val_auc: {max(history1.history['val_auc']):.4f}")

# ============================================================
# STAGE 2: Fine-tune with Focal Loss
# ============================================================
print(f"\n[Stage 2] Fine-tuning with focal loss ({EPOCHS_STAGE2} epochs)...")

# Unfreeze base model
base_model.trainable = True

# Recompile with focal loss and lower learning rate
focal_loss = BinaryFocalCrossentropy(gamma=2.0, alpha=0.75)

model.compile(
    optimizer=keras.optimizers.Adam(learning_rate=1e-5),
    loss=focal_loss,
    metrics=["accuracy", keras.metrics.AUC(name="auc")]
)

trainable_params_stage2 = sum([tf.size(w).numpy() for w in model.trainable_weights])
print(f"Trainable parameters (Stage 2): {trainable_params_stage2:,}")

history2 = model.fit(
    train_gen,
    validation_data=val_gen,
    epochs=EPOCHS_STAGE2,
    class_weight=class_weight_dict,
    callbacks=[
        callbacks.EarlyStopping(
            monitor="val_auc",
            patience=7,
```

```
            restore_best_weights=True,
            verbose=1
        )
    ],
    verbose=0
)

stage2_epochs = len(history2.history['loss'])
print(f"Stage 2 completed in {stage2_epochs} epochs")
print(f"Best val_auc: {max(history2.history['val_auc']):.4f}")

training_time = time.time() - start_time

# Combine histories
history = {
    'loss': history1.history['loss'] + history2.history['loss'],
    'accuracy': history1.history['accuracy'] + history2.history['accuracy'],
    'auc': history1.history['auc'] + history2.history['auc'],
    'val_loss': history1.history['val_loss'] + history2.history['val_loss'],
    'val_accuracy': history1.history['val_accuracy'] + history2.history['val_accuracy'],
    'val_auc': history1.history['val_auc'] + history2.history['val_auc'],
}

return model, history, training_time, total_params

# ============================================================
# EVALUATION FUNCTION
# ============================================================
def evaluate_model(model, val_gen):
    """
    Comprehensive evaluation with threshold optimization
    """
    print("\nEvaluating model...")

    # Get predictions
    val_gen.reset()
    y_pred_probs = model.predict(val_gen, verbose=0).ravel()
    y_true = val_gen.classes

    # Find optimal threshold
    best_threshold = 0.5
    best_f1 = 0

    for threshold in np.linspace(0.2, 0.7, 51):
        y_pred = (y_pred_probs > threshold).astype(int)
        f1 = f1_score(y_true, y_pred)
        if f1 > best_f1:
            best_f1 = f1
            best_threshold = threshold

    # Make final predictions with optimal threshold
    y_pred = (y_pred_probs > best_threshold).astype(int)

    # Calculate metrics
    metrics = {
        'threshold': best_threshold,
        'accuracy': accuracy_score(y_true, y_pred),
        'balanced_accuracy': balanced_accuracy_score(y_true, y_pred),
        'precision': precision_score(y_true, y_pred),
```

```
        'recall': recall_score(y_true, y_pred),
        'f1_score': f1_score(y_true, y_pred),
        'auc': roc_auc_score(y_true, y_pred_probs),
    }

    # Confusion matrix
    cm = confusion_matrix(y_true, y_pred)
    tn, fp, fn, tp = cm.ravel()

    metrics['sensitivity'] = tp / (tp + fn) if (tp + fn) > 0 else 0
    metrics['specificity'] = tn / (tn + fp) if (tn + fp) > 0 else 0
    metrics['confusion_matrix'] = cm

    # ROC curve data
    fpr, tpr, _ = roc_curve(y_true, y_pred_probs)
    metrics['roc_curve'] = (fpr, tpr)

    print(f"\nOptimal threshold: {best_threshold:.3f}")
    print(f"Accuracy: {metrics['accuracy']:.4f}")
    print(f"Balanced Accuracy: {metrics['balanced_accuracy']:.4f}")
    print(f"AUC: {metrics['auc']:.4f}")
    print(f"F1-Score: {metrics['f1_score']:.4f}")
    print(f"Sensitivity: {metrics['sensitivity']:.4f}")
    print(f"Specificity: {metrics['specificity']:.4f}")

    return metrics

# ============================================================
# TRAIN ALL MODELS
# ============================================================
print("\n" + "="*70)
print("STARTING MODEL TRAINING AND COMPARISON")
print("="*70 + "\n")

results = {}

for model_name, model_func in MODELS.items():
    try:
        # Train model
        model, history, training_time, total_params = train_model(
            model_name, model_func, train_gen, val_gen, class_weight_dict
        )

        # Evaluate model
        metrics = evaluate_model(model, val_gen)

        # Store results
        results[model_name] = {
            'model': model,
            'history': history,
            'metrics': metrics,
            'training_time': training_time,
            'total_params': total_params
        }

        print(f"\n✓ {model_name} completed successfully!")
        print(f"  Training time: {training_time/60:.2f} minutes")

        # Clear memory
```

```
        del model
        keras.backend.clear_session()

    except Exception as e:
        print(f"\n✗ {model_name} failed with error: {str(e)}")
        results[model_name] = None

print("\n" + "="*70)
print("ALL MODELS TRAINED!")
print("="*70 + "\n")

# ============================================================
# CREATE COMPARISON TABLE
# ============================================================
print("Creating comparison table...")

comparison_data = []
for model_name, result in results.items():
    if result is not None:
        metrics = result['metrics']
        comparison_data.append({
            'Model': model_name,
            'Parameters (M)': result['total_params'] / 1e6,
            'Training Time (min)': result['training_time'] / 60,
            'Accuracy': metrics['accuracy'],
            'Balanced Acc': metrics['balanced_accuracy'],
            'Precision': metrics['precision'],
            'Recall': metrics['recall'],
            'F1-Score': metrics['f1_score'],
            'AUC': metrics['auc'],
            'Sensitivity': metrics['sensitivity'],
            'Specificity': metrics['specificity'],
            'Threshold': metrics['threshold']
        })

df_comparison = pd.DataFrame(comparison_data)
df_comparison = df_comparison.sort_values('AUC', ascending=False)

print("\n" + "="*100)
print("COMPREHENSIVE MODEL COMPARISON RESULTS")
print("="*100)
print(df_comparison.to_string(index=False))
print("="*100 + "\n")

# Save to CSV
df_comparison.to_csv('model_comparison_results.csv', index=False)
print("✓ Results saved to: model_comparison_results.csv\n")

# ============================================================
# VISUALIZATION 1: PERFORMANCE METRICS COMPARISON
# ============================================================
print("Creating visualizations...")

fig = plt.figure(figsize=(20, 12))

# Metrics to compare
metrics_to_plot = ['Accuracy', 'Precision', 'Recall', 'F1-Score', 'AUC', 'Sensitivity', 'Specificity']
colors = plt.cm.Set3(np.linspace(0, 1, len(df_comparison)))
```

```
# 1. Bar chart for each metric
for idx, metric in enumerate(metrics_to_plot):
    ax = plt.subplot(3, 3, idx + 1)
    bars = ax.bar(df_comparison['Model'], df_comparison[metric], color=colors, edgecolor='black',
linewidth=1.5)
    ax.set_ylabel(metric, fontsize=11, fontweight='bold')
    ax.set_ylim([0, 1.05])
    ax.grid(axis='y', alpha=0.3, linestyle='--')
    ax.set_xticklabels(df_comparison['Model'], rotation=45, ha='right', fontsize=9)

    # Add value labels on bars
    for bar in bars:
        height = bar.get_height()
        ax.text(bar.get_x() + bar.get_width()/2., height + 0.01,
                f'{height:.3f}', ha='center', va='bottom', fontsize=8, fontweight='bold')

    # Highlight best model
    best_idx = df_comparison[metric].idxmax()
    bars[best_idx].set_edgecolor('red')
    bars[best_idx].set_linewidth(3)

# 8. Training time comparison
ax8 = plt.subplot(3, 3, 8)
bars = ax8.bar(df_comparison['Model'], df_comparison['Training Time (min)'],
               color=colors, edgecolor='black', linewidth=1.5)
ax8.set_ylabel('Training Time (minutes)', fontsize=11, fontweight='bold')
ax8.grid(axis='y', alpha=0.3, linestyle='--')
ax8.set_xticklabels(df_comparison['Model'], rotation=45, ha='right', fontsize=9)
for bar in bars:
    height = bar.get_height()
    ax8.text(bar.get_x() + bar.get_width()/2., height + 0.5,
             f'{height:.1f}', ha='center', va='bottom', fontsize=8, fontweight='bold')

# 9. Model size comparison
ax9 = plt.subplot(3, 3, 9)
bars = ax9.bar(df_comparison['Model'], df_comparison['Parameters (M)'],
               color=colors, edgecolor='black', linewidth=1.5)
ax9.set_ylabel('Parameters (Millions)', fontsize=11, fontweight='bold')
ax9.grid(axis='y', alpha=0.3, linestyle='--')
ax9.set_xticklabels(df_comparison['Model'], rotation=45, ha='right', fontsize=9)
for bar in bars:
    height = bar.get_height()
    ax9.text(bar.get_x() + bar.get_width()/2., height + 1,
             f'{height:.1f}M', ha='center', va='bottom', fontsize=8, fontweight='bold')

plt.suptitle('Comprehensive Model Performance Comparison',
             fontsize=16, fontweight='bold', y=0.995)
plt.tight_layout()
plt.savefig('model_comparison_metrics.png', dpi=300, bbox_inches='tight')
plt.show()

# ============================================================
# VISUALIZATION 2: ROC CURVES COMPARISON
# ============================================================
fig, (ax1, ax2) = plt.subplots(1, 2, figsize=(16, 7))

colors_roc = plt.cm.tab10(np.linspace(0, 1, len(results)))

for idx, (model_name, result) in enumerate(results.items()):
```

```
    if result is not None:
        fpr, tpr = result['metrics']['roc_curve']
        auc_score = result['metrics']['auc']

        # Full ROC
        ax1.plot(fpr, tpr, lw=2.5, color=colors_roc[idx],
                 label=f'{model_name} (AUC={auc_score:.4f})')

        # Zoomed ROC
        ax2.plot(fpr, tpr, lw=2.5, color=colors_roc[idx],
                 label=f'{model_name} (AUC={auc_score:.4f})')

# Full ROC styling
ax1.plot([0, 1], [0, 1], 'k--', lw=2, label='Random (AUC=0.5000)')
ax1.set_xlim([0.0, 1.0])
ax1.set_ylim([0.0, 1.05])
ax1.set_xlabel('False Positive Rate', fontsize=13, fontweight='bold')
ax1.set_ylabel('True Positive Rate', fontsize=13, fontweight='bold')
ax1.set_title('ROC Curves - All Models (Full View)', fontsize=14, fontweight='bold')
ax1.legend(loc='lower right', fontsize=9)
ax1.grid(alpha=0.3, linestyle='--')

# Zoomed ROC styling
ax2.plot([0, 1], [0, 1], 'k--', lw=2)
ax2.set_xlim([0.0, 0.3])
ax2.set_ylim([0.7, 1.0])
ax2.set_xlabel('False Positive Rate', fontsize=13, fontweight='bold')
ax2.set_ylabel('True Positive Rate', fontsize=13, fontweight='bold')
ax2.set_title('ROC Curves - All Models (Zoomed View)', fontsize=14, fontweight='bold')
ax2.legend(loc='lower right', fontsize=9)
ax2.grid(alpha=0.3, linestyle='--')

plt.tight_layout()
plt.savefig('model_comparison_roc.png', dpi=300, bbox_inches='tight')
plt.show()

# ============================================================
# VISUALIZATION 3: CONFUSION MATRICES
# ============================================================
n_models = len([r for r in results.values() if r is not None])
fig = plt.figure(figsize=(18, 3 * ((n_models + 3) // 4)))

plot_idx = 1
for model_name, result in results.items():
    if result is not None:
        ax = plt.subplot((n_models + 3) // 4, 4, plot_idx)
        cm = result['metrics']['confusion_matrix']

        sns.heatmap(cm, annot=True, fmt='d', cmap='Blues', ax=ax,
                    xticklabels=['Benign', 'Malignant'],
                    yticklabels=['Benign', 'Malignant'],
                    cbar_kws={'label': 'Count'})

        acc = result['metrics']['accuracy']
        auc_score = result['metrics']['auc']
        ax.set_title(f'{model_name}\nAcc: {acc:.3f} | AUC: {auc_score:.3f}',
                     fontsize=11, fontweight='bold')
        ax.set_xlabel('Predicted', fontsize=10)
        ax.set_ylabel('True', fontsize=10)
```

```
        plot_idx += 1

plt.suptitle('Confusion Matrices - All Models', fontsize=16, fontweight='bold')
plt.tight_layout()
plt.savefig('model_comparison_confusion_matrices.png', dpi=300, bbox_inches='tight')
plt.show()

# ============================================================
# VISUALIZATION 4: TRAINING HISTORY
# ============================================================
fig = plt.figure(figsize=(18, 4 * ((n_models + 1) // 2)))

plot_idx = 1
for model_name, result in results.items():
    if result is not None:
        history = result['history']

        # Loss
        ax1 = plt.subplot((n_models + 1) // 2, 4, plot_idx)
        ax1.plot(history['loss'], label='Train Loss', linewidth=2)
        ax1.plot(history['val_loss'], label='Val Loss', linewidth=2)
        ax1.set_title(f'{model_name} - Loss', fontsize=11, fontweight='bold')
        ax1.set_xlabel('Epoch')
        ax1.set_ylabel('Loss')
        ax1.legend()
        ax1.grid(alpha=0.3)

        # Accuracy
        ax2 = plt.subplot((n_models + 1) // 2, 4, plot_idx + 1)
        ax2.plot(history['accuracy'], label='Train Acc', linewidth=2)
        ax2.plot(history['val_accuracy'], label='Val Acc', linewidth=2)
        ax2.set_title(f'{model_name} - Accuracy', fontsize=11, fontweight='bold')
        ax2.set_xlabel('Epoch')
        ax2.set_ylabel('Accuracy')
        ax2.legend()
        ax2.grid(alpha=0.3)

        plot_idx += 2

plt.suptitle('Training History - All Models', fontsize=16, fontweight='bold')
plt.tight_layout()
plt.savefig('model_comparison_training_history.png', dpi=300, bbox_inches='tight')
plt.show()

# ============================================================
# FINAL SUMMARY
# ============================================================
print("\n" + "="*100)
print("FINAL SUMMARY - BEST PERFORMING MODELS")
print("="*100)

# Rank by different metrics
metrics_ranking = ['AUC', 'Accuracy', 'F1-Score', 'Balanced Acc']

for metric in metrics_ranking:
    top_3 = df_comparison.nlargest(3, metric)[['Model', metric]]
    print(f"\nTop 3 by {metric}:")
    for idx, row in top_3.iterrows():
```

```
        print(f"  {idx+1}. {row['Model']}: {row[metric]:.4f}")

print("\n" + "="*100)
print("RECOMMENDATION FOR PAPER")
print("="*100)

best_model = df_comparison.iloc[0]
print(f"\nBest Overall Model: {best_model['Model']}")
print(f"  - AUC: {best_model['AUC']:.4f}")
print(f"  - Accuracy: {best_model['Accuracy']:.4f}")
print(f"  - F1-Score: {best_model['F1-Score']:.4f}")
print(f"  - Balanced Accuracy: {best_model['Balanced Acc']:.4f}")
print(f"  - Training Time: {best_model['Training Time (min)']:.2f} minutes")
print(f"  - Parameters: {best_model['Parameters (M)']:.2f}M")

# Find best lightweight model (< 10M parameters)
lightweight = df_comparison[df_comparison['Parameters (M)'] < 10]
if not lightweight.empty:
    best_lightweight = lightweight.iloc[0]
    print(f"\nBest Lightweight Model: {best_lightweight['Model']}")
    print(f"  - AUC: {best_lightweight['AUC']:.4f}")
    print(f"  - Accuracy: {best_lightweight['Accuracy']:.4f}")
    print(f"  - Parameters: {best_lightweight['Parameters (M)']:.2f}M")

print("\n" + "="*100)
print("All results saved!")
print("  - model_comparison_results.csv")
print("  - model_comparison_metrics.png")
print("  - model_comparison_roc.png")
print("  - model_comparison_confusion_matrices.png")
print("  - model_comparison_training_history.png")
print("="*100)

print("\n✓ COMPARISON COMPLETE! All visualizations and data ready for your paper.")
```

Neural Network Model Architecture:

Layer (type)	Output Shape	Param #
input_layer_2 (InputLayer)	(None, 224, 224, 3)	0
conv1 (Conv2D)	(None, 112, 112, 32)	864
conv1_bn (BatchNormalization)	(None, 112, 112, 32)	128
conv1_relu (ReLU)	(None, 112, 112, 32)	0
conv_dw_1 (DepthwiseConv2D)	(None, 112, 112, 32)	288
conv_dw_1_bn (BatchNormalization)	(None, 112, 112, 32)	128

conv_dw_1_relu (ReLU)	(None, 112, 112, 32)	0
conv_pw_1 (Conv2D)	(None, 112, 112, 64)	2,048
conv_pw_1_bn (BatchNormalization)	(None, 112, 112, 64)	256
conv_pw_1_relu (ReLU)	(None, 112, 112, 64)	0
conv_pad_2 (ZeroPadding2D)	(None, 113, 113, 64)	0
conv_dw_2 (DepthwiseConv2D)	(None, 56, 56, 64)	576
conv_dw_2_bn (BatchNormalization)	(None, 56, 56, 64)	256
conv_dw_2_relu (ReLU)	(None, 56, 56, 64)	0
conv_pw_2 (Conv2D)	(None, 56, 56, 128)	8,192
conv_pw_2_bn (BatchNormalization)	(None, 56, 56, 128)	512
conv_pw_2_relu (ReLU)	(None, 56, 56, 128)	0
conv_dw_3 (DepthwiseConv2D)	(None, 56, 56, 128)	1,152
conv_dw_3_bn (BatchNormalization)	(None, 56, 56, 128)	512
conv_dw_3_relu (ReLU)	(None, 56, 56, 128)	0
conv_pw_3 (Conv2D)	(None, 56, 56, 128)	16,384
conv_pw_3_bn (BatchNormalization)	(None, 56, 56, 128)	512
conv_pw_3_relu (ReLU)	(None, 56, 56, 128)	0
conv_pad_4 (ZeroPadding2D)	(None, 57, 57, 128)	0
conv_dw_4 (DepthwiseConv2D)	(None, 28, 28, 128)	1,152
conv_dw_4_bn (BatchNormalization)	(None, 28, 28, 128)	512
conv_dw_4_relu (ReLU)	(None, 28, 28, 128)	0
conv_pw_4 (Conv2D)	(None, 28, 28, 256)	32,768
conv_pw_4_bn (BatchNormalization)	(None, 28, 28, 256)	1,024
conv_pw_4_relu (ReLU)	(None, 28, 28, 256)	0
conv_dw_5 (DepthwiseConv2D)	(None, 28, 28, 256)	2,304
conv_dw_5_bn (BatchNormalization)	(None, 28, 28, 256)	1,024

conv_dw_5_relu (ReLU)	(None, 28, 28, 256)	0
conv_pw_5 (Conv2D)	(None, 28, 28, 256)	65,536
conv_pw_5_bn (BatchNormalization)	(None, 28, 28, 256)	1,024
conv_pw_5_relu (ReLU)	(None, 28, 28, 256)	0
conv_pad_6 (ZeroPadding2D)	(None, 29, 29, 256)	0
conv_dw_6 (DepthwiseConv2D)	(None, 14, 14, 256)	2,304
conv_dw_6_bn (BatchNormalization)	(None, 14, 14, 256)	1,024
conv_dw_6_relu (ReLU)	(None, 14, 14, 256)	0
conv_pw_6 (Conv2D)	(None, 14, 14, 512)	131,072
conv_pw_6_bn (BatchNormalization)	(None, 14, 14, 512)	2,048
conv_pw_6_relu (ReLU)	(None, 14, 14, 512)	0
conv_dw_7 (DepthwiseConv2D)	(None, 14, 14, 512)	4,608
conv_dw_7_bn (BatchNormalization)	(None, 14, 14, 512)	2,048
conv_dw_7_relu (ReLU)	(None, 14, 14, 512)	0
conv_pw_7 (Conv2D)	(None, 14, 14, 512)	262,144
conv_pw_7_bn (BatchNormalization)	(None, 14, 14, 512)	2,048
conv_pw_7_relu (ReLU)	(None, 14, 14, 512)	0
conv_dw_8 (DepthwiseConv2D)	(None, 14, 14, 512)	4,608
conv_dw_8_bn (BatchNormalization)	(None, 14, 14, 512)	2,048
conv_dw_8_relu (ReLU)	(None, 14, 14, 512)	0
conv_pw_8 (Conv2D)	(None, 14, 14, 512)	262,144
conv_pw_8_bn (BatchNormalization)	(None, 14, 14, 512)	2,048
conv_pw_8_relu (ReLU)	(None, 14, 14, 512)	0
conv_dw_9 (DepthwiseConv2D)	(None, 14, 14, 512)	4,608
conv_dw_9_bn (BatchNormalization)	(None, 14, 14, 512)	2,048
conv_dw_9_relu (ReLU)	(None, 14, 14, 512)	0

conv_pw_9 (Conv2D)	(None, 14, 14, 512)	262,144
conv_pw_9_bn (BatchNormalization)	(None, 14, 14, 512)	2,048
conv_pw_9_relu (ReLU)	(None, 14, 14, 512)	0
conv_dw_10 (DepthwiseConv2D)	(None, 14, 14, 512)	4,608
conv_dw_10_bn (BatchNormalization)	(None, 14, 14, 512)	2,048
conv_dw_10_relu (ReLU)	(None, 14, 14, 512)	0
conv_pw_10 (Conv2D)	(None, 14, 14, 512)	262,144
conv_pw_10_bn (BatchNormalization)	(None, 14, 14, 512)	2,048
conv_pw_10_relu (ReLU)	(None, 14, 14, 512)	0
conv_dw_11 (DepthwiseConv2D)	(None, 14, 14, 512)	4,608
conv_dw_11_bn (BatchNormalization)	(None, 14, 14, 512)	2,048
conv_dw_11_relu (ReLU)	(None, 14, 14, 512)	0
conv_pw_11 (Conv2D)	(None, 14, 14, 512)	262,144
conv_pw_11_bn (BatchNormalization)	(None, 14, 14, 512)	2,048
conv_pw_11_relu (ReLU)	(None, 14, 14, 512)	0
conv_pad_12 (ZeroPadding2D)	(None, 15, 15, 512)	0
conv_dw_12 (DepthwiseConv2D)	(None, 7, 7, 512)	4,608
conv_dw_12_bn (BatchNormalization)	(None, 7, 7, 512)	2,048
conv_dw_12_relu (ReLU)	(None, 7, 7, 512)	0
conv_pw_12 (Conv2D)	(None, 7, 7, 1024)	524,288
conv_pw_12_bn (BatchNormalization)	(None, 7, 7, 1024)	4,096
conv_pw_12_relu (ReLU)	(None, 7, 7, 1024)	0
conv_dw_13 (DepthwiseConv2D)	(None, 7, 7, 1024)	9,216
conv_dw_13_bn (BatchNormalization)	(None, 7, 7, 1024)	4,096
conv_dw_13_relu (ReLU)	(None, 7, 7, 1024)	0
conv_pw_13 (Conv2D)	(None, 7, 7, 1024)	1,048,576

conv_pw_13_bn (BatchNormalization)	(None, 7, 7, 1024)	4,096
conv_pw_13_relu (ReLU)	(None, 7, 7, 1024)	0
global_average_pooling2d_2 (GlobalAveragePooling2D)	(None, 1024)	0
batch_normalization_2 (BatchNormalization)	(None, 1024)	4,096
dense_4 (Dense)	(None, 512)	524,800
dropout_2 (Dropout)	(None, 512)	0
dense_5 (Dense)	(None, 1)	513

Logbook

Logbook (FYDP-P):

Member name	***Name***	***ID***
1.	FARRDIN NOWSHAD	21321007
2	MD. ABU ANAS MRIDUL	22121024
3.	ABRAR MAKSUD NAHEAN	22121076
4.	MOHAMMAD FASIUL ABEDIN KHAN	22121092

ATC Panel Details		
Chair	Dr. Nahid Akhter Jahan	nahid.jahan@bracu.ac.bd
Member-1	Tasfin Mahmud	tasfin.mahmud@bracu.ac.bd

Log-book of Group 11**(FYDP-P)**				
Date/Time	**Attendee**	**Summary of the meeting**	**Responsible**	**Comment by ATC**
08-02-2025	Farrdin	Brainstorming day 1	All	N/A
	Anas			
	Nahean			N/A
	Fasiul			

10-02-2025	Farrdin	Brainstorming day 2	All	N/A
	Anas			
	Nahean			N/A
	Fasiul			
13-02-2025	Farrdin	Brainstorming day 3	All	N/A
	Anas			
	Nahean			N/A
	Fasiul			
16-02-2025	Farrdin	Brainstorming day 4	All	N/A
	Anas			
	Nahean			N/A
	Fasiul			
18-02-2025	Farrdin	Shortlisting project ideas	Vortex-based power generation	N/A
	Anas		Noninvasive Breast cancer detection	
	Nahean		Smart glass	N/A
	Fasiul		SWARM drones	
20-02-2025	Fasiul	First meeting with the ATC panel, demonstrating all 4 ideas to the panel. The panel suggested dropping 2 ideas and choosing the ideal ones (2) out of the 4.	Shortlisting two ideas out of 4. And a feasibility test	Suggestion to cancel out 2 ideas out of 4
	Anas			
	Farrdin		Power calculation of an air vortex-based power generation plant.	Suggestion to cancel out 2 ideas out of 4
	Nahean			
25-02-2025	Farrdin	Redoing background research and feasibility check, identifying pros and cons of all 4 ideas, and finalizing the best 2 ideas for the panel to choose from.	All	N/A
	Anas			
	Nahean			N/A
	Fasiul			
03-03-2025	Farrdin	2nd ATC panel meeting. After presenting the ideas, the ATC panel suggested going with the idea or concept of early cancer detection.	All	Asked to choose the idea with which we were confident to move on
	Anas			
	Nahean			Asked to choose the idea with which we were confident to move on
	Fasiul			
04-03-2025	Farrdin	started writing a literature review on early cancer screening in the field of breast cancer and lung cancer. And started	All	N/A
	Anas			
	Nahean			N/A
	Fasiul			

		writing the draft concept note.		
05-03-2025	Farrdin	Took feedback from ATC panel members on our draft concept note, and fixed issues identified by the Panel members.	All	Suggested to add budget
	Anas			
	Nahean			Suggested to revise our technical specification
	Fasiul			
06-03-2025	Farrdin	Submitted the Draft concept note.	All	N/A
	Anas			
	Nahean			N/A
	Fasiul			
07-03-2025	Farrdin	Started writing the final concept note.	All	Provided thoughts on the draft concept note
	Anas			
	Nahean			Provided thoughts on the draft concept note
	Fasiul			
08-03-2025	Farrdin	Got feedback on the Final concept note from the ATC panel.	All	Suggested to add block block diagram
	Anas			
	Nahean			Suggested to add block block diagram
	Fasiul			
15-03-2025	Farrdin	Started preparing for the progress presentation	All	Suggested to start making slides
	Anas			
	Nahean			Suggested to start making slides
	Fasiul			
03-04-2025	Farrdin	Started making presentation slides	All	Instructed to perform a demo presentation
	Anas			
	Nahean			Instructed to perform a demo presentation
	Fasiul			
16-04-2025	Farrdin	Sent demo presentation slide to ATC panel, and according to their feedback back made some changes	All	Suggested to add a flow chart
	Anas			
	Nahean			Suggested to add CO/PO box
	Fasiul			
24-04-2025	Farrdin	Presented our progress in front of the ATC panel. Got Feedback and ideas about the Final Presentation slides.	All	Suggested to add block block diagram
	Anas			
	Nahean			Suggested to add budget
	Fasiul			
26-04-2025	Farrdin	Group meeting about the project proposal	All	N/A
	Anas			
	Nahean			N/A
	Fasiul			

28-04-2025	Farrdin	Started writing the draft project proposal.	All	N/A
	Anas			
	Nahean			
	Fasiul			N/A
29-04-2025	Farrdin	Got feedback about the project proposal from the ATC panel.	All	Provided some feedback to make some small changes.
	Anas			
	Nahean			Instructed related to the structure of the proposal.
	Fasiul			
01-05-2025	Farrdin	Submitted draft project proposal.	All	N/A
	Anas			
	Nahean			
	Fasiul			N/A
03-05-2025	Farrdin	Started preparing for the Final presentation	All	N/A
	Anas			
	Nahean			
	Fasiul			N/A
06-05-2025	Farrdin	Took feedback from ATC panel members on the Final presentation slides	All	Told us to make our flow chart font bigger.
	Anas			
	Nahean			
	Fasiul			
07-05-2025	Farrdin	Performed a mock presentation in front of ATC panel members.	All	Give suggestions about Q/A sessions.
	Anas			
	Nahean			Suggested to rearrange some slide positions
	Fasiul			
08-05-2025	Farrdin	Final presentation	All	N/A
	Anas			
	Nahean			
	Fasiul			N/A
10-05-2025	Farrdin	started going over our draft proposal and writing the final version based on that.	All	N/A
	Anas			
	Nahean			
	Fasiul			N/A
13-05-2025	Farrdin	Submitted project proposal to the ATC panel and got their feedback.	All	Suggested to make some changes in the alignment and formatting.
	Anas			
	Nahean			Suggested some sentence rearrangement
	Fasiul			
14-05-2025	Farrdin	Group meeting to review project proposals and resolve issues.	All	N/A
	Anas			
	Nahean			N/A

	Fasiul			
15-05-2025	Farrdin	Project proposal submission	All	N/A
	Anas			
	Nahean			
	Fasiul			N/A

Log-book (FYDP-D):

Member name	***Name***	***ID***
1.	FARRDIN NOWSHAD	21321007
2	MD. ABU ANAS MRIDUL	22121024
3.	ABRAR MAKSUD NAHEAN	22121076
4.	MOHAMMAD FASIUL ABEDIN KHAN	22121092

ATC Panel Details		
Chair	Dr. Nahid Akhter Jahan	nahid.jahan@bracu.ac.bd
Member-1	Dr. Farjana Akter Jhuma	farjana.jhuma@bracu.ac.bd

Log-book of Group 11 **(FYDP-D)**				
Date/Time	**Attendee**	**Summary of the meeting**	**Responsible**	**Comment by ATC**
10-06-2025	Farrdin	Research on the required software		
	Anas			
	Nahean			
	Fasiul			
12-06-2025	Farrdin	Planning and finalizing the required software before sitting in a meeting with Tashfin sir		
	Anas			
	Nahean			
	Fasiul			
14-06-2025	Farrdin	Discussion with Tashfin sir about submittables		
	Anas			
	Nahean			
	Fasiul			

16-06-2025	Farrdin	Divided work between group members	Farrdin: Approach 1 Circuit and Power simulation	
	Anas		Fasiul: Run ML model for approach 1	
	Nahean		Nahean: Run ML model for approach 2	
	Fasiul		Anas: Compilation of all findings	
22-06-2025	Farrdin	Went to South-East University for collaboration with their Pharmacy department Prof. Dr. Md. Siddiqul Islam		
	Anas			
	Nahean			
	Fasiul			
23-06-2025	Farrdin	Initiated a meeting with Dr. Mosaddekur Rahman for advice on fulfiling the data requirement and getting his reference to contact with Ahsania Mission Cancer Hospital		
	Anas			
	Nahean			
	Fasiul			
23-06-2025	Farrdin	Contacted a hospital personnel (Dr. Raihan Sharif) with the reference of Dr. Mosaddekur Rahman		
	Anas			
	Nahean			
	Fasiul			
25-06-2025	Fasiul	Discussion on work plan and division		
	Anas			
	Nahean			
	Farrdin			
28-06-2025	Farrdin	Started working on the whole process	Proteus Simulation of VOC	
	Fasiul		ML model	
	Nahean		ML model data collection	
	Anas		VOC data collection and analysis	
	Farrdin	Work on progress	Simulink simulation	
	Fasiul		ML model	
	Nahean		Research on breath mask design	
	Anas		VOC data collection and analysis	
	Farrdin	Work on progress		
	Fasiul			

	Nahean			
	Anas			
13-08-2025	Farrdin	Progress Presentation		
	Anas			
	Nahean			
	Fasiul			
14-08-2025	Farrdin	Received feedback from the ATC panel and started working on it		
	Anas			
	Nahean			
	Fasiul			
15-08-2025	Farrdin	Work in progress	PCB design	
	Anas		VOC data collection and analysis	
	Nahean		VOC data analysis (Theoretical proof)	
	Fasiul		ML model	
20-08-2025	Farrdin	Meeting with the ATC panel with revised work		
	Anas			
	Nahean			
	Fasiul			
21-08-2025	Farrdin	Conducting Simulations and 3D designs		
	Anas			
	Nahean			
	Fasiul			
24-08-2025	Farrdin	Work on progress and report writing		
	Anas			
	Nahean			
	Fasiul			
26-08-2025	Farrdin	Making presentation slides on further progress		
	Anas			
	Nahean			
	Fasiul			
28-08-2025	Farrdin	FYDP-D Presentation		
	Anas			
	Nahean			
	Fasiul			

01-09-2025	Farrdin Anas Nahean Fasiul	Continuation in report writing		
04-08-2025	Farrdin Anas Nahean Fasiul	Started the procedure of purchasing the required components		
11-09-2025	Farrdin Anas Nahean Fasiul	FYDP-D Report Submission		

Log-book (FYDP-C):

Member name	***Name***	***ID***
1.	FARRDIN NOWSHAD	21321007
2	MD. ABU ANAS MRIDUL	22121024
3.	ABRAR MAKSUD NAHEAN	22121076
4.	MOHAMMAD FASIUL ABEDIN KHAN	22121092

ATC Panel Details		
Chair	Dr. Nahid Akhter Jahan	nahid.jahan@bracu.ac.bd
Member-1	Dr. Farjana Akter Jhuma	farjana.jhuma@bracu.ac.bd
Member-2	Subhan Zawad Bihan	subhan.bihan@bracu.ac.bd

Log-book of Group 11 (FYDP-D)				
Date/Time	**Attendee**	**Summary of the meeting**	**Responsible**	**Comment by ATC**
25-10-2025	Farrdin Anas Nahean	Meeting with ATC	All	

	Fasiul			
10-11-2025	Farrdin	Group discussion on further procedures	All	
	Anas			
	Nahean			
	Fasiul			
12-11-2025	Farrdin	Visit to Ahsania Mission Cancer Hospital	All	
	Anas			
	Nahean			
	Fasiul			
18-11-2025	Farrdin	ML model accuracy improvement & setup build	All	
	Anas			
	Nahean			
	Fasiul			
03-12-2025	Farrdin	Progress Presentation	All	
	Anas			
	Nahean			
	Fasiul			
05-12-2025	Fasiul	Procurement of all the components	All	
	Anas			
	Farrdin			
	Nahean			
07-12-2025	Farrdin	Assembling the device	All	
	Anas			
	Nahean			
	Fasiul			
14-12-2025	Farrdin	Preparing the image chamber or booth	All	
	Anas			
	Nahean			
	Fasiul			
20-12-2025	Farrdin	Integrating the thermal camera with different ML models	All	
	Anas			
	Nahean			
	Fasiul			
21-12-2025	Farrdin	Work on progress	All	
	Anas			
	Nahean			
	Fasiul			
22-12-2025	Farrdin	Work on progress	All	
	Anas			
	Nahean			

	Fasiul			
23-12-2025	Farrdin	Work on progress	All	
	Anas			
	Nahean			
	Fasiul			
27-12-2025	Farrdin	Identifying the suitable model with better accuracy	All	
	Anas			
	Nahean			
	Fasiul			
28-12-2025	Farrdin	Work in progress & extended writing to finalize the whole report	All	
	Anas			
	Nahean			
	Fasiul			
01-01-2026	Farrdin	Work in progress	All	
	Anas			
	Nahean			
	Fasiul			
02-01-26	Farrdin	Preparing the poster for showcase	All	
	Anas			
	Nahean			
	Fasiul			
03-01-2026	Farrdin	Meeting with the ATC panel to report all the works completed till now and the designed poster	All	
	Anas			
	Nahean			
	Fasiul			
04-01-2026	Farrdin	Final run of the whole setup and making a video of the whole screening process	All	
	Anas			
	Nahean			
	Fasiul			
05-01-2026	Farrdin	FYDP showcase	All	
	Anas			
	Nahean			
	Fasiul			